The Reactions in Viral Nucleic Acids During Photolysis and Chlorine Disinfection

by

Zhong Qiao

A dissertation submitted in partial fulfillment
of the requirements for the degree of
Doctor of Philosophy
(Environmental Engineering)
in the University of Michigan
2018

Doctoral Committee:

Assistant Professor Krista R. Wigginton, Chair
Associate Professor Rose M. Cory
Associate Professor Michael Dodd, University of Washington
Associate Professor Terese M. Olson

Zhong Qiao

zhqiao@umich.edu

ORCID iD: 0000-0001-5180-7128

Dedication

I dedicate this work to my grandmother Bingxiang Zhou and my grandfather Chengjin Qiao, who raised me from when I was born. Both of my grandparents had zero school education, but they taught me the most about life. They worked extremely hard to provide me with the best that they had. They were the most sacrificial grandparents I've ever known, as well as the strongest. It is so unfortunate that they passed away before I finished this work. They had no way of knowing how much impact they had on my life.

I also dedicate this to my mother Guanghua Ren and my father Yu Qiao. I thank my parents for bringing me to this beautiful and peaceful world. I appreciate that they always worked their best to offer me a home full of love. I learned from them that money cannot buy you happiness but love can. Knowing there is a door that is always open for me makes me loved and happy all the time.

Finally, I dedicate this to my beautiful wife Dehuizi Meng and my baby boy Alex Qiao. Getting married before finishing my Ph.D is the best decision that I have ever made. Life is so good when I have them by my side. And they are the most fulfilling part of my life. I love them forever.

Acknowledgements

First, I would like to express my deep gratitude to Professor Krista R. Wigginton for being my doctoral advisor, a close friend, and a great mentor during the past five years. She has given me tremendous guidance and support from the start to the completion of this dissertation. Her advice is invaluable, and her patience is incredible. When I felt frustrated and doubtful of my capability, it was her continuous encouragement and trust that drove me forward towards the finish line. Without her assistance and contribution, I would not have been able to complete my Ph.D research.

My acknowledgement also goes to my committee members Professor Terese M. Olson, Professor Rose M. Cory, and Professor Michael Dodd from the University of Washington for their feedback on my research proposal and their suggestions on my experimental design. I want to thank Dr. Collin Ward in Professor Rose Cory's group for his help on my simulated sunlight study.

I want to convey appreciation to my current and previous colleagues in the Wigginton research group who have created an amazing working environment. I want to especially thank Yinyin Ye for teaching me experimental techniques and providing me with tons of insightful discussions. Many thanks go to Pin Hsuan Chang and Devibaghya Thirunarayanan for their help and contributions to my research projects. Further, I want to acknowledge other members in the

Environmental Biotechnology group for their help on safety and instrument training. I also want to thank Thomas Yavaraski for his guidance on Oribitrap-MS and HPLC analyses, and Nivea Vydiswaran for her laboratory support.

Next, I would like to express my sincere acknowledgement to my family. I want to thank my grandparents for raising, caring, and providing me with the happiest childhood. The memories about the time that we spent together are the most valuable treasure of my life. I also want to acknowledge my father and my mother for their endless support and unconditional love. Home is always the place I miss most no matter how far I go. My deepest thanks go to my dear wife and lovely son for their love, company, and understanding. Having them in my life makes me the happiest man in the whole world.

Table of Contents

List of Tables

List of Figures

List of Appendices

Abstract

Virus-induced diseases pose risks to public health and cause significant impacts on our economy. People can become infected by waterborne virus pathogens when they come into contact with drinking water and recreational water that was not properly treated and disinfected. Nucleic acids (DNA/RNA) carry the genetic instructions for viruses to replicate in their host cells; therefore, damaging viral nucleic acids is an effective way to inactivate viruses and reduce risks of waterborne infection. UV_{254} and chlorine are two disinfection methods commonly used in water treatment, and both lead to reactions in viral genomes. Despite the widespread use of disinfection, scientists and engineers still lack a comprehensive understanding of the reactions that take place in viral nucleic acids, the impact of higher order structure on viral genome reactivity during UV_{254} and chlorine disinfection. With this knowledge, it might become possible to predict the inactivation kinetics of newly emerged viruses and other viruses that are not readily culturable.

To address these knowledge gaps, this dissertation explores the reactions that occur in viral nucleic acids during photolysis and chlorine disinfection. The research spans several levels of nucleic acid reactivity, from the short nucleic acid oligomer level, up to the entire viral genome incorporated in virus particles. In the first portion of this work, the photochemical reactions that take place in viral RNA oligomers were investigated. Specifically, RNA oligomer segments from the genome of bacteriophage MS2 were exposed to UV_{254}, simulated sunlight, and singlet oxygen ($^1O_2$), and the oligomer reaction kinetics were analyzed with RT-qPCR and quantitative

MALDI-TOF mass spectrometry (MS). One especially important finding of this work was that quantitative MALDI-TOF-MS detected significantly more RNA modifications than RT-qPCR. This suggests that certain chemical modifications in the RNA are not detected by the reverse transcriptase enzyme. High-resolution ESI-Orbitrap MS identified pyrimidine photohydrates as the major UV_{254} products, which may have contributed to the discrepancy between the MS- and RT-qPCR-based results.

In the second portion, the influence of viral nucleic acid higher order structure on UVC photolysis was examined. We measured the direct UV_{254} photolysis kinetics of four model viral genomes composed of single-stranded and double-stranded RNA, as well as single-stranded and double-stranded DNA, in ultrapure water, in phosphate buffered saline, and encapsidated in their native virus particles. The photolysis rate constants of naked nucleic acids measured by qPCR (RT-qPCR for RNA) and normalized by the number of bases measured in a particular sequence exhibited the following trend: ssDNA > dsDNA ≈ ssRNA > dsRNA. Interestingly, encapsidation of viral genomes did not affect the photoreactivity of most genome sequences. A large difference in photoreactivity was observed between single and double strands of both RNA and DNA.

In the final portion, the impact of viral genome higher order structure on reactivity with free chlorine was characterized. Chlorine reaction kinetics of the same four model viral genomes were measured when they were naked in solution and when they were incorporated in their native virus particles, respectively. We observed that for most of the nucleic acid regions studied, the naked viral genomes reacted with chlorine significantly faster than encapsidated genomes. The research suggests that dsDNA was the least reactive of the genome types tested.

Specifically, the two T3 dsDNA regions were ~72 times more resistant than the ssDNA regions, which was the most reactive genome type tested.

Chapter 1   Background

1.1   Human viruses

1.1.1   Viruses and their impact to public health

Viruses are a class of microorganisms that cause numerous illnesses and epidemics among humans, plants, and domestic and wild animals. In humans, viruses are responsible for many severe diseases including poliomyelitis, aseptic meningitis, and some hepatitis. Viruses are responsible for numerous disease outbreaks and pandemics. For example, the severe acute respiratory syndrome (SARS) outbreak was caused by a coronavirus and took the lives of 774 people globally in 2003 [1]. The Ebola outbreak in 2014-2015, which was caused by an Ebola virus, led to 11,310 deaths worldwide [2]. Finally, the Spanish flu pandemic in 1918 was caused by an influenza virus (H1N1) and resulted in the deaths of 50 to 100 million [3]. These virus-induced diseases impose significant stress on our economy, such as the expenses on health care and anti-viral strategies. In the United States alone, influenza epidemics cause an estimated economic burden of $87.1 billion, including $10.4 billion of direct medical expenses and $16.3 billion of lost earnings due to illnesses and deaths [4]. The Ebola outbreak resulted in over 1.6 billion US dollars in medical costs [2]. Even less severe virus diseases, like human norovirus, can have major impacts. Each year, norovirus infection causes an estimated 21 million cases of acute gastroenteritis, resulting in more than 56,000 hospitalizations and 570-800 deaths in the United States [5], [6].

Viruses can be transmitted through a variety of pathways, including direct person-to-person contact and indirect contact via airborne droplets, aerosols, or contaminated food, water, medical equipment, and other environment surfaces [7], [8]. Human enteric viruses such as adenoviruses, reoviruses, and noroviruses, are transmitted through the fecal-oral pathway [9]. This often involves exposure to contaminated drinking or recreational waters that have not been appropriately treated or through food consumption that was contaminated with water. Disinfection is an important engineered process that interrupts the indirect route of viral transmission [10]. Disinfectants, such as UV and chlorine, react with viral components (e.g. viral proteins and genomes) and interrupt their biological function, thus leading to inactivation of virus.

1.1.2   *Virus composition, structure, and life cycle*

All viruses consist of at least two components, including a nucleic acid genome and a protective protein capsid. The genome can consist of either DNA or RNA, can be either single-stranded or double-stranded, and can be either linear or circular. The capsid can be helical or icosahedral in structure [11] and consists of two or more different types of proteins. Some viruses also contain a lipid bilayer (i.e., envelope), which originates from the host cell membrane or endoplasmic reticulum (E.R.) membrane [11], and can contain proteins encoded by the virus genome. Interestingly, there is no conserved region of the virus nucleic acid genome and this makes sequencing efforts more difficult for viruses than other classes of organisms. A fully assembled infectious virus particle is called a virion.

Viruses cannot generate energy or propagate outside of their host cells. Instead, they rely on the specialized host cells to provide the complicated machinery necessary to build new virus particles, as well as the necessary basic building blocks, such as nucleotides, amino acids, and lipids [12]. The virus life cycle includes the whole process of virus reproduction, including virus attachment, genome entry, genome replication, virion assembly, and virion release [12]. Attachment is the stage in which the viruses recognize and bind to their respective host cells. In this process, viral proteins on the capsid or envelope interact with specific receptors on the outer surface of the host cell. This unique recognition helps determine the host range of a virus. Once attached, the viral genome can enter into a host cell through several pathways. Certain bacterial viruses (i.e., bacteriophages), inject their genomes into the host through contraction of the tail sheath. Other viruses can induce conformational changes of cellular membranes, which allows the full virion to enter the cell via receptor-mediated endocytosis. Inside the host cell, the viral genome is uncoated and the genome replication process is initiated. Meanwhile, new virus proteins are synthesized by transcription and translation of the viral genome. Ultimately, thousands of copies of the replicated viral genome are packed into newly assembled capsid proteins to form virions. In the final stages, mature virus particles are released through either lysing of the infected cell or by budding out of the host cell.

1.1.3   Virus inactivation

Understanding the virus life cycle sheds light on how viruses might be inactivated. For a successful virus infection, the viral proteins have to be sufficiently intact in order to recognize and attach to the receptor on the host cell surface, and to deliver the genome into the host cell. Meanwhile, the viral genomes must be sufficiently intact so that when they enter the cell, they

can serve as templates for genome replication and protein synthesis. Protein and genome damage inflicted by disinfecting agents can therefore derail these critical steps in infection. To combat the transfer of infective viruses via the aqueous environment, chemical oxidants such as chlorine and ozone, and radiation techniques such as UV_{254} are commonly used to disinfect recreational waters, treated drinking water, potable reuse waters and wastewater effluents [13]-[15].

1.2 Inactivation of viruses in water disinfection

By definition, disinfection is the process of eliminating or reducing pathogenic and harmful microorganism such as viruses. In contrast, sterilization is the process of destroying all microorganisms, including spores, regardless of if they are harmful or not.

1.2.1 Chemical disinfection

Chemical disinfection is a traditional and widely applied method to control the spread of infectious pathogens. Proper chemical disinfection involves adding an oxidizing chemical to a water or surface, or generating the oxidizing chemical in air or solution. Effective disinfection relies on a variety of factors including disinfectant type, disinfectant concentration, contact time, and the presence of material besides the intended target that consumes the disinfectant (e.g., organic matter) [16]. The most common chemical disinfectants applied in water treatment include free chlorine, chloramine, and ozone. Other chemicals such as chlorine dioxide, bromine, and hydrogen peroxide are also effective in certain scenarios.

Chlorination is the most widely applied method for primary water disinfection in the United States [17]. It is also commonly added into treated drinking water just before water enters the

distribution system to prevent the re-growth of pathogens and to combat pathogens that infiltrate the distribution system. When chlorine is added into water, it quickly reacts with water to form hypochlorite ions (OCl^-) and hypochlorous acid (HOCl). Hypochlorious acid is the antimicrobial species and is the predominant species present when the pH is less than the pKa of 7.5 [18]. The term "free chlorine" represents the combination of hypochlorous acid and hypochlorite ions.

Chorine disinfection can inactivate nonenveloped viruses by damaging either the capsid proteins or viral genome [19], [20]. This leads to interruptions in the key steps of virus replication cycles, such as attaching to host cells and genome replication [21]-[23]. Previous research on nucleic acid reactivity with chlorine has revealed that reactions between DNA and chlorine preferentially form 8-chloroadenine and 5-chlorocytosine [24]. Products resulting from reaction of chlorine with RNA include 8-chloroguanosine, 5-chlorocytidine, and 8-chloroadenosine [25]. The formation of 8-oxo-7,8-dihydro-2'-deoxyguanosine (8-oxodG) is commonly used as a marker for general oxidative damage in nucleic acids [26]-[29]. The less abundant reports on RNA oxidation mention that RNA genome damage in the cell can lead to decreased protein synthesis rates [30] and increased replication error rates. The specific reactions that take place in RNA as opposed to DNA have not been well characterized. In terms of reactions between chlorine and viral proteins, chlorine-induced protein damage can result in the virus losing its ability to attach to the host cell [31], the inhibition of genome injection into its host [20], and the interruption of endocytosis and nuclear delivery processes [22].

The widespread application of free chlorine disinfection results from its low cost, ease of use, and highly reliable performance as a broad spectrum antimicrobial disinfectant. However, there

are some disadvantages associated with chlorination, such as the irritation it causes to mucous membranes and human skin at high concentrations, the corrosion it causes during its storage, handling, and shipping, and the toxic effects it can have on aquatic life in the natural environment [32]. Another major drawback is chlorination leads to the formation of hazardous byproducts, including trihalomethanes (THMs) and other halogenated hydrocarbons, by the reactions between chlorine and natural organic matter present in water [17]. THMs formed in chlorine-treated drinking water have drawn considerable attention because of their possible association with rectal, colon, and bladder cancers [33]-[35]. Due to the negative effects that these compounds might have on human health, the United States Environmental Protection Agency (U.S. EPA) has set strict regulatory standards on four THMs, namely trichloromethane (chloroform), bromodichloromethane (BDCM), dibromochloromethane (DBCM), and tribromomethane (bromform) [36].

Driven primarily by the undesirable disinfection by-products (DBPs) associated with free chlorine, other chemical disinfectants have been introduced and applied for water treatment. Chloramines, for example, which are formed by combining ammonia with chlorine, are increasingly used as a secondary disinfectant to maintain residual disinfection in distribution systems. Monochloramine is the second most commonly used chemical disinfectant in US drinking water treatment systems after free chlorine. Based on a survey conducted in 2004, 29% of water utilities used chloramines for secondary disinfection [37]. Chloramines form lower amounts of THMs compared to free chlorine [38]. Also, chloramines are less reactive than free chlorine, so they can persist longer within distribution systems. Amongst the chloramines, monochloramine is the most effective at inactivating pathogens and is the predominant species

when the pH is above 7. Another benefit is that chloramines tend to create fewer taste and odor issues than free chlorine. One major drawbacks of using chloramines is that chloramines are less reactive with microorganisms, such as *Legionella* [39], [40]; consequently, chloramines require longer contact times than free chlorine to achieve the same level of inactivation of waterborne pathogens. Other disadvantages include an associated risk of anemia in kidney dialysis patients, increased leaching of lead in drinking water, and the formation of nitrite from enhanced microbial activities in biofilms that exist in the distribution system [40], [41].

Ozonation is another disinfection technique that has been applied in a great number of water treatment plants throughout the world. For drinking water disinfection, ozone is usually produced on site by passing a stream of pure oxygen or dry air though a pair of electrodes that generate a high electrical discharge [17]. Ozone is a powerful oxidant that is effective over a wide pH and temperature range and rapidly reacts with bacteria, protozoa, and viruses. Ozone inactivates viruses by attacking both viral proteins and genomes. During ozonation, hydroxyl and superoxide-free radicals can also be formed and react with viral components. In poliovirus, ozone damaged the protein capsid, which interrupted virus attachment with its host cell [42]. Another study showed that at a concentration of 0.37 mg/L and within a contact time of 10 seconds, ozone caused > 3 logs of genome degradation to Norwalk virus, poliovirus 1, and bacteriophage MS2 at pH 7 and 5 °C [43]. Ozone generates fewer DBPs than chlorination, although bromate formation can be an issue [44]. Ozonation also results in few, if any, taste or odor issues. Due to its high reactivity, however, ozone has a very short lifetime in water, and thus cannot serve as a residual disinfectant in drinking water distribution systems [45], [46]. Chlorine and chloramines have been used in conjunction with ozone to solve this problem. The

generation of ozone requires reliable power supplies and high power consumption, which makes ozonation more expensive to operate and maintain than chlorination [47].

1.2.2 Disinfection by UV radiation

Some disinfection technologies harness radiation rather than chemicals. Ultraviolet (UV) germicidal irradiation and solar spectrum irradiation, for example, are commonly used for disinfection. Radiation-mediated virus inactivation can occur via three distinct pathways: direct, indirect endogenous, and indirect exogenous photolysis [48]. In the first mechanism, viral components (e.g., nucleic acids) that are able to absorb UV light are directly damaged during irradiation. This has been reported extensively with germicidal UV (i.e., UVC, 100-280 nm) and using UV regions of the solar spectrum (primarily UVB, 290-315 nm) [49]-[51]. The second and third mechanisms are indirect photochemical pathways that can be initiated by both visible and UV light. In the presence of dissolved oxygen, the excitation of sensitizers (i.e., light-absorbing compounds that are able to transfer energy/electrons to other molecules) results in the formation of reactive oxygen species (ROS), such as singlet oxygen ($^1O_2$) and hydroxyl radicals ($\bullet OH$). Once formed, these strong oxidants can react with viral constituents [50]. In endogenous photoinactivation, sensitizers are located within the virus particles (e.g. viral genome) [52], whereas in exogenous photoinactivation, sensitizers are located outside of the organism (e.g., natural organic matter (NOM)) [53], [54].

Photochemical disinfection treatments primarily target the viral nucleic acids [55], [56], although there are reports of protein damage following UV radiation [52], [57]. Previous studies on photochemical reactions in nucleic acids, primarily with DNA, have identified three major direct

photochemical pathways [58]-[60]. In the first two pathways, the excitation of neighboring pyrimidines lead to the formation of either cyclobutane pyrimidine dimers (CPD) [61], [62] or pyrimidine-pyrimidone 6-4 photoproducts (namely 6-4 products) [63], [64]. In the third pathway, when nucleic acids are present in water, reactions with UV results in the formation of pyrimidine photohydrates [65]. In DNA, thymine dimers have significant impact on biological functions, whereas the hydrates reportedly have less biological significance [66]. Some dsDNA viruses can utilize genome repair machineries in the host cell to mitigate pyrimidine dimer modifications that have occurred in the viral genome [67], [68]. A similar phenomenon has not been identified in viruses with ssDNA genomes or RNA genomes.

The advantages of UV disinfection include easy installation and operation, small space requirements, the lack of taste and odor issues, no adverse effects on plumbing, and no potential risk of overdosing [69], [70]. Another major benefit of UV irradiation is that it does not generate toxic or carcinogenic by-products unless UV treatment is applied in conjunction with chemical disinfection [41]. Similar to ozone, the major drawback of UV irradiation is the lack of residual disinfectant in the treated water, although this can be overcome by adding a secondary disinfectant such as chlorine or chloramine [17], [71]. Other disadvantages of UV include higher capital and energy costs compared to chlorination, lower disinfection efficiency for water with high turbidity and no measurable residual to monitor and control the efficacy of disinfection [17].

1.3 Methods for detecting viruses and studying their genome reactivity

1.3.1 Plaque assays

In order to evaluate the efficacy of disinfection techniques, dose-response curves are typically established by measuring the concentrations of pathogens that survive after various doses. Infective viruses are commonly enumerated before and after disinfecting treatments using culture assays, but this is only possible if the target viruses are culturable on available cell lines [72]-[74]. Plaque assays are a common virus culture and enumeration method conducted in petri dishes or multi-well plates. In particular, aliquots of samples that contain viruses are prepared with different dilution ratios. The samples are inoculated onto a monolayer of host cells that corresponds to the virus of interest in the sample. During incubation, cells that are infected by some viruses will lyse and release thousands of viruses, which subsequently infect nearby cells. Over time, the repeated infection of neighboring cells results in plaques, which can be visible to the naked eye or with the aid of dyes and an optical microscope [75]. The number of formed plaque units and dilution factors are used to calculate the number of infective virions per sample unit volume, usually reported as plaque forming units per mL (i.e., PFU/mL). This is based on the assumption that each plaque-forming unit represents one infectious virus particle [76], [77], and thus can result in incorrect virus concentrations if virions are in an aggregated state. One major advantage of virus culture methods, like plaque assays, is that they measure the infectivity of viruses directly, which is valuable for assessing the efficacy of disinfection techniques.

Many viruses cannot be readily cultured, and thus other quantitative methods are required for their detection and enumeration. Furthermore, when research goes beyond the survival of viruses

and explores the mechanistic fate of viruses through water disinfection processes, a suite of additional methods beyond culturing is necessary.

1.3.2   qPCR and RT-qPCR

The infectivity of many important viruses, such as human norovirus (HuNoV) [78], either cannot be measured or are difficult to measure due to the lack of cell lines that are readily infected by the viruses. This situation applies to emerging viruses because it takes time to develop new culture systems that effectively propagate and enumerate the newly identified viruses. Consequently, culture-independent molecular methods such as quantitative polymerase chain reaction (qPCR) and reverse transcription quantitative polymerase chain reaction (RT-qPCR) are often applied to quantify viruses present in water and other types of samples [56], [79], [80].

PCR is a common laboratory technique used to identify and amplify a specific region of target DNA. In particular, primers with complimentary sequences to the target DNA first locate and bind to the region of interest. Then, DNA polymerase is employed to synthesize new strands of DNA through a number of cycles. In every cycle, the number of this specific sequence is doubled, which leads to an exponential amplification of the target DNA after many cycles (typically 30 to 45 cycles) [81]. For quantitative PCR, or qPCR, there are two additional steps beyond PCR: 1) the amplified DNA segments are labeled with fluorescence dyes; 2) the number of DNA in a sample is quantified based on the assumption that the quantity of the amplified DNA is proportional to the amount the sample fluoresces. The number of the cycles it takes for the fluorescence to be detected by a fluorometer is termed the "Ct value". The higher the Ct value required for detection, the lower the initial copy numbers of the target DNA in a sample

[82]. Since the polymerases used in PCR only work with DNA, a reverse transcription (RT) step is used first for RNA detection. RT-qPCR has been developed to identify and quantify target RNA regions. In RT-qPCR, the RNA template (e.g. region of target viral RNA) is reverse transcribed into complementary DNA (cDNA) by RT and then the cDNA is amplified and quantified with qPCR.

Compared to plaque assays, there are a couple of major advantages of PCR-based methods, including fast response times, high specificity, and its ability to detect non-culturable viruses [83]. Therefore, PCR and RT-qPCR have been widely applied to enumerate viral genomes [78]-[80] and to study the kinetics of reactions that take place in viral genomes during water disinfection [20], [84]. However, there are limitations that need to be considered while using PCR based methods for measuring virus presence and fate through disinfection processes. First, PCR does not provide information regarding virus infectivity because it detects the presence of viral nucleic acids. In other words, the presence of nucleic acids does not equate to the presence of infective viruses in the sample. Some research has used qPCR to measure the fate of viruses through unit processes, but measuring nucleic acids before and after unit processes does not provide sufficient information on the effectiveness of the unit process at inactivating viruses [20]. qPCR methods only measure a small fraction of the entire genome [56], so the results do not relate what has happened in the entire genome. For example, the size of a PCR target region is typically 100-500 base pairs, but the genome of human Adenovirus serotype 5 contains 35,938 base pairs [85]. This becomes problematic when genome damage occurs outside of the region targeted by PCR. Another issue with using qPCR to study virus genome fate is that the results

provide no information on reaction products. Hence, it is inappropriate to use PCR methods to investigate specific reaction pathways in virus genomes during water disinfection.

1.3.3   Mass spectrometry

Another culture-independent method to detect viral components is mass spectrometry (MS). Mass spectrometry is a rapid and powerful tool for characterizing reactions in polar biomolecules, such as peptides and nucleic acids. A mass spectrometer typically involves the ionization of analytes and a means of separating and measuring the mass-to-charge (m/z) ratio of the resulting ions [86]. The molecular weight of the compound can be calculated based on the charge and the m/z ratio of the ion. The mass information obtained from mass spectrometers provides evidence for the chemical composition of a compound. In addition to identifying unknown chemical species, the mass spectrometer can quantify the amount of a chemical species in a sample.

In recent years, mass spectrometry-based methods have been developed to characterize the sequence, quantity, structure, and chemical modifications of nucleic acids [87]-[89]. There are two common soft ionization techniques that can be applied in nucleic acids analysis, namely matrix assisted laser desorption ionization (MALDI) and electrospray ionization (ESI) [90]. MALDI coupled with time-of-flight mass spectrometry (MALDI-TOF-MS) has several benefits including short analysis time, a simple spectrum, the production of mainly single charged ions, and an ease of operation relative to other MS techniques [90]. ESI is often applied in conjunction with liquid chromatography (LC) in the front and an ion trap, single or triple quadrupole, or time-of-flight mass analyzer in the back (LC-MS) [87], [90]. Unlike MALDI, ESI tends to form

a range of multiply charged ions, which enables the analysis of larger biomolecules such as peptides and genome segments, but the more complex mass spectra makes data interpretation more difficult. LC systems often feed into mass spectrometers. These can separate compounds from complex matrices before they are ionized and detected by the mass analyzer. This increases the sensitivity and specificity of MS methods. High-resolution ESI-LC-MS systems provide the additional benefit of higher mass accuracy. This offers opportunity for high-level qualitative analysis, such as the identification of unique/signature masses of the chemical species.

One application of MS-based methods is to detect products resulting from reactions that take place in viral nucleic acids during disinfection treatments. This is easiest if products have a different mass than the original molecule. For example, pyrimidine photohydrates, which are formed from reactions between nucleic acids and UV, have a mass difference of +18.015 Da (=H_2O) from the original pyrimidine bases, and thus can be easily detected by mass spectrometry [91]. For products that do not cause mass shifts, such as pyrimidine dimers, either highly resolved LC separations or tandem MS (MS-MS) strategies must be utilized to identify products based on their structural differences [87]. Beyond its application for identifying reaction products, quantitative-MS based methods can help obtain the reaction kinetics of nucleic acids. The key to quantitative mass spectrometry for biomolecules is applying appropriate internal standard. For example, ^{18}O-labeled oligomer internal standards can be introduced when genomes are digested with RNase in ^{18}O water [92]. An alternative quantitative MS technique uses target-specific internal standards that consist of two additional bases (AU) at the 5' end of the target oligomer sequence [93]. Until now, results obtained with these MS approaches have not been compared with results obtained with qPCR methods.

1.4 Motivations and research objectives

1.4.1 Motivation

A mechanistic understanding of virus inactivation helps identify features in viruses that make them more or less susceptible to natural or engineered stressors. This is important because it will never be possible to study every type of virus in every type of water treatment, natural environment, etc. Consequently, for some viruses, we can only predict their fate in disinfection processes and other environments based on their structure, chemistry, and microbiology. A mechanistic description of virus inactivation requires a fundamental understanding of the reactivity of viral components. Compared to bacterial and protozoan pathogens, viruses have relatively simple chemical structures and do not replicate outside of their host. This means that viruses are essentially large, inert biomolecules. Unveiling the links between viral chemical composition and their susceptibility to common disinfectants will enable us to predict the susceptibility of nonculturable and newly emerging viruses to disinfection based on molecular composition and structure. Likewise, an improved understanding of the link between virus composition and inactivation will assist in developing improved disinfection techniques based on virus molecular structure.

Previous research has identified specific chemical modifications that occur in virus components during disinfection processes and lead to virus inactivation [22], [31], [94]-[96]. Most of this research has focused on reactions that take place in viral proteins and the biological significance of those reactions.[20], [52], [57], [97] Protein modifications caused by disinfectants can result in changes in protein tertiary and quaternary structure [98], [99], and subsequently lead to protein

15

unfolding [98], protein cross-linking [100], and increased susceptibility to protease cleavage [83], [100].

When it comes to viral nucleic acids, many important enteric virus pathogens, such as norovirus and poliovirus, contain RNA genomes. Understanding the reactions that take place in viral RNA during water disinfection is therefore important for comprehensive descriptions of virus inactivation. Unfortunately, compared to proteins and DNA, the specific reactions that take place in RNA when exposed to oxidants and radiation, and the impact of these modifications on biological functions, are less studied [101]. Specifically, oxidants- and radiation-induced viral RNA reactions have not been adequately characterized. It is commonly assumed that the reactions that occur in DNA also apply to RNA. However, due to the deficiency of RNA studies, the differences between DNA bases and RNA bases is unclear.

Studying the mechanistic fate of viral RNA through disinfection treatments requires reliable analytical methods. RT-qPCR has been widely applied to track the fate of viral RNA due to its specificity and high sensitivity [83], [102]. RT-qPCR measurements rely on reverse transcription to convert target RNA to complimentary DNA (cDNA); however, reverse transcriptase has a high error rate [87], making inaccurate base matches while transcribing. It is therefore possible that RT-qPCR fails to recognize all RNA modifications that take place during disinfection reactions, some of which may be important for virus infectivity. The sensitivity of RT-qPCR detect modifications that occur in RNA has not been previously reported.

The reactivity of viral genomes is likely impacted by the higher order structure of the genome and its incorporation into the virion. For example, some common secondary structures found in single-stranded RNA, such as stem-loop and pseudoknots, can increase the compactness of RNA genome and potentially alter its reactivity. Also, the incorporation of the nucleic acids into virus particles may protect viral nucleic acids from disinfectants [103].

To date, there have been few studies that examine the overall impact of virus genome higher order structure on reactivity. For naked nucleic acids, the physical orientation of nucleic acid bases and the structures surrounding them at the time of UV irradiation can have an impact on DNA/RNA photoreactivity [104]-[106]. For viruses, it was reported previously that UV_{254} primarily reacts with viral genomes [20] and causes only little protein damage [52], which suggests capsid proteins may provide minimal protection to nucleic acids against UVC irradiation. One early study did report that tobacco mosaic virus genomes are inactivated more rapidly when naked than when incorporated in a virus capsid [107], but this effect has not been reported in other viruses.

With regards to chemical disinfection, a previous study examined the reactivity of extracted poliovirus RNA with chlorine dioxide using RT-PCR and showed that denatured virus RNA reacted significantly slower than native virus RNA [13]. This suggests an influence of higher order genome structure on viral nucleic acid reactivity with oxidants. Although it is likely that the protein capsid protects packed genomic material from oxidants such as chlorine, we do not yet know the extent of this protection and how it varies from virus to virus. Furthermore, for envelope viruses, the impact that the lipid bilayer has on the genome reaction kinetics has not

previously been explored. Ultimately the influence that higher order viral structure has on viral genome reactivity with oxidants could help someday predict the relative kinetics of virus inactivation without the need for conducting culture methods.

1.4.2   Research objectives

The overall aim of this work is to characterize the reactions that occur in viral nucleic acids during water disinfection process, from the short oligomer level up to the entire genome within a virus particle. To address the knowledge gaps and research questions described above, this dissertation seeks to address three major research objectives in the three research chapters. Each of the three objectives is listed below as well as the specific tasks that were necessary to address the objectives.

<u>Objective 1: Characterize photochemical reactions that occur in RNA oligomers with quantitative mass spectrometry and RT-qPCR</u>

a) Develop a quantitative MALDI-TOF-MS method and a specific RT-qPCR assay to track reaction kinetics of short RNA oligomers.

b) Obtain reaction rate constants of RNA oligomers reacting with UV_{254}, sunlight, and reactive oxygen species with the quantitative MALDI-TOF-MS and RT-qPCR methods.

c) Compare rate constants of RNA oligomers determined by quantitative mass spectrometry with those determined by RT-qPCR.

d) Analyze the reaction products that result from the photolysis of RNA oligomers using mass spectrometry.

Objective 2: Assess viral nucleic acid photoreactivity with UV$_{254}$ and the impact of virus encapsidation

a) Predict reaction rate constants of target viral nucleic acids with UVC irradiation based on sequence information and published photochemical constants.

b) Develop and optimize qPCR and RT-qPCR assays that quantify two target regions of a model ssRNA virus, a model dsRNA virus, a model ssDNA virus, and a model dsDNA virus.

c) Characterize the UV$_{254}$ reaction kinetics of target genome regions in the four model viruses under three scenarios, namely, when the genomes are naked in water, when the genomes are naked in phosphate buffer, and when the genomes are within the virus particles (RT-) qPCR.

d) Compare the predicted rate constants with the measured rate constants and compare the experimental rate constants of naked genomes with rate constants of encapsidated genomes.

Objective 3: Investigate the reactions of viral nucleic acids with free chlorine and determine the influence of virus encapsidation

a) With a continuous flow system, characterize the chlorine reaction kinetics of target genome regions in four model viruses.

b) Study the role of encapsiation by comparing rate constants of naked genomes with rate constants of encapsided genomes.

c) Examine the impact of location and sequence on reactivity of viral nucleic acids with free chlorine.

Chapter 2 Direct and Indirect Photochemical Reactions in Viral RNA Measured with RT-qPCR and Mass Spectrometry

2.1 Introduction

Many illnesses are transmitted by enteric viruses [9], often by exposure to drinking or recreational waters that have not been appropriately treated. Disinfection is the main line of defense for inactivating viruses in water. Understanding virus disinfection mechanisms helps improve treatment technologies and also predict the fate of non-culturable or newly emerged viruses during disinfection processes. Most enteric viruses are composed of a small RNA or DNA genome that is protected by a protein capsid. The specific chemical reactions that take place in viral proteins during disinfection and the biological significance of those reactions have been the focus of recent studies [20], [52], [57], [97], but our understanding of the specific reactions that take place in viral nucleic acids is more limited.

Disinfection treatments that harness photochemistry, including ultraviolet (UV) germicidal irradiation and solar water disinfection (SODIS), primarily target the viral genome [55], [56]. Photochemical reactions in viral genomes can take place via direct or indirect photolysis pathways [48]. In the direct mechanism, viral nucleic acids absorb UV light and then react to form photoproducts [49]. In indirect pathways, exogenous sensitizers outside of the organism (e.g., NOM) absorb light and then react with the nucleic acids or react with other constituents in the water to form reactive species (e.g., singlet oxygen ($^1O_2$), hydroxyl radical ($\bullet OH$)) that

subsequently react with the nucleic acids [50]. Alternatively, endogenous molecules within the virus particle can also act as sensitizers [52].

Most of the past research on nucleic acid photochemistry has focused on DNA. The major DNA modifications induced by UV radiation include cis-syn cyclobutane pyrimidine dimers (CPD), (6-4) photoproducts, and pyrimidine hydrates, with other modifications occurring at lower levels [108]. Oxidants that form from indirect photolysis pathways, like $^1O_2$, preferentially react with guanine bases in DNA [109], although all four bases are susceptible to oxidative damage [110]. The oxidation product 8-oxo-7,8-dihydro-2'-deoxyguanosine (8-oxodG) is often used as a marker of oxidative damage in deoxynucleosides [26]-[29].

Studying the mechanistic fate of viral RNA through photochemical treatment processes requires both microbiological and analytical methods. Infective viruses can be enumerated before and after disinfecting treatments, as long as the viruses of interest are culturable [72]-[74]. A number of important waterborne viruses, however, are not culturable or are difficult to culture with available cell lines (e.g., human norovirus, hepatitis A virus). Quantitative RT-PCR (RT-qPCR) is widely used to enumerate viral genomes when viruses are not readily cultureable [56], [79], [80] and to study the kinetics of reactions that take place in viral genomes [20], [84]. When used to track genome inactivation, there is a common assumption that RT-qPCR tracks all of the modifications in RNA, but the validity of this assumption has not been readily examined [56], [111]. Reverse transcriptase has a high error rate [112]; for example, it makes inaccurate base modifications while transcribing RNA into DNA. It is therefore possible that RT-qPCR fails to

recognize all RNA modifications that take place during direct and indirect photolysis reactions, some of which may be important for virus infectivity.

The goal of this study was to characterize RNA reactions during direct and indirect photolysis. In particular, we studied direct photolysis by UV_{254} and sunlight radiation, and indirect photolysis with $^1O_2$. We focused on $^1O_2$ due to the fact that it is a principal oxidant involved with virus inactivation in waters containing NOM [50]. Using quantitative Matrix Assisted Laser Desorption Ionization time-of-flight mass spectrometry (MALDI-TOF-MS), high-resolution Electrospray ionization (ESI) Orbitrap mass spectrometry, and RT-qPCR, we characterized the photolysis reaction kinetics and products in two RNA oligomers from the genome of bacteriophage MS2.

2.2 Experimental methods

2.2.1 Chemicals and reagents

Furfuryl alcohol (98%), THAP (2'-4'-6' Trihydroxyacetophenone monohydrate), dibasic ammonium citrate ($HOC(CO_2H)(CH_2CO_2NH_4)_2$) and Rose Bengal (dye content 95%) were purchased from Sigma-Aldrich (St. Louis, MO). HPLC grade acetonitrile (ACN) was purchased from Acros Organics (New Jersey, USA). UltraPure DNase/RNase-Free distilled water was purchased from ThermoFisher Scientific, (Grand Island, NY).

2.2.2   UV$_{254}$, solar spectrum, and $^1O_2$ reaction protocols

Two RNA oligonucleotides were designed with sequences from selected regions of the bacteriophage MS2 viral genome (Table 2.1). Oligomer A was rich in pyrimidine bases, including several pairs of neighboring pyrimidines, and poor in guanines. Oligomer B was poor in pyrimidines and rich in guanines. The size of the synthetic RNA oligomers (24-mer) was small enough for quantitative RNA mass spectrometry measurements and large enough for RT-qPCR measurements. The photolysis experiments were conducted in DNA/RNAse-free water and run in triplicate.

Table 2.1 The sequences and masses of the RNA oligonucleotides from MS2 genome and corresponding internal standards

RNA segment	Sequence	Average Mass Monoisotopic Mass (Da)
Oligomer A	5'- ^{982}AUCCAUAUCACACCCUUUUCCACG^{1005} -3'	7453.521 7449.990
Oligomer A Internal Standard	5'- AUCCAUAUCACACCCUUUUCCACGAU -3'	8088.898 8085.067
Oligomer B	5'- ^{168}UGGAAGCAGGGAUCGCAGGCGCAA^{191}-3'	7832.846 7829.137
Oligomer B Internal Standard	5'- UGGAAGCAGGGAUCGCAGGCGCAAAU-3'	8468.224 8464.214

In the UV$_{254}$ irradiation treatments, 20 µL RNA solution in DNase/RNase-free distilled water (4 µM, pH 6.2) was added to the wells of a 96-well plate (Eppendorf, Hauppauge, NY). The plate was placed approximately 25 cm below four 15 W germicidal low-pressure mercury vapor lamps (model G15T8, Philips, Andover, MA) inside a collimated beam unit. Based on chemical actinometry measurements [113], the UV irradiance was 0.17 mW/cm^2 at 254 nm. The RNA

23

oligomer samples were irradiated for up to 20 minutes, or a dose of 204 mJ/cm^2. Shielding calculations indicated that 99% of the incident light was transmitted through the sample, thus shielding corrections were not deemed necessary.

For solar spectrum irradiation and $^1O_2$ experiments, samples of oligomers (1 mL, 1.2 µM) were pipetted into 5 mm diameter quartz NMR tubes (Wilmand, Vineland, NJ). The tubes were placed in a test chamber of a Suntest XLS+ solar simulator (Atlas Material Testing Technology, Mt Prospect, IL). The solar simulator spectrum (300 to 800 nm) was monitored with a built-in photo-diode detector, with measured irradiances equal to 34 W/m^2 and 1.4 W/m^2 for the UVA (320-400 nm) and UVB (280-320 nm) ranges, respectively. This is equivalent to approximately 2.4× and 3.4× the intensity of midday sun in Ann Arbor, MI during the summer (Figure A-1). The temperature in the test chamber was maintained at 25 ºC by an air- and water-cooling system.

For the $^1O_2$ experiments, Rose Bengal was added to the tubes to a concentration of 1.5 mg/L (1.5 µM). To maintain a constant $^1O_2$ concentration, Rose Bengal was replenished in the experimental solution to the initial concentration of 1.5 mg/L every 20 minutes. This approach resulted in a relatively constant $^1O_2$ concentration of 9 x 10^{-11} M throughout the experiment, as measured with the $^1O_2$ probe compound furfuryl alcohol (Figure A-2) [50]. Control experiments conducted either in the dark (i.e. Dark Control) or without Rose Bengal (i.e. No Rose Bengal Control) were included in each set of $^1O_2$ experiments.

In both the $^1O_2$ experiments and direct photolysis experiments, aliquots of the experimental solutions were collected from the reaction tubes in the simulator chamber periodically and stored refrigerated in the dark. The $^1O_2$ experiments were conducted for two hours and the direct photolysis experiments were conducted for five hours. Samples were analyzed immediately after the completion of the experiments by RT-qPCR and mass spectrometry.

2.2.3   Stem-loop primer based RT-qPCR assay

The stem-loop quantitative RT-qPCR method applied here was originally developed to quantify MicroRNAs (miRNAs) and therefore works well for RNA oligomers that are 18-25 bases long [114]. In brief, stem-loop RNA primers were designed for the two 24-mer RNA targets (Table 2.1). The RNA oligomer standards for RT-qPCR calibration curves were prepared at concentrations between 1.3×10^{-3} and 8.0×10^{-2} pmole/µL (7.5×10^8 and 4.8×10^{10} copies/µL). The RT reaction solutions (15 µL) consisted of 0.15 µL Deoxynucleotides (dNTPs; 100 mM), 1.00 µL MultiScribe™ Reverse Transcriptase (50 U/µL), 1.50 µL 10X Reverse Transcription Buffer, 0.19 µL RNase Inhibitor (20 U/µL; TaqMan® MicroRNA Reverse Transcription Kit, ThermoFisher Scientific, Grand Island, NY), 3.0 µL 5X Stem-loop RT primer (Custom TaqMan® Small RNA Assay, ThermoFisher Scientific, Grand Island, NY), 4.16 µL nuclease-free water, and 5.0 µL of the RNA oligomer stock. RT was performed in a thermal cycler (Eppendorf AG 22331 Hamburg, Hauppauge, NY) at 16 ℃ for 30 minutes followed by 42 ℃ for 30 minutes. Finally, the preparation was heated at 85 ℃ for 5 minutes to denature RNA-DNA hybrids and inactivate reverse transcriptase. The resulting cDNA was then amplified by qPCR.

The 20 µL qPCR reactions included 1.33 µL of the cDNA solution, 1.00 µL of TaqMan® Small RNA Assay (20X), 10.00 µL of 2X TaqMan® Universal PCR Master Mix II with UNG (ThermoFisher Scientific, Grand Island, NY), and 7.67 µL of nuclease-free water. Amplification and detection were performed with a RealPlex^2 Mastercycler system (Eppendorf, Hauppauge, NY). The amplification procedure included two hold programs, 2 minutes at 50 ℃ to activate the uracil N'-glycosylase and then 10 minutes at 95 ℃ to activate the hot start DNA polymerases, followed by 40 cycles consisting of 15 seconds at 95 ℃ and 60 seconds at 60 ℃. Real-time fluorescence measurements were analyzed with the RealPlex system software. Experimental RNA samples and RNA standards were reverse transcribed and amplified in parallel in each analysis.

2.2.4   MALDI-TOF-MS analysis

The RNA oligomer samples were analyzed with a quantitative MALDI-TOF-MS technique in negative-ion mode on a Bruker Autoflex Speed system (Madison, WI). A 20 mg/L solution of THAP in 50% ACN/50% H_2O with 50 mg/mL ammonium citrate hydrate was used as the MALDI matrix. For quantification, a 26-mer internal standard was designed for each viral RNA segment by adding one adenine (A) and one uracil (U) to the 24-mer sequence at the 3' end (Table 2.1) [93]. Calibration curves for oligomer quantification were prepared by mixing 1 µM 26-mer with different 24-mer concentrations, ranging from 0.2 to 2 µM (Figure A-3). The resulting calibration curve R^2 values were always greater than 0.99. Following the UV, solar spectrum, and $^1O_2$ experiments, 5 µL aliquots of the treated oligomer solutions were combined with 5 µL of the corresponding internal standard solutions with 1 µM as concentration. These

mixtures were then combined with the matrix solution at a 1:1 ratio and spotted on a polished

steel MALDI target plate (Bruker, Madison, WI) and allowed to air dry.

The MALDI mass measurements were calibrated externally with a mixture of five

oligonucleotides ranging in masses from 1488 to 9137 Da. MALDI spectra were generated in

linear mode with 12,000 laser shots randomly collected across the sample spot. Samples were

scanned from 2,000 to 10,000 m/z.

2.2.5   ESI-Orbitrap mass spectrometry

High-resolution mass analyses were performed with a qExactive ESI-Orbitrap mass spectrometer

(Thermo Fisher Scientific, MA, USA) coupled with an EQuan Max Plus LC system. The

samples were separated on a Hypersil GOLD UHPLC column (50 x 2.1 mm, 1.9 µM particle

size, Part No.: 25002-052130, Thermo Fisher Scientific, MA, USA). The mass spectrometer was

operated in negative-ion mode with 3.8 kV spray voltage, 320 ℃ capillary temperature and 50 S-

lens. The spectrometer was externally calibrated with Pierce ESI Negative Ion calibration

solution (Prod #: 88324, Thermo Fisher Scientific, MA, USA). For each analysis, 15 µL of

sample was injected with a mobile phase of 2% Hexafluoro-iso-propanol (HFIP) + 0.4%

Triethylamine (TEA) in water and 2% Hexafluoro-iso-propanol (HFIP) + 0.4% Triethylamine

(TEA) in methanol. The gradient information is provided in Table A-1. For product detection

and identification, RNA oligomer samples were scanned from 400 to 2000 m/z in full-scan mode

with a resolution power of 70,000. Product fragmentation was performed in Target-MS-MS

mode with isolation as 4 amu and an HCD level of 20. A scan window of m/z 400 to 1200 was

collected at a resolution power of 17,500. Mass spectra were processed and analyzed by Xcalibur Qual Browser software (Thermo Fisher Scientific, MA, USA).

2.2.6 Statistical analysis

Details on how rate constants were calculated are presented in the Appendix A section. To test whether there were statistical differences between RNA reaction rate constants measured with RT-qPCR and mass spectrometry, multiple linear regression analyses were conducted using StatPlus (AnalystSoft Inc., Walnut, CA). The null hypothesis was that the kinetics from each experiment were not significantly different. The P values were computed and compared at a confidence level of 95%.

2.3 Results and discussion

Prior to conducting the reaction kinetics experiments, we developed the stem-loop RT-qPCR assay and quantitative MALDI-TOF-MS assay for the two MS2 oligomers. Once optimized, both quantitative methods resulted in calibration curves with R^2 values greater than 0.99 and the stem-loop RT-qPCR efficiencies were consistently greater than 0.85 (Figure A-3 and Figure A-4). The calibration curve linear concentration ranges differed between the two techniques, so that it was necessary to dilute the RNA samples 20-100× prior to RT-qPCR analysis, but no dilution was necessary for the MALDI-TOF-MS analyses.

2.3.1 Direct photochemical reactions with UV_{254}

We exposed the two RNA oligomers to UV_{254} doses up to 204 mJ/cm^2, and tracked RNA reaction kinetics with the quantitative PCR and MS methods. For context, this dose of UV_{254} causes approximately 5-log inactivation of MS2 virus [20]. The two RNA oligomers degraded significantly during the UV_{254} experiment (Figure 2.1) and no RNA loss was detected when samples were incubated in the dark over the same timeframe. The decay of both oligomers measured by MALDI-TOF-MS and RT-qPCR followed first-order kinetics over the studied dose range (Figure 2.1), with Oligomer A reacting at a faster rate than Oligomer B (Table 2.2). In particular, the MALDI-TOF-MS results show that 70% of Oligomer A segments reacted after 204 mJ/cm^2 of UV_{254} irradiation, whereas only 32% of Oligomer B segments reacted. Meanwhile, RT-qPCR results also suggested that Oligomer A reacted faster than Oligomer B segments following exposure to UV_{254} (45% and 24%, respectively). Past research on reactions in nucleic acids suggests that pyrimidine bases are the most reactive with UVC [115]-[117]. We therefore expected Oligomer A to react faster than Oligomer B due to the fact that it contains 17 pyrimidine bases compared to 7 pyrimidine bases.

Figure 2.1 Reactions of two MS2 viral RNA oligomers with UV_{254} irradiation measured by RT-qPCR and quantitative MALDI-TOF-MS. Experiments were run in triplicate. Experimental conditions: $[\text{RNA segment}]_0 = 4\ \mu M$ in nuclease free water, pH 6.2.

Table 2.2 First-order rate constants of oligomer reactions with UV_{254} and second-order rate constants of oligomer reactions with $^1O_2$ measured with RT-qPCR and quantitative MALDI-MS. Errors reflect the 95% confident internal values of rate constants, based on a single linear regression of triplicate experimental data. Arrows indicate there are significant differences between rate constants ($p < 0.05$; multiple linear regression test).

RNA Segment	UV_{254} ($mJ^{-1}cm^2$)		$^1O_2$ ($M^{-1}s^{-1}$)	
	MALDI-MS	RT-qPCR	MALDI-MS	RT-qPCR
Oligomer A	$5.7 \times 10^{-3} \pm 2.5 \times 10^{-4}$ ⟷	$2.6 \times 10^{-3} \pm 2.0 \times 10^{-4}$	$1.1 \times 10^6 \pm 6.1 \times 10^4$	$1.1 \times 10^6 \pm 1.4 \times 10^5$
Oligomer B	$1.9 \times 10^{-3} \pm 1.4 \times 10^{-4}$ ⟷	$1.2 \times 10^{-3} \pm 3.4 \times 10^{-4}$	$5.9 \times 10^6 \pm 6.1 \times 10^5$	$6.5 \times 10^6 \pm 3.3 \times 10^5$

For each of the two oligomers, the first-order rate constants measured by MALDI-TOF-MS were significantly higher than the rate constants determined by RT-qPCR (Table 2.2; $p < 0.01$). Specifically, Oligomer A and Oligomer B rate constants measured with MALDI-TOF-MS were

2.2× and 1.6× higher than rate constants measured with RT-qPCR. This indicates that the MALDI-TOF-MS technique is more sensitive to different photochemical products than the RT-qPCR technique.

Previous research on nucleic acid photochemistry, primarily with DNA, has identified three major direct photochemical pathways [58]-[60]. The first and second pathways involve reactions between neighboring pyrimidines that lead to the formation of cyclobutane pyrimidine dimers (CPD) [61], [62] and pyrimidine-pyrimidone 6-4 photoproducts (termed 6-4 products) [63], [64]. A third pathway forms pyrimidine photohydrates when the reactions take place in aqueous solutions [65]. Reactions that form pyrimidine photohydrate products result in a mass change of +18.015 Da ($=H_2O$), whereas the dimer products do not cause a mass change (Figure A-5). In our experiments, more damage was detected using MALDI-TOF-MS compared to RT-qPCR, despite the fact that the MALDI-TOF-MS technique was not sensitive to the pyrimidine dimer products. This indicates that certain products were not efficiently detected with the RT enzymes.

Pyrimidine hydrates were the major products detected in the UV-treated samples based on the product peaks in the MALDI-TOF-MS and high-resolution ESI-Orbitrap-MS spectra (Figure 2.2). Products of Oligomer A included a single pyrimidine photohydrate (mass difference of +18.02 Da) and a double pyrimidine photohydrate (mass difference of +36.03 Da; Figure A-6). The concentration of the single pyrimidine photohydrate product, monitored as the peak height of the product relative to the internal standard, reached a maximum at a UV_{254} dose of 81.6 mJ/cm^2 and then decreased until the final dose of 204 mJ/cm^2 (Figure 2.2). A single pyrimidine photohydrate product of Oligomer B was also detected, but its intensity relative to the internal

standard was lower than the corresponding Oligo A photohydrate product (Figure 2.2). A double pyrimidine photohydrate product of Oligomer B was not detected.
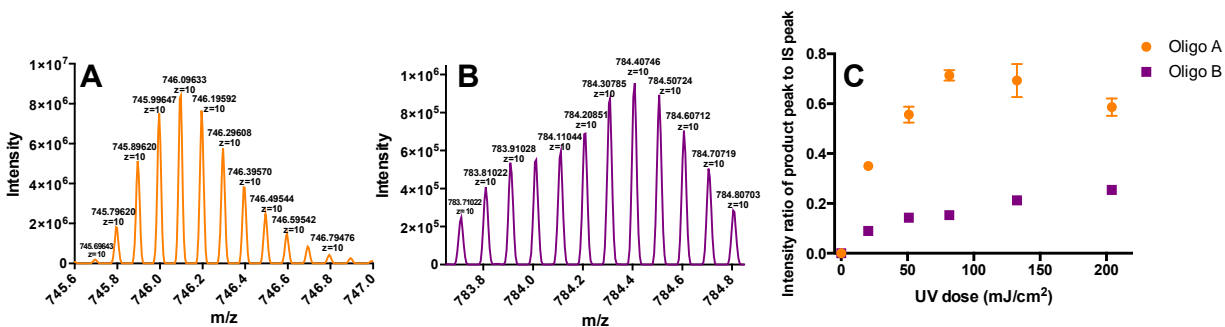
Figure 2.2 Pyrimidine photohydrates resulting from reactions of oligomers with UV_{254}. A) High-resolution mass spectrum of Oligomer A pyrimidine photohydrate product with -10 charge. B) High-resolution mass spectrum of Oligomer B pyrimidine photohydrate product with -10 charge. C) Ratio of pyrimidine photohydrates peak intensities to internal standard peak intensities (26-mer internal standards with constant concentration of 2 µM), measured with MALDI-TOF-MS. Experimental error bars represent standard error (n = 3 experiments); some error bars are smaller than the symbols.

Our results agree with an early report on RNA photochemistry that suggested hydrated residues are the major photoproducts after large doses of UVC irradiation [118]. More recent studies tend to assume that pyrimidine dimers in RNA are the major photoproduct [119], [120], likely because that is true for DNA [121]. The discrepancy between RNA and DNA products may be due to the fact that the rate-limiting step of dimerization is the conformational change that creates favorable base alignment at the time of excitation, and this may be more prevalent with DNA [122].

The RT enzyme was inhibited or halted by certain RNA products, which may include pyrimidine dimers, pyrimidine hydrates, or some other products that have not been identified. Pyrimidine dimers are bulkier modifications than the hydrates (Figure A-5) and thus may be more likely to impact the reverse transcriptase. Although the impact of pyrimidine dimers on RT has not been reported, DNA polymerase enzymes can be stopped by certain DNA modifications, depending on the type of DNA modification [123] and on the specific polymerase. Taq polymerases, for example, do not read over pyrimidine dimer lesions, whereas A- and B- family polymerases do replicate sequences with pyrimidine dimers [124].

The decrease of RT-qPCR response through water treatment processes and environmental processes is often assumed to correlate with the loss of virus infectivity [79], [125]. There are issues with making this assumption, including that the inactivation pathway might not target the genome [20], [126], the RT-qPCR measures only a fraction of the viral genome [13], [56], and that the RT enzyme might not detect the same type of damage that inactivates the viral RNA genome. Whereas publications have addressed the first two points, the specific RNA chemistry that inactivates the virus and how that compares to RT-qPCR remains largely unexplored.

Within the host cell, the genome of (+)ssRNA viruses (e.g., MS2, poliovirus, norovirus) must be sufficiently intact to serve as messenger RNA for the host cell ribosomes to make new virus proteins and to serve as a template for RNA dependent RNA polymerases to make new RNA genomes. With RT-qPCR, on the other hand, the RNA must be sufficiently intact for reverse transcriptase to make a complimentary DNA strand that is then amplified by PCR. Previously, a one-hit genome inactivation model was suggested for MS2 treatment with UV_{254} when RNA

damage was monitored by RT-qPCR [56]. In other words, the RNA modifications detected by RT-qPCR were sufficient to explain the extent of MS2 inactivation. In our experiments, much more RNA damage was detected by mass spectrometry than by RT-qPCR (Figure 2.1). Assuming the one-hit model with RT-qPCR detection is accurate for MS2 and other (+)ssRNA viruses, our data suggests a large fraction of UV_{254}-induced RNA reaction products do not inactivate viruses.

2.3.2   *Direct photochemical reactions with simulated sunlight*

Neither Oligomer A or Oligomer B decreased significantly in concentration after 5 hours of simulated sunlight exposure, regardless of the method used to quantify the oligomer concentration (Figure 2.3). This dose of UVB solar irradiation (5100 J/m^2 UVB and 1.2 x 10^5 J/m^2 UVA) is equivalent to approximately 1.5 hours of noontime irradiation in Ann Arbor, Michigan during the summer (Figure A-1). Previous research suggests that direct photolysis plays a role in virus inactivation in sunlit waters, with UVB wavelengths causing most of the photoinactivation [74], [127], [128]; we therefore anticipated reactions in the RNA oligomers.
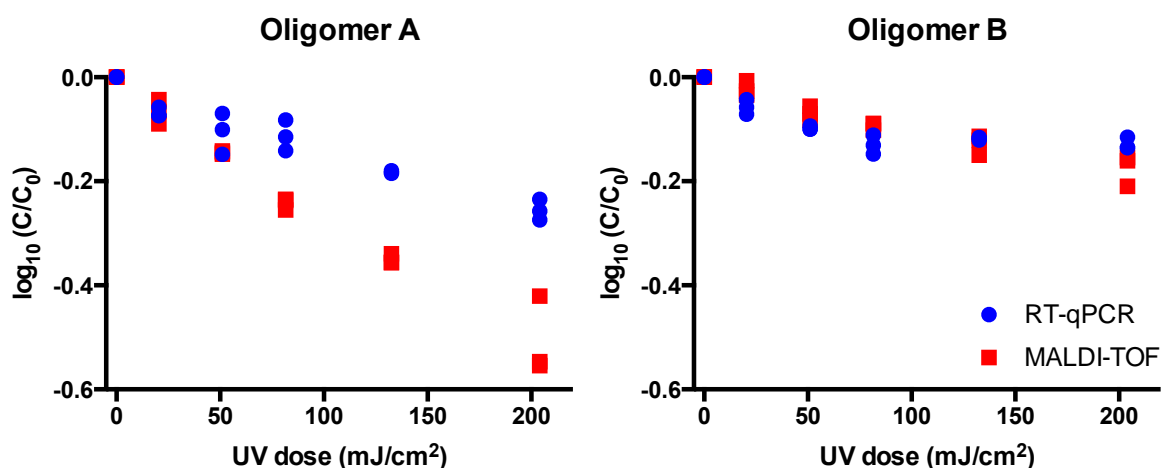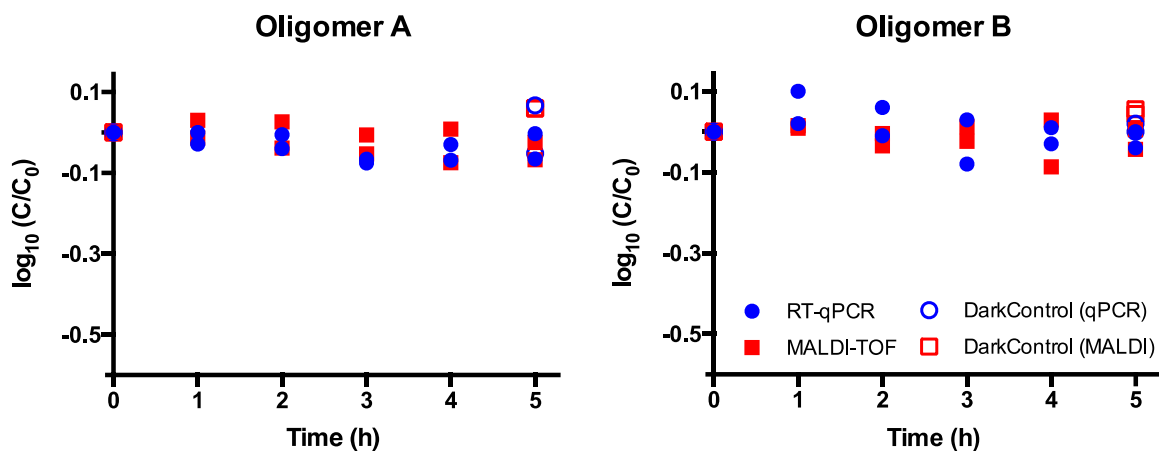
Figure 2.3 Reaction of two MS2 viral RNA oligomers with simulated solar irradiation measured by RT-qPCR and quantitative MALDI-TOF-MS. Control experiments were conducted in dark environment at the same time. Experiments were run in duplicate. Experimental conditions: [RNA segment]$_0$ = 1.3 µM in nuclease free water, pH 6.2.

The rate of MS2 inactivation was reportedly 0.22 h^{-1} in sensitizer-free water with UVA/UVB intensities similar to those used here [74]. The explanation for our lack of detectable reaction is most likely due to the short RNA segments, which are only 0.7% of the length of the MS2 genome. Although the data on RNA reactions due to solar radiation is scarce, the rate constants for pyrimidine dimer formation in dsDNA from UVA or UVB radiation was reportedly 1.4×10^{-7} and 1.0×10^{-4} per kbp per J/m^2 respectively [129]. Rate constants for the formation of other DNA photoproducts with UVA and UVB were not readily available in the literature. We applied these reaction rate constants for DNA pyrimidine dimer formation to the full MS2 RNA genome and our 24-mer oligomers. For the MS2 genome, the predicted pyrimidine formation rates were approximately $2 - 5\times$ faster than the MS2 direct photoinactivation rates reported by Silverman et al [74]. There are several potential explanations for this discrepancy, including that reactions may be slower in RNA than in DNA, that incorporation in a virus particle may influence the

RNA reaction kinetics, that there were differences in the UVA/UVB spectra emitted by the lamps, and that other products are responsible for inactivating the MS2 genome. Regardless of the reason for the discrepancy, the DNA pyrimidine formation rate constants did an adequate job of predicting MS2 inactivation with sunlight. When these same rate constants were applied to our 24-mer oligomers, calculations predicted a ~3% decrease in oligomer concentration due to pyrimidine dimer formation after 5 hours of solar simulator irradiation. This is in agreement with our lack of observed oligomer decay with RT-qPCR and mass spectrometry over the experiment timeframe. Future experiments should expose RNA oligomers in our size range to much higher solar UV doses (e.g., >50,000 J/m^2 of solar UVB) in order to readily observe reactions in the oligomers.

2.3.3   Indirect photochemical reactions with simulated sunlight

When irradiated in the presence of the Rose Bengal sensitizer, Oligomers A and B decreased in concentration according to first order kinetics and Oligomer B decreased more rapidly than Oligomer A (Figure 2.4). This trend in reactivity with $^1O_2$ is opposite than what was observed in the direct photochemical reactions and is most likely due to the relative number of guanine bases in the oligomers (10 in Oligomer B and 1 in Oligomer A). Whereas uracil and cytosine are the most sensitive bases to direct photo-oxidation, guanine bases are the most reactive with $^1O_2$ and other oxidants [130].
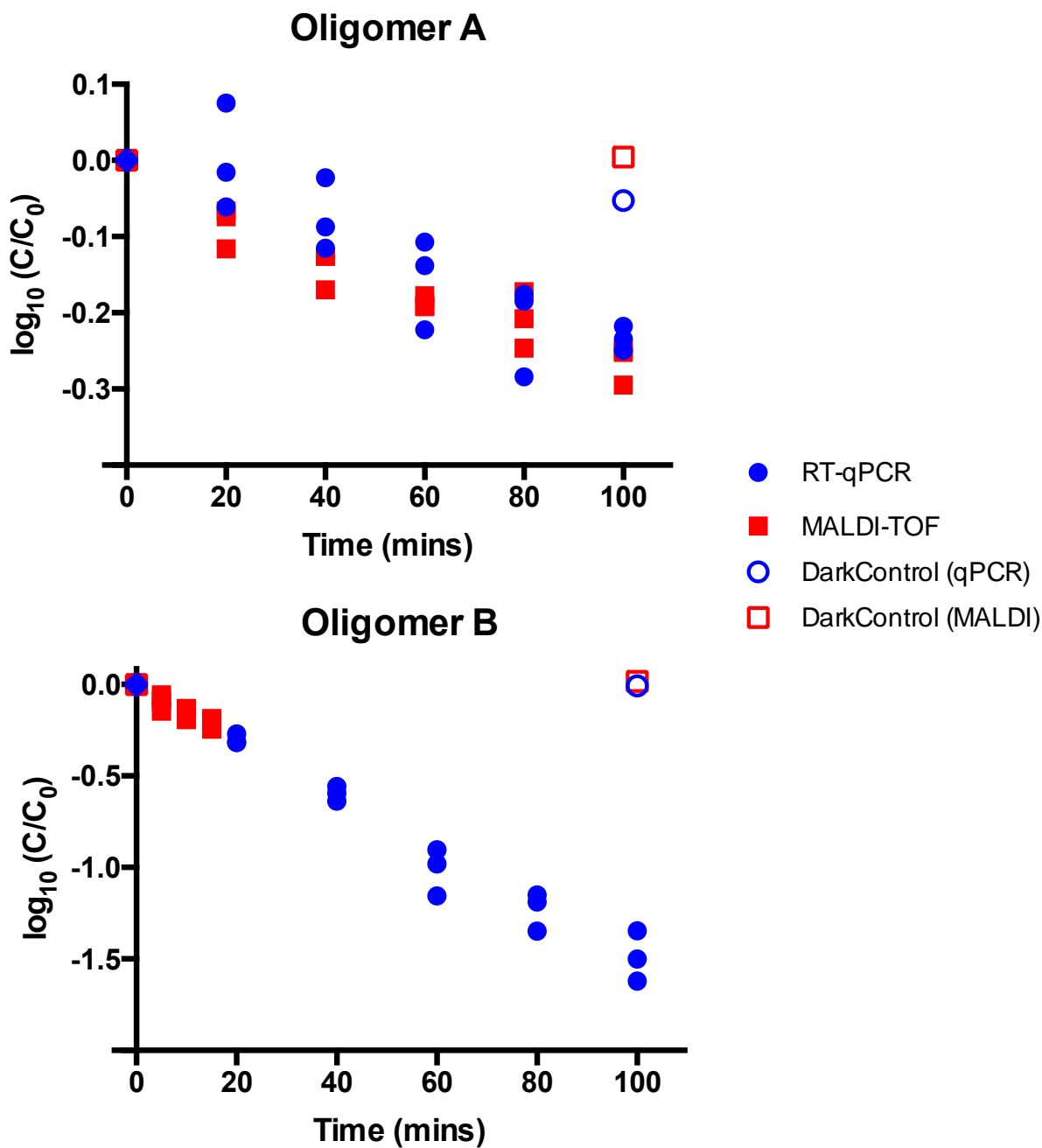
Figure 2.4 Reaction of two MS2 viral RNA oligomers with $^1O_2$ measured by RT-qPCR and quantitative MALDI-TOF-MS. Control experiments were conducted in dark environment at the same time. Experiments were run in triplicate. Experimental conditions: [RNA segment]$_0$ = 1.0 μM in 1.5 mg/L Rose Bengal solution, pH 6.6.

There was no statistical difference in reaction kinetics measured by quantitative MALDI-TOF-MS and RT-qPCR (Figure 4.4, Table 2.2), suggesting that the same $^1O_2$-induced RNA damage is detected by both techniques. It should be noted that reactions between the oligomers and $^1O_2$ resulted in products that interfered with the MALDI oligomer peaks. Consequently, we limited the oligomer measurements by MALDI-TOF-MS to the initial 50% of the Oligomer A and Oliogmer B reactions (Figure 2.4). This product interference was not observed with RT-qPCR measurements, so the oligomer reactions were monitored by RT-qPCR over the entire experimental timeframe (i.e., 100 minutes). Previous research demonstrated that oxidative damage in RNA inhibited the synthesis of cDNA by RT, although the products were not identified [131]. Here, following thirty minutes of $^1O_2$ exposure, ESI-Orbitrap-MS detected a major product for Oligomer A and two major products for Oligomer B (Figure 2.5). The Oligomer A product had a mass of 7469.579 Da; this product, which is 16.05 Da heavier than the reactant, likely involves the formation of an 8-hydroxyguanosine (8-OHG) adduct, which is a common marker for RNA oxidation. Products of Oligomer B included a species with mass change of +6.00 Da (Product B1) and a species with a mass change of +13.00 Da (Product B2; Figure 2.5). The masses of Product B1 and Product B2 are not indicative of common RNA adducts reported in the literature, such as 8-hydroxyadenosine, 5-hydroxycytidine, and 5-hydroxyuridine. The products were not resolved with chromatography, thus the fragmentation data was inconclusive.
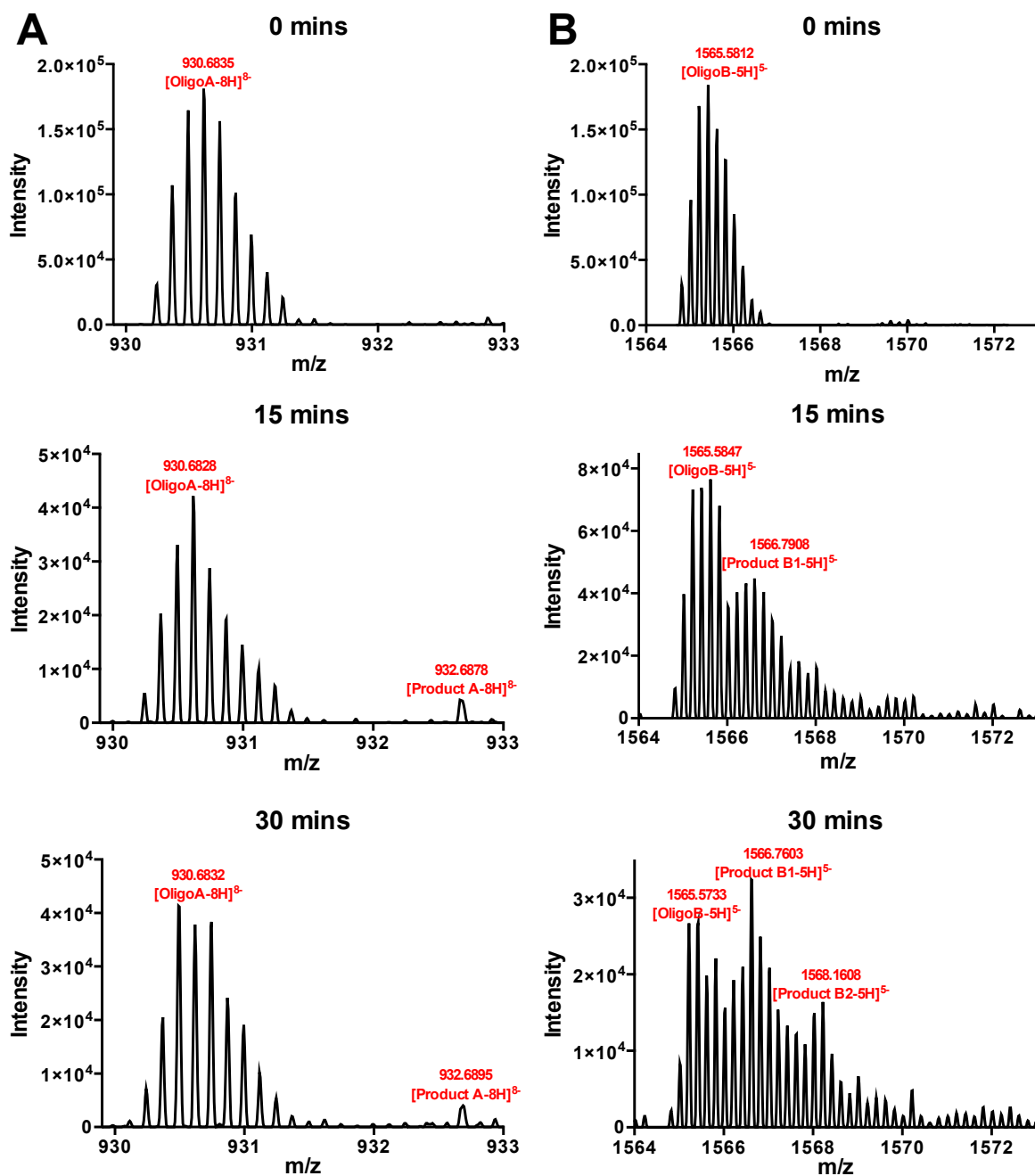
Figure 2.5 High-resolution mass spectra of two MS2 viral RNA oligomers treated with $^1O_2$ for 0, 15 and 30 minutes, obtained by ESI-Orbitrap MS under full-scan negative-ion mode. (A) Oligomer A and reaction products. (B) Oligomer B and reaction products.

Reported reaction rate constants for $^1O_2$ with RNA monomer bases offer an opportunity to relate our results with established chemical kinetics [130], [132]. By summing up the reported rate constants of the individual bases in our oligomers, we predicted second order rate constants of 7.8 x 10^6 $M^{-1}s^{-1}$ for Oligomer A and 1.3 x 10^7 $M^{-1}s^{-1}$ for Oligomer B (Table A-2). The predicted rate constants are 7× and 2× higher than the measured rate constants, respectively. This may be due to inaccuracies in the reported $^1O_2$ rate constants (see discussion in Appendix A) or due to the impact of primary structure on base reactivity. The predicted rates do agree with our finding that $^1O_2$ is more reactive with Oligomer B than with Oligomer A.

The impact that RNA oxidation products have on viral RNA-dependent RNA polymerases has not been studied, but the major DNA oxidation product 8-oxoG leads to mutations during transcription by DNA-dependent RNA polymerases [133], [134]. If RNA-dependent RNA polymerases undergo the same error, oxidation products in the genome may cause mutations that lead to non-infective viruses. Likewise, oxidized mRNAs can cause ribosome stalling and thus result in defective proteins synthesis [134]-[137]; in viral RNA, this may lead to incomplete or flawed viral capsids that are unable to recognize and interact with host cells.

2.4 Environmental implications

We studied the photochemical reactivity of purified MS2 RNA oligomers to understand the influence of genome sequence on RNA reactivity during water disinfection processes. Our results demonstrate that different regions of viral RNA genomes have distinct photoreactivities and regions that are most susceptible to direct photolysis may be least susceptible to indirect photolysis. Furthermore, not all of the photochemical reactions that take place in RNA were

readily detectable by RT-qPCR or MS, which has direct implications for analytical techniques used to define reaction kinetics. Because the detection of RNA modifications that cause virus inactivation are of most interest, future research efforts should seek out the RNA products that inhibit RNA-dependent RNA polymerases and ribosomes.

RNA bases incorporated in a virus particle likely react differently than RNA bases in an oligomer. We expect that the direct photolysis reaction rate constants observed in our 24-mers with UV_{254} would vary slightly when they are incorporated in the full virus, with additional products forming due to interactions between the RNA and capsid proteins. With indirect photolysis involving $^1O_2$, we expect that reaction rate constants would be significantly reduced when the oligomers are incorporated into the virus particle due to the fact that the protein capsid and RNA genome reduce the accessibility of $^1O_2$ to the RNA oligomers. RNA-protein interactions in virus particles likely cause additional RNA oxidation products. The exact impact that RNA higher-level order has on RNA base photochemistry reactivity remains to be investigated. Filling these remaining fundamental knowledge gaps on RNA photochemistry and the biological significance of photochemical products will not only be important for understanding the inactivation of waterborne viruses, but across all domains of life in natural and engineered waters exposed to photochemical stresses.

Chapter 3   Nucleic Acid Photolysis by UV_{254} and the Impact of Virus Encapsidation

3.1   Introduction

Nucleic acids are ubiquitous biopolymers that carry the code for all domains of life, yet several types of nucleic acids are undesirable in the aquatic environment due to their potential impacts on human and ecological health. Disinfection processes often target nucleic acids of problematic microorganisms, but extracellular nucleic acids also pose a potential risk. Antimicrobial resistance genes (ARGs) released from municipal wastewaters and animal farming activities, for example, can transfer resistance to other microorganisms [138]. Double-stranded RNA (dsRNA) pesticides in genetically modified crops have the potential to be released into surface waters [139]. Furthermore, many infectious environmental viruses consist of nucleic acids protected by a simple protein coat.

The nitrogenous bases in DNA and RNA molecules strongly absorb UV radiation, leading to a number of photochemical reactions. This high photoreactivity of nucleic acids is the main reason why UVC is commonly employed for disinfection in water, air, or on surfaces. The effectiveness of UV at inactivating microorganisms, along with the low levels of disinfection byproducts that form relative to chemical disinfectants, has led to a sustained growth of the UV disinfection industry. By 2019, the UV disinfection market is expected to reach nearly \$1 billion, or 1/3 of the total disinfection market [140]. Due to the widespread application of UV disinfection, the

reaction kinetics that drive the inactivation of microorganisms and nucleic acids should be well-defined.

The pyrimidine bases in nucleic acids (thymine (T), cytosine (C), and uracil (U)) are more photoreactive with UVC than purine bases (adenine (A), guanine (G)), and the reactions that take place between neighboring thymine bases have been the most extensively studied to-date. The TT dimer products from neighboring pyrimidine bases include the cyclobutane pyrimidine dimer (CPD), pyrimidine pyrimidone photoadducts (i.e., 6−4 products), and their Dewar valence isomers [141]. Of these, the CPD products have the highest quantum yields [142], [143]. In addition to TT dimers, TC, CT, CC, and UU dimer products have also been characterized [142], [143]. Hydration, protein-nucleic acid linkages, covalent crosslinks between complimentary strands, and backbone breaks also take place in nucleic acids exposed to UVC [121]. Pyrimidine photohydrate reactions are the most prevalent of these, and form readily on uracil and cytosine bases, but not on thymine bases [144]. Consequently, hydration reactions are more important in RNA than in DNA.

The physical orientation of bases and the structures that surround them at the time of irradiation impact the base photoreactivity. Dimer formation, for example, requires neighboring pyrimidine bases to have well-aligned double bonds and the correct intrabond separation at the time of UV exposure [104], [122]. Several studies have characterized the role that the flanking bases of neighboring pyrimidines have on dimer quantum yields [105], [145], [146], which directly influence photoreactivity. Purine neighboring bases, in general, and guanine bases at the 5' end, in particular, reduce dimerization quantum yields [145]. Photohydrate formation is not as

impacted by the chemistry of the neighboring bases, but the reactions are impacted by access to water molecules [147]. The presence of bases in either a single-strand or double-strand can also affect quantum yields; in general, the increased order of double-stranded nucleic acids decreases pyrimidine quantum yields [106], [122]. An early study reported that viral ssRNA in solution is more susceptible to UVC inactivation than the encapsidated ssRNA genome [107], but to our knowledge, the work has not been extended to other viruses or genome types.

Predicting the kinetics of nucleic acid UVC photolysis is complicated by the fact that many quantum yield values available in the literature were collected with DNA oligomers with repeated base sequences or under varied experimental conditions (e.g., UV wavelength, pH, ionic strength, etc.). Furthermore, RNA photochemistry is comparatively much less represented in the literature than DNA photochemistry, making it difficult to draw conclusions about the overall relative reactivity of single stranded and double stranded RNA and DNA molecules. RNA photochemistry is of particular interest for disinfection purposes because viruses can contain genomes with ssRNA and dsRNA, in addition to ssDNA and dsDNA. In viruses, the dsDNA viruses are typically considered more resistant to UVC radiation than viruses with other genomes types [148]. Interestingly, this is not due to relatively lower photoreactivity of dsDNA, but due to the ability of host cells to repair dsDNA [67].

To address the role that structure plays in nucleic acid photochemistry, we investigated the reactions that take place in single-stranded and double-stranded DNA and RNA viral genomes with UV_{254}. As model systems, we compared photolysis rates of four viral genomes within and outside of virus particles to assess the impact of virus particles incorporation on nucleic acid

reactivity. We employed quantitative polymerase chain reaction (qPCR) techniques to target specific regions of the genomes, as these methods are commonly used for detecting nucleic acids in water and tracking microorganism fate through water treatment processes. Finally, we compared our measured reaction rate constants to those predicted with quantum yield values in the literature.

3.2 Experimental methods

3.2.1 Virus preparation

Four model viruses were selected to represent four types of nucleic acid genomes, namely MS2 (ss RNA), φ6 (ds RNA), φX174 (ssDNA), and T3 (dsDNA). The characteristics of these viruses and their genomes are provided in Table 3.1.

Table 3.1 Four model viruses used in this study, including details of the genome regions analyzed.

Virus	Family/Genus*	Genome type	Genome size	Particle size (nm)	Enveloped /nonenveloped	Regions Analyzed	Region Location	Region size (bases or base pairs)
MS2	Leviviridae/ Levivirus	ssRNA (linear)	3.6 kb	~25	Nonenveloped	Region A Region B	944-1439 2693-3189	496 b 497 b
φ6	Cystoviridae/ Cystovirus	dsRNA (segmented)	2.9 kbp (S) 4.1 kbp (M) 6.4 kbp (L)	~85	Enveloped	Region A Region B	S1141-S1639 L1510-L1993	499 bp 484 bp
φX174	Microviridae/ Phix174microvirus	ssDNA (circular)	5.4 kb	~25	Nonenveloped	Region A Region B	571-1074 1717-2209	504 b 493 b
T3	Podoviridae/ T7virus	dsDNA (linear)	38.2 kbp	~50 × 20 (tailed)	Nonenveloped	Region A Region B	1678-2186 11826-12324	509 bp 499 bp

*Family and genus were based on the International Committee on Taxonomy of Viruses (ICTV), https://talk.ictvonline.org/taxonomy/

Escherichia viruses MS2 and T3, and their corresponding *E. coli* hosts were purchased from American Type Culture Collection (ATCC 15597 and 11303, respectively). MS2 and T3 stock were propagated, enriched, and enumerated based on previously published methods [83]. Enriched virus stock solutions were purified using a Fast Protein Liquid Chromatography system (Econo, Bio-Rad) equipped with a HiPrep Sephacryl S-400 HR column (GE). The purified stocks were filter sterilized with 0.22 µm polyethersulfone (PES) membrane filters (Millipore). The final MS2 and T3 virus stocks (~10^{11} PFU/mL) were stored in phosphate buffered saline (PBS; 5 mM NaH_2PO_4, 10mM NaCl, pH 7.5) at 4 °C.

Pseudomonas virus $\varphi6$ and its host *Pseudomonas syringae* pv. phaseolicola were kindly provided by Dr. Linsey Marr at Virginia Tech. $\varphi6$ was added to *Pseudomonas syringae* grown to OD_{640} of 0.1 in Luria-Bertani (LB) medium (5 g L^{-1} NaCl) at 26 °C with a multiplicity of infection (MOI) of 2, and the virus and host mixture was incubated for 7 to 9 hours. Due to its lipid envelope, $\varphi6$ was concentrated and purified differently than the other three bacteriophages. Cell lysates were filtered through 0.22 µm PES membranes, and were concentrated with a lab-scale tangential flow filtration system (Millipore) with a 30 kDa cellulous filter. The $\varphi6$ concentrate was purified by centrifuging at $65,700 \times g$, 4 °C in a 10-40% (w/v) step sucrose gradient for 1.5 hours, then by centrifuging at $65,700 \times g$, 4 °C in a 40-60% (w/v) linear sucrose gradient for 15 hours overnight. The $\varphi6$ virus band was collected with a needle and was transferred to PBS with a 100 kDa centrifugal ultrafilter (Millipore). The final $\varphi6$ virus stocks (~10^{12} PFU/mL) were filter sterilized through 0.22 µm PES membranes, and stored in PBS at -80 °C.

Escherichia virus *φ*X174 and its corresponding bacterial host *E. coli* ATCC 13706 were kindly provided by Dr. Charles Gerba at the University of Arizona. *φ*X174 virus was propagated by the agar overlay technique. Specifically, soft tryptic soy agar (TSA; 0.7% w/v agar) was mixed with *φ*X174 virus and host bacteria, was overlaid on hard TSA (1.5% w/v agar), and was incubated at 37 °C overnight. The soft agar layer was collected and diluted in PBS to release *φ*X174 from the agar. The agar was removed by centrifuging at 3,000 × g for 10 minutes. The supernatant containing *φ*X174 was treated with a chloroform extraction, filtered through a 0.22 µm PES membrane, and stored in PBS at 4 °C.

3.2.2   UV$_{254}$ photolysis

UV photolysis of viral genomes were studied when the genomes were within the virus capsids (i.e., encapsidated) and when they were extracted from the virus capsids (i.e., naked nucleic acids in ultrapure nuclease-free water and in nuclease-free PBS). The prepared PBS was heated to 90 °C for 30 minutes to eliminate the activity of nucleases. For each UV treatment, the nucleic acids were extracted from the virus stocks immediately before the UV$_{254}$ treatment with Maxwell 16 Viral Total Nucleic Acid Purification Kits (Promega) according to the manufacturer's instructions. The concentrations of the extracted virus nucleic acids were determined with a Qubit 2.0 (Life Technologies) in ng/mL and converted to genome copies (gc)/µL using the genome's molecular mass and Avogadro's constant, and then diluted to a final concentration of ~10^6 gc/µL with ultrapure nuclease free water (ThermoFisher) or nuclease free PBS. The encapsidated nucleic acids were prepared by directly diluting the virus stocks to a similar genome concentration ~10^6 gc/µL with PBS. At this concentration, the absorbance of our

experimental solutions at 254 nm was below 0.01; it was therefore not necessary to correct the UV$_{254}$ radiation doses for shielding.

Samples of the virus in PBS and the extracted nucleic acids in either ultrapure water or PBS (50 µL) were added to the wells of 96-well plate with flat bottoms (Costar). The plate was placed approximately 25 cm below four 15 W germicidal UV lamps (model G15T8, Philips) inside a collimated beam unit. The UV irradiance at 254 nm (0.17 mW/cm^2) was determined by chemical actinometry measurements [113]. The virus and genome solutions were irradiated up to doses of 408 mJ/cm^2 at room temperature. Aliquots of the experimental solutions were collected from the samples periodically and stored at 4 °C in the dark. Dark control samples were stored at room temperature in the dark for the duration of the longest UV exposure to capture background nucleic acid decay. The experiments were repeated at least four times for every genome type. Following UV treatment, the encapsidated viral nucleic acids were extracted from the virus samples with Maxwell 16 Viral Total Nucleic Acid Purification Kits. The UV-treated samples and dark controls were analyzed by qPCR or RT-qPCR immediately after the completion of the UV experiments.

3.2.3 qPCR assay for UV-treated viral genomes

Two sets of PCR primers were designed to target two regions of approximately 500 bases or base pairs on each viral genome (Table 3.1, Table B-1). The entire genome of ssRNA of MS2 and dsRNA of φ6 were directly extracted from the purified virus stocks, and were used as standards; gBlock standards containing two target regions (Integrated DNA Technologies) were purchased for φX174 ssDNA and T3 dsDNA. Both experimental samples and standards were quantified in

parallel using qPCR or RT-qPCR assays in a RealPlex2 Mastercycler system (Eppendorf). The reaction rate constants of the target regions were calculated based on a first-order reaction model:

$$\ln\left(\frac{C}{C_0}\right) = -k_{exp} \cdot D_{UV_{254}}$$

Where C_0 is the initial concentration of viral genome segment; C is the concentration of the viral genome segment after UV$_{254}$ treatment; k_{exp} is the first-order rate constant; $D_{UV_{254}}$ is the UV$_{254}$ dose (mJ/cm^2).

3.2.3.1   RT-qPCR assay for MS2 ssRNA

The 20 µL one-step RT-qPCR reactions consisted of 10 µL of 2× GoTaq qPCR Master Mix (Promega), 0.4 µL of 50× GoScript RT Mix, 0.6 µL of 10 µM forward primer, 0.6 µL of 10 µM reverse primer, 6.4 µL of nuclease-free water, and 2 µL of RNA sample. The following thermocycling conditions were used: 15 min at 40 °C, 10 min at 95 °C, 45 cycles of 95 °C for 15 s, 55 °C for 30 s, and 72 °C for 45 s, followed by a melting curve analysis from 68 to 95 °C for 5 minutes.

3.2.3.2   RT-qPCR assays for φ6 dsRNA

For φ6 genome samples, dsRNA samples were mixed with 10 µM forward primer and 10 µM reverse primer at a volume ratio of 10:1.5:1.5. The sample-primer mixture was heated at 99 °C for 5 minutes, and immediately chilled on ice before the RT-qPCR assays. The 20 µL RT-qPCR reactions consisted of 10 µL of 2× GoTaq qPCR Master Mix, 0.4 µL of 50× GoScript RT Mix, 5.2 µL of the pre-treated sample-primer mixture, 4 µL of 5 M Betaine (Sigma-Aldrich), and 0.4 µL of nuclease-free water. The following thermocycling conditions were used: 15 min at 40 °C,

10 min at 95 °C, 40 cycles of 95 °C for 15 s, 59 °C for 30 s, and 72 °C for 45 s, followed by a melting curve analysis from 60 to 95 °C for 10 minutes.

3.2.3.3   qPCR assays for φX174 ssDNA and T3 dsDNA

For both φX174 ssDNA and T3 dsDNA, each qPCR reaction was run in 10 µL total volume consisting of 5 µL of EvaGreen qPCR Master Mix (Biotium), 0.25 µL of 25 mg/mL bovine serum albumin (BSA) solution (Sigma-Aldrich), 0.4 µL of 10 µM forward primer, 0.4 µL of 10 µM reverse primer, 2.95 µL of nuclease-free water, and 1 µL of DNA samples. The following thermocycling conditions were used for φX174 ssDNA: 5 min at 95 °C, 40 cycles of 95 °C for 20 s, 55 °C for 20 s, and 72 °C for 20 s, followed by a melting curve analysis from 68 to 95 °C for 5 minutes. The following thermocycling conditions were used for T3 dsDNA: 2 min at 95 °C, 35 cycles at 95 °C for 5 s, 60 °C for 5 s, and 72 °C for 25 s, followed by a melting curve analysis from 55 to 95 °C for 5 minutes.

3.2.4   Statistical analysis

Linear regressions and statistical analyses were conducted using Prism 7 (GraphPad Software, Inc. La Jolla, CA) on pooled data from replicate experiments of each tested region (n ≥ 4). Analysis of Covariance (ANCOVA) tests were conducted to determine whether there were significant differences between the rate constants of two groups (i.e. naked genome vs encapsidated genome, ssDNA vs dsDNA). When p was less than 0.05, we concluded that the rate constants of two groups were significantly different.

3.3 Results and discussion

3.3.1 Photolysis of naked nucleic acids in ultrapure water

The 500 base (b) regions of the naked ssRNA and ssDNA and the 500 base pair (bp) regions of the naked dsRNA and dsDNA in ultrapure water generally reacted according to first order kinetics, although tailing was observed in region B of MS2 ssRNA and regions A and B of T3 dsDNA (Figure B-1). Tailing has been repeatedly observed when nucleic acids are exposed to UV_{254} [119], [149]-[151] and a number of explanations have been suggested, including the presence of aggregated particles (for viruses) and the presence of UV-resistant nucleic acid sequences. We propose that the commonly observed tailing effect is due to pyrimidine dimer reactions reaching photostationary state, as described in early UV photolysis literature [152], [153]. The reason tailing was observed in region B of MS2 after the same UV_{254} dose as region A may be due to the greater number of neighboring uracil bases in the sequence (32 in region B, 19 in region A, Table B-2). Further research will be necessary to characterize the extent of dimer reversion in different nucleic acids with varied sequences and structures.

For each region in ultrapure water, we pooled data from replicate experiments ($n \geq 7$) and conducted linear regressions on the data that exhibited first order kinetics (Figure 3.1; Table B-3). Control samples stored in the dark did not react over the timeframe of the experiments, suggesting that the background decay was negligible (Figures B-1). The first order rate constants of the two measured regions in naked dsRNA were not statistically different ($p = 0.15$), nor were the two regions of naked dsDNA ($p = 0.32$; Table B-4). The two regions analyzed in ssRNA had statistically different kinetics ($p = 0.001$), as did the two regions in ssDNA ($p < 0.0001$; Table B-

4). This was likely due to the different number of neighboring pyrimidine bases in the two regions of ssRNA and the two regions of ssDNA (Table B-2).
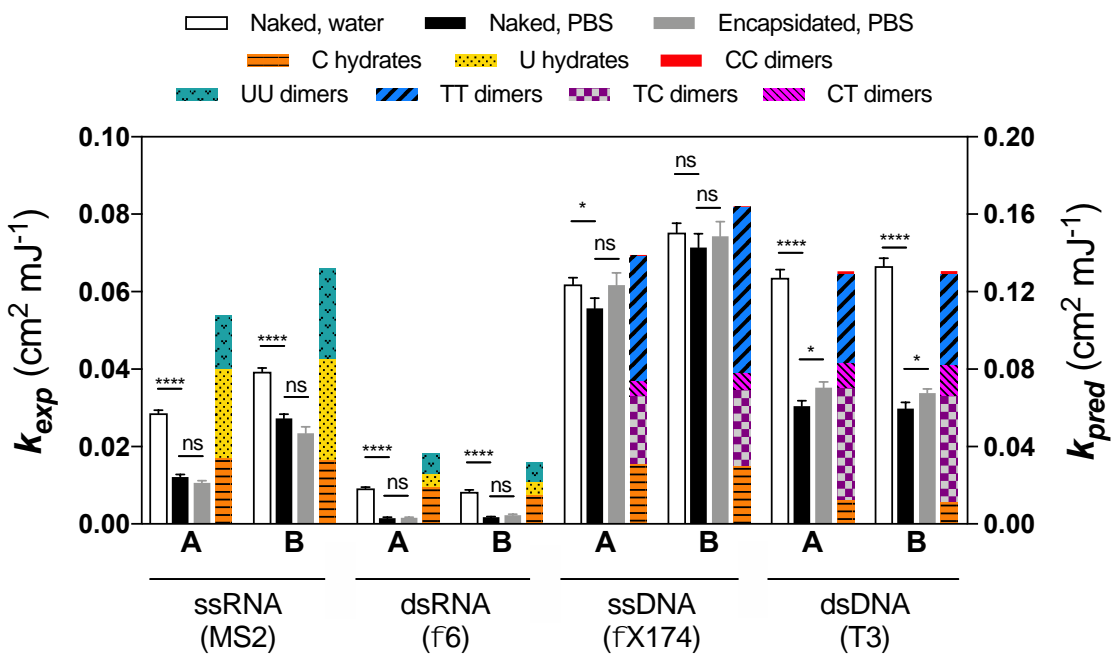
Figure 3.1 Measured UV$_{254}$ rate constants of virus genome regions A and B in naked forms (white and black bars) and in encapsidated forms (grey bars) and predicted rate constants of the same genome regions (bars with patterns). Error bars represent standard error for replicate experiments ($n \geq 4$). Asterisks indicate rate constants are significantly different (one asterisk for $0.01 < p < 0.05$, four asterisks for $p < 0.0001$) and ns indicates that rate constants are not significantly different ($p > 0.05$). The ANCOVA analysis p values are presented in Table B-4.

$\varphi 6$ and T3 are dsRNA and dsDNA viruses, respectively, and MS2 and φX174 are ssRNA and ssDNA viruses, respectively; thus, the analyzed 500 bp regions in $\varphi 6$ and T3 have twice as many bases as the 500 b regions of MS2 and φX174. It was therefore not possible to directly compare the measured rate constants of the single-stranded regions with the double-stranded regions. By

comparing the ssRNA regions with the ssDNA regions, and the dsRNA regions with the dsDNA regions, it was evident that the DNA regions reacted faster than the RNA regions. Specifically, the two ssDNA regions reacted ~2× faster than the two ssRNA regions, and the two dsDNA regions reacted ~8× faster than the two dsRNA regions. A study on the UV_{254} photolysis of short DNA and RNA hairpin structures with HPLC also concluded that DNA is more photoreactive than RNA [154].

Viral nucleic acids can act as sensitizers with UV_{254}, leading to other reactions in virus particles [52]. We therefore assessed the role that $^1O_2$ and $\cdot OH$ played in the UV_{254} photolysis of naked T3 dsDNA in ultrapure water (see Appendix B). The reaction kinetics of the naked dsDNA in D_2O were no different than it was in ultrapure water (Figure B-2, $p = 0.83$), and no difference in reaction kinetics was observed between dsDNA with methanol and dsDNA in ultrapure water (Figure B-2, $p = 0.95$). These results demonstrate that neither $^1O_2$ nor $\cdot OH$ was contributing significantly to the decay of the naked dsDNA. We therefore concluded that the observed nucleic acid reactions in ultrapure water were due to direct photolysis.

3.3.2   *Photolysis of naked nucleic acids in PBS*

For the naked ssRNA, dsRNA, and dsDNA regions, the photolysis rate constants in PBS were substantially lower than in ultrapure water (Figure 3.1, Table B-3). Specifically, the ssRNA rate constants were, on average, 1.7× higher in ultrapure water than PBS, the dsRNA rate constants were, on average, 5.3× higher in ultrapure water, and the dsDNA rate constants were, on average, 2.2× higher in ultrapure water. For ssDNA, only region A had faster kinetics in ultrapure water based on ANCOVA analysis, and the difference in this case was minor (1.1×, $p =$

0.04). The reason that the photoreactivities of MS2 ssRNA, ϕ6 dsRNA, and T3 dsDNA were much more impacted by solution chemistry than φX174 ssDNA is not clear, but may involve the circularity of the ϕX174 ssDNA genome. The MS2 and T3 genomes are linear, and the ϕ6 genome is linear and segmented.

Our PBS buffer consisted of 5 mM NaH_2PO_4 and 10 mM NaCl (pH 7.5), whereas our suspensions of nucleic acids in ultrapure water solutions were approximately pH 5.8. Pyrimidine dimer quantum yields are generally not impacted by pH [143], [147] and early work with cytosine and uracil hydrates suggest their quantum yields are relatively consistent above pH 5 [155]. It is therefore unlikely that our observed differences in ultrapure water and PBS were due to pH. In terms of ionic strength, Douki observed a 20% decrease of TT dimer quantum yields and a 300% increase in TC dimer quantum yields when 20 mM NaCl was added to calf thymus DNA in pure water [143]. In that study, the DNA dimer quantum yields were consistent when the NaCl concentrations increased above 20 mM. Pyrimidine photohydrate quantum yields are also impacted by ionic strength, as well as buffer type [155]. These observed effects of ionic strength and buffer type on quantum yield are likely related to nucleic acid structure. Hydrate formation, for example, requires water molecules to access bases; this occurs more readily when double helix RNA structures are denatured [155]. Dimer formation requires that neighboring pyrimidines are favorably aligned at the time of excitation, and this can be inhibited when structures are highly ordered [122]. Here, the nucleic acids in PBS likely had more ordered structures than the nucleic acids in ultrapure water, thus inhibiting dimer and hydrate formation.

3.3.3 Predicted photolysis rate constants

We next predicted the theoretical photolysis rate constants, k_{pred}, for the eight nucleic acid regions based on a base composition method. Specifically, we used the sequences in our ssRNA, dsRNA, ssDNA, and dsDNA regions and the RNA and DNA extinction coefficients and quantum yields in the literature (Table B-2), and summed the rate constants of the major potential reactive bases in the regions:

$$k_{pred,i} = \frac{2.3}{U} b \cdot \varepsilon_{254} \cdot \Phi$$

$$k_{pred} = \sum_i^n k_{pred,i} = \sum_i^n \left(\frac{2.3}{U} b \cdot \varepsilon_{254} \cdot \Phi \right)$$

Here, k_{pred} (cm^2 mJ^{-1}) is the predicted rate constant of the nucleic acid regions, $k_{pred,i}$ (cm^2 mJ^{-1}) is the predicted rate constant of the reactive nucleic acid monomer or doublets i, including C, U, UU, and CC for RNA, and C, TT, CT, TC, and CC for DNA, ε_{254} (M^{-1} cm^{-1}) is the extinction coefficient of the nucleic acid monomer or dimer at 254 nm in M^{-1} cm^{-1}, Φ (mol eins^{-1}) is the quantum yield of a particular reaction, U is a constant of the number of joules per einstein at 254 nm (4.7×10^5 J eins^{-1}), and b is the number of reactive nucleic acid monomers or dimers in the nucleic acid region [156]. For the dsRNA and dsDNA regions, the sequences of both strands were included in the k_{pred} calculation.

The resulting predicted rate constants of the eight regions exhibited trends similar to the experimental rate constants (k_{exp}) of the naked nucleic acid regions (Figure 3.1). For both the experimental and predicted rate constants, the two ssDNA regions had the fastest kinetics, on

average, followed by the dsDNA and ssRNA regions, and the dsRNA regions were the least reactive. The trends observed between the measured rate constants of the two regions in ssDNA (region B > region A) and the two regions in ssRNA (regions B > region A) were also predicted based on the different numbers of reactive monomers and dimers in their sequences (Table B-2).

For each region, the predicted rate constant was larger than the measured values in ultrapure water and in PBS. The predictions were closest for ssDNA, with the predicted rate constants within a factor of 2 of the measured rate constants in both ultrapure water and PBS. The predictions for dsRNA were the furthest from the measured values, with up to a 24-fold difference between the predicted rate constant and the measured rate constant. The differences were more pronounced when ssRNA, dsRNA, and dsDNA were in PBS than when in ultrapure water (Figure 3.1). The discrepancies between predicted rate constants and measured rate constants have several possible explanations. First, many of the quantum yield values available in the literature were measured on short oligomers with repeated bases (e.g. UUUUUUU), and these likely react differently than longer sequences with mixed bases. Quantum yield values available in the literature were measured under a range of temperatures, solution pH, UVC wavelengths, or ionic strengths that differed from our experimental conditions; these parameters can affect photolysis quantum yields [157], [158].

Quantum yields can also be impacted by the technique by which they are measured. In many of the early reports, quantum yields were measured using the nucleic acid base chromophore decay, and this can suffer from interference by the formed products [147]. The molecular methods used here may not detect all of the reactions that take place in the RNA and DNA. Updated quantum

yield measurements under a variety of experimental conditions and a better characterization of PCR method tolerance to nucleic acid photolysis products would help address some of the observed discrepancies.

We present each k_{pred} value with the contributing reactions ($k_{pred,i}$) identified by color (Figure 3.1; Table B-2); this highlights the relative importance of hydration and dimerization reactions in RNA versus DNA, as predicted with quantum yields in the literature. In both the ssRNA and dsRNA regions, most of k_{pred} (~70%) is due to hydration reactions, with the rest from dimerization reactions. In DNA regions, the opposite is true, with most of k_{pred} (~85%) resulting from dimerization reactions. Another interesting observation from the photolysis predictions is the relative contributions of TT dimers in the ssDNA and dsDNA reactions. TT dimers are commonly assumed to be the most prevalent UV photoproducts in DNA, but here, the sum of the predicted C hydrate contribution and TC dimer contribution is greater than the TT dimer contribution. We should note that C hydrates can revert back to cytosines under some conditions, and that was not included in our predictions [155]. The CT, TC, and CC quantum yields used in k_{pred} were based on a study in which DNA photoproducts were quantified following the exposure of calf thymus DNA to UV_{254} [142]. We used the relative yields of TC, CT, or CC dimer products to TT dimer products in that study, along with the well-established TT cyclobutane dimer quantum yield for UV_{254} to estimate TC, CT, and CC quantum yields (Table B-2). We were unable to locate quantum yield values for UC and CU reactions in RNA; the predicted RNA rate constants would have been even higher if those reactions had been included.

3.3.4   Single stranded versus double stranded photoreactivity

As mentioned above, the measured rate constants of the single stranded and double stranded nucleic acid regions were not directly comparable due to the regions containing different numbers of bases. We therefore normalized the rate constants by the number of bases in the analyzed regions (Figure 3.2) to observe the impact of double-strand structures on RNA and DNA reactivity. In ultrapure water, RNA bases reacted, on average, 7.7× faster in the single-stranded regions than in the double-stranded regions; in buffer, the difference in kinetics increased to 24×. For DNA in ultrapure water, the single-stranded DNA regions reacted, on average, 2.1× faster than the double-stranded genome, whereas in buffer, that difference increased to 4.3×. In the case of DNA, some of the observed differences were likely due to the higher proportion of adjacent TT bases in the two ssDNA regions (36 and 48 TT pairs in 500 bases; Table B-2) compared to the two dsDNA regions (46 and 47 TT pairs in 1000 bases; Table B-2). The ss and ds RNA sequences, however, had similar proportions of reactive bases, thus the lower photoreactivity of dsRNA compared to ssRNA was likely due to the impact of the double helix.
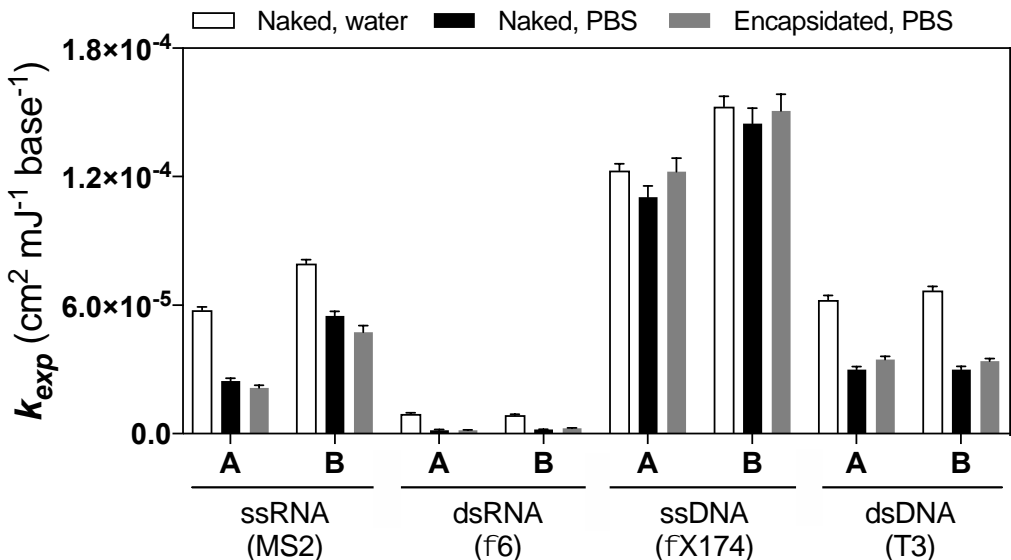
Figure 3.2 Experimental first order rate constants of target viral genome regions normalized by the number of bases in corresponding region. Error bars represent standard error.

Together, these results demonstrate that the double helix has a greater impact on RNA photoreactivity than on DNA photoreactivity, and that the impact of the double helix was enhanced in buffer solution compared to ultrapure water. An early study of RNA exposed to UV_{280} found that hydrates formed $10\times$ faster in polyU oligomers in ssRNA than in polyU:polyA in dsRNA, while dimers formed $5\times$ faster in ssRNA compared to dsRNA [106]. By comparison, in DNA, reported TT dimer quantum yields differ by less than $2\times$ in ssDNA and dsDNA [122], [159]. Our results underscore the high resistance of dsRNA to UV_{254} photolysis compared to other nucleic acids, particularly in buffered solutions. The resistance of dsRNA rotavirus to UVC inactivation has been noted previously [160].

3.3.5 Photolysis of encapsidated nucleic acids

To explore how the incorporation of nucleic acids in viral particles impacts the rate of direct photolysis by UV_{254}, we conducted experiments with the same nucleic acids analyzed above, but encapsidated in virus particles and suspended in PBS (Figure 3.1). We hypothesized that that genomes compressed inside a protein capsid would be less photoreactive, due to possible decreased availability of H_2O molecules for hydrate formation, the restriction of motions necessary for dimer formations, and the potential for energy transfer to virus proteins. In fact, for three of the four viruses tested, namely MS2 (ssRNA), $\phi 6$ (dsRNA), and $\varphi X174$ (ssDNA), encapsidation did not impact the reaction kinetics of the nucleic acids (Table B-4; $p > 0.05$). We observed slightly faster reaction kinetics (~1.2×) for both T3 dsDNA regions when encapsidated, although the ANCOVA analysis p values were barely below our 0.05 cutoff for statistical significance (Table B-4). These results of little or no effect from encapsidation contradict an early report on the UV photolysis of tobacco mosaic virus ssRNA; that research found that the ssRNA genome was 6x more sensitive to UV when outside of the virus capsid than when inside the capsid [107].

3.3.6 Literature review of nucleic acid photolysis kinetics

A number of previous studies have measured the UV_{254} photodegradation of viral nucleic acids and extracellular DNA with qPCR or RT-qPCR [20], [111], [151], [160]-[167]. It is normally difficult to compare these results because the regions they target have a range of sizes. We therefore normalized the literature rate constants by the number of bases in the analyzed regions and compared the normalized rate constants from different studies and from different genome types (Table B-5). The nucleic acid UV_{254} photolysis rate constants in the literature generally

agree with one another and with our data (Figure 3.3). The compiled data confirms that the ssDNA encapsidated genomes are the most reactive with UV_{254} and that the encapsidated dsRNA genomes are the least reactive with UV_{254}. The average rate constants per base (mean $\pm$ 95% C.I.) for encapsidated ssRNA, dsRNA, ssDNA, and dsDNA were $3.1 \times 10^{-5} \pm 1.0 \times 10^{-5}$, $4.3 \times 10^{-6} \pm 5.8 \times 10^{-6}$, $1.8 \times 10^{-4} \pm 1.9 \times 10^{-5}$, and $1.7 \times 10^{-5} \pm 8.3 \times 10^{-6}$ cm^2 mJ^{-1} base^{-1}, respectively. The average rate constants per base for naked dsDNA was $4.8 \times 10^{-5} \pm 2.2 \times 10^{-5}$ cm^2 mJ^{-1} base^{-1}. The scatter observed for each genome type is likely due to variations in the analyzed region sequences (e.g., number of TT sequences) and differences in experimental conditions between laboratories (e.g., buffer, temperature, etc.).
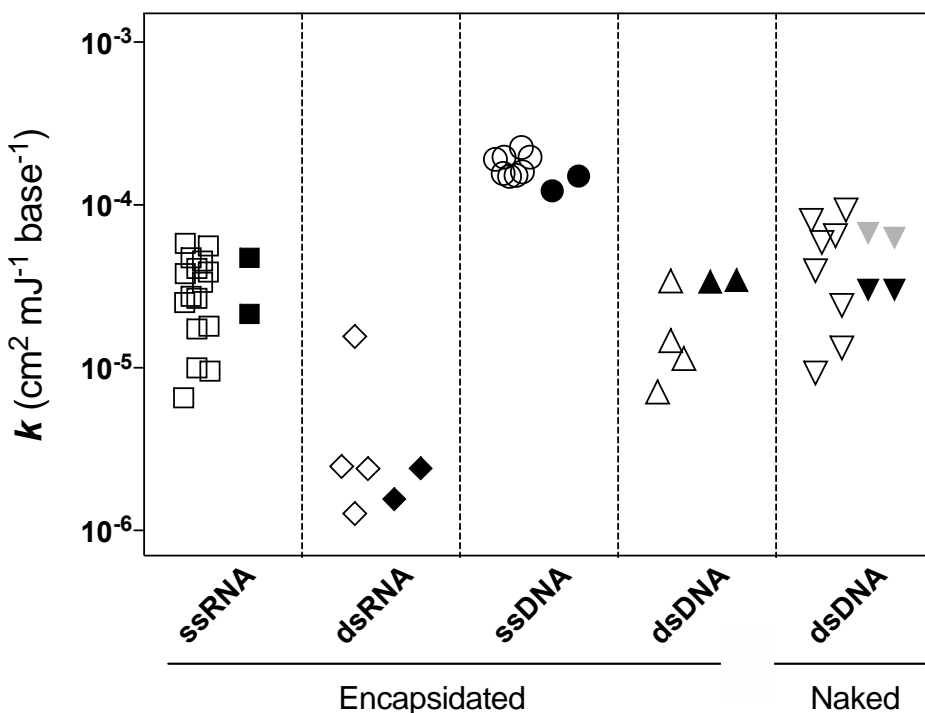
Figure 3.3 Comparison of the first order rate constants measured in this study on two regions of each genome with first order rate constants reported in the literature normalized by the number

of bases in the PCR amplicon. Black points represent data from this study conducted in PBS, gray points represent data from this study conducted in ultrapure water, and white points represent data from the literature.

3.4   Environmental implications

Our research demonstrates the relatively high resistance of dsRNA compared to the other genome types. The dsRNA rate constants measured here were ~80× lower than the ssDNA rate constants, which exhibited the highest rate constants on a per base basis. The dsRNA rate constants from this work will help with future efforts to disinfect dsRNA viruses and help predict the environmental fate of dsRNA plant incorporated protectants, which are increasingly applied to combat agricultural pests. Our results suggest that dsRNA viruses and dsRNA plant-incorporated protectants likely persist after other forms of nucleic acids have degraded from photochemical reactions.

Another important conclusion of this work is the large impact that higher order structure and solution chemistry plays in nucleic acid photochemistry, particularly for RNA. This complicates efforts to predict the UV_{254} inactivation rate constants of virus genomes using published nucleic acid quantum yields in combination with the genome size and sequence. The ssDNA of φX174 was the only genome unaffected by the solution chemistry. Future research will be needed to determine if this is the case for all ssDNA viruses or for all circular genomes.

Finally, it is worth discussing the implications of employing qPCR and RT-qPCR methods to quantify intact RNA and DNA, respectively. These two approaches employ different enzymes to detect damage. Namely, qPCR uses polymerase to copy intact DNA regions and RT-qPCR uses

reverse transcriptase to convert intact RNA regions to complimentary DNA. The relative tolerances of polymerase and reverse transcriptase to photolysis products is not currently known, but our earlier work demonstrated that the photolysis kinetics of short RNA oligomers were faster when measured with a mass spectrometry method than when measured with RT-qPCR [91]. We selected qPCR and RT-qPCR methods for this research, as opposed to HPLC or LC-MS methods, in order to obtain region-specific rate constants in the genomes; this information is lost when genomes are digested and individual bases are quantified by HPLC or LC-MS. Furthermore, the hydrate products that form with UV_{254} can undergo facile dehydration, a reaction that is acid-catalyzed [144]. Consequently, acid digestion steps and acidic mobile phases in LC separations will affect the measured UV_{254} reaction rates and this is avoided with qPCR and RT-qPCR. Future research should characterize the specific reactions measured by the polymerases used in qPCR and the reverse transcriptases used in RT-qPCR, as well as the photoproducts that impact the biological activity of RNA and DNA.

Chapter 4   Reactivity of Viral Nucleic Acids with Chlorine and the Impact of Virus Encapsidation

4.1   Introduction

Nucleic acids encode and store the genetic information for life and reproduction. Oxidation reactions that take place in nucleic acids can be detrimental to humans, as DNA lesions can lead to mutations that result in diseases such as cancer [168]-[170]. On the other side, these reactions can also be beneficial such as when pathogenic microorganisms are purposely treated with disinfecting oxidants such as chlorine and ozone [23], [95], [171]. From the perspective of water purification, environmental engineers often consider certain types of DNA and RNA as pollutants in aquatic environments, since they make up antibiotic resistance genes (ARGs) and the genomes of human pathogens such as viruses, and some new types of dsRNA pesticides [139]. Mechanistic understandings how nucleic acids react and lose their biological activity provides insight into how microorganisms lose their infectivity. It ultimately may allow researchers to predict the fate of various microorganisms and nucleic acids of interest in disinfecting treatments.

Chlorine is long known as an effective germicidal agent, and chlorine disinfection is widely employed for drinking water and wastewater treatment due to its low cost and high efficacy at inactivating pathogenic microorganism [172], [173]. Free chlorine is present primarily as a combination of hypochlorous acid (HOCl, pKa of 7.5) and its conjugate base, hypochlorite ion

(OCl⁻), under the conditions of typical water treatment [174]. Given that HOCl is a much more effective oxidant than OCl⁻, the effectiveness of free chlorine as a disinfectant is dependent on the pH of the solution [175].

The chemical reactions between free chlorine and nucleotide monomers have been studied extensively [24], [30], [176], [177], and the majority of the reports on nucleic acid oxidation have been on DNA under oxidative stress in Eukaryotes [178], [179]. Previous studies found that HOCl reacts relatively slowly with 2'-deoxyadnosine 5'-monophosphate (dAMP) and 2'-deoxycytidine 5'-monophosphate (dCMP), and the exocyclic NH_2 group is likely the reaction site. The reactions are much faster with thymidine 5'-monophosphate (TMP) and uridine 5'-monophosphate (UMP), in which the heterocyclic NH group is the primarly reaction site [178], [179]. 2'-deoxyguanodine 5'-monophosphate (dGMP) is the most reactive base and it has both reaction sites [178]. In contrast to other nucleotides, dGMP interacts with free chlorine with biphasic kinetics: in the primary phase, HOCl reacts quickly with the heterocyclic ^{1}NH-group, and in the secondary phase, HOCl reacts with the ^{6}C-amino group [178]. The reactions of free chlorine with these groups results in the formation of a number of stable chlorinated products, including 5-chlorouracil [180], [181], 8-chloroadenine [182], and 5-chlorocytosine [183]-[185]. The less abundant reports on RNA oxidation have detected the formation of 8-chloroguanosine, 5-chlorocytidine, and 8-chloroadenosine to a lesser extent in cellular RNA when treated with HOCl [25].

When nucleotide monomers are assembled in single-stranded (ss) and double-stranded (ds) genomes (DNA and RNA), higher order structures are also formed. It has been reported that the

secondary structures of ssDNA and ssRNA share many common features [186], and some common secondary structures found in single-stranded nucleic acids include stacking, stem-loop, pseudoknots, hairpins, and mismatched duplex [187]-[190]. The antiparallel helical structure of double-stranded genomes (dsDNA and dsRNA) can also form some higher order configurations such as duplex twisting, supercoiling, and chromatin loops [191], [192]. The chlorine reactivity of the nucleotide bases can be altered by incorporation into higher order genome structures. For example, previous research showed that free chlorine reactivity with dsDNA is dramatically slower compared to its reactivity with nucleotides monomers [178]. This has been attributed to the protection of the primary reaction sites, such as the heterocyclic NH group in TMP and the exocyclic NH_2 group in dAMP, by base pairing between two complimentary DNA strands driven by hydrogen bonding. A early literature reported high chlorine doses were required to cause fragmentation of plasmid DNA, which suggests a high resistance of dsDNA to free chlorine [193]. Also, the chlorination of NH- and NH_2-groups of the individual monomers can induce denaturation of double-stranded nucleic acids because the loss of fydrogen bonding can result in the double helix dissociates into single stands [178]. Accordingly, free chlorine reacted about 10 times faster with heat-denatured DNA and RNA (ssDNA and ssRNA) compared to native dsDNA due to the increased exposure of reactive sites on the single strands [179].

The reactivity of nucleic acids with chlorine is also impacted by their incorporation into microorganism structures. In bacteria, free chlorine reacts primarily with the outer layers of bacterial cells, such as membrane proteins; however free chlorine can also penetrate into the bacterial cell and react with nucleic acids [194]. Chlorine induced modifications can interfere with the vital biological functions of nucleic acids. DNA lesions can interpret genome replication

and transcription, and potentially lead to wider-scale mutations that threaten cell viability [168]. For instance, chlorination of transforming DNA can result in the destruction of its transforming activity [195]. HOCl also inhibits the function of DNA repair machinery, and this makes fixing genome damage challenging for the cells [196]. Inside cells, RNA damage can lead to decreased protein synthesis and the formation of aggregated and truncated peptides due to the interruption of mRNA translation and decreased ribosome function [30].

Compared to bacterial cells, our understanding of chlorine reactions that occur in viral nucleic acids and their impacts on biological functions is limited. When extracted poliovirus ssRNA was reacted with another disinfectant, chlorine dioxide, RT-qPCR analysis showed that the heat-denatured viral RNA reacts significantly slower than native virus RNA that contains secondary structures [13]. This underlines the impact of higher order genome structure on RNA susceptibility to oxidant attack. In the ssRNA of Hepatitis A, RT-qPCR analysis demonstrated that the 5' non-translated region (NTR) that is rich in secondary structures, was more susceptible to chlorine attack than the coding regions [23]. However, the mechanistic explanation for this observation remains unclear. Virus nucleic acids are packed into a capsid protein shells. To our knowledge, the potential protection of the nucleic acids by the protein coat to oxidant attack has not been examined in a systematic manner.

In this study, we investigate the reactivity of viral genomes as the viruses are inactivated with free chlorine treatment. Four model viruses with four different genome types were selected to represent viruses in the water environment, namely bacteriophage MS2, φ6, φX174, and T3. We analyzed the reaction kinetics of both naked and encapsidated nucleic acids using qPCR/RT-

qPCR to evaluate the impact that incorporation in virus particles plays on nucleic acid reactivity. The second order reaction rate constants of two regions in each viral genome were calculated and compared. The results from this study demonstrate the protective effect of protein capsids on viral genomes and highlight the large differences in free chlorine reactivity with the four virus genome types.

4.2   Experimental methods

4.2.1   Chemicals and reagents

Monosodium phosphate (NaH_2PO_4), sodium chloride (NaCl), disodium phosphate (Na_2HPO_4), and monopotassium phosphate (KH_2PO_4) were obtained from Fisher Scientific (Fair Lawn, NJ). Bovine serum albumin (BSA), betaine solution (5 M), disodium ethylenediamine tetraacetate dehydrate (EDTA-Na_2), and sodium hypochlorite solution (NaOCl) were purchased from Sigma-Aldrich (St. Louis, MO). N,N-Diethyl-p-phenylenediamine (DPD) indicator solution for residual chlorine analysis was ordered from Ricca Chemical (Arlington, TX). UltraPure Tris-HCl buffer (pH 7.5) was obtained from Invitrogen (Carlsbad, CA). GoTaq 1-step RT-qPCR system, Maxwell 16 viral total nucleic acid purification kit, and ultrapure nuclease-free water were purchased from Promega (Madison, WI). Fast Evagreen qPCR master mix was obtained from Biotium (Fremont, CA) and gBlocks gene fragments were ordered from Integrated DNA Technologies (IDT, Coralville, IA).

4.2.2   Virus preparation

There are four different kinds of nucleic acids serving as viral genomes. In this study, one model

virus was picked to represent each viral genome type, namely MS2 for ssRNA, φ6 for dsRNA,

φX174 for ssDNA, and T3 for dsDNA. We selected these four bacteriophage viruses for various

reasons including that they are easy to work with, can easily be propagated to high titers, and that

they are commonly applied as surrogates for human viruses. The characteristics of these four

model viruses are provided in Table 3.1.

MS2 virus (ATCC 15597-B1) and its corresponding bacterial host *Escherichia coli* (*E. coli*;

ATCC 15597) were purchased from American Type Culture Collection (ATCC). The details on

MS2 propagation and purification were previously published [83]. In brief, the enriched MS2

virus solution was purified by a Fast Protein Liquid Chromatography system (Econo, Bio-Rad)

equipped with a HiPrep Sephacryl S-400 HR column (GE), followed by a filtration using 0.22

μM polyethersulfone (PES) membrane filters (Millipore). The final MS2 stocks were stored at 4

°C in phosphate buffered saline (PBS; 5 mM NaH_2PO_4, 10mM NaCl, pH 7.5).

Pseudomonas virus φ6 and its host cell *Pseudomonas syringae* pv. phaseolicola were received

from Professor Linsey Marr's research group at Virginia Tech. φ6 stocks were propagated and

purified based on a published method [166]. Briefly, φ6 was mixed with its host in Luria-Bertani

(LB) medium (5 g L^{-1} NaCl) at 26 °C and incubated for 7 to 9 hours. The virus suspensions were

filtered through 0.22 μm PES membranes to remove cells and debris, and were concentrated ~50

times using a bench-scale tangential flow filtration system (Millipore) equipped with a 30 kDa

cellulous filter. The φ6 concentrates were further purified by two-step centrifugation at 65,700 $\times$

g, 4 °C. The first step was in a 10-40% (w/v) step sucrose gradient for 1.5 hours and the second step was in a 40-60% (w/v) linear sucrose gradient for 15 hours. The band, which contained $\varphi6$ viruses, was collected with a needle and was then buffer exchanged into PBS using a 100 kDa centrifugal ultrafilter (Millipore). Finally, the $\varphi6$ virus stocks were filtered through 0.22 µm PES membranes, and stored at -80 °C until use.

Bacteriophage T3 and its *E. coli* host ATCC 11303 were purchased from ATCC. T3 virus was propagated by the agar overlay technique. Specifically, soft agar (0.7% w/v) containing a mixture of T3 viruses and host cells was overlaid on a layer of hard agar (1.5% w/v) in a petri dish that was incubated at 37 °C overnight. The soft agar layer was carefully separated from the hard layer and resuspended in PBS. The suspensions were then centrifuged at 3,000 × g for 10 minutes to remove the agar. The viruses in the supernatant were extracted from host bacterial cells by chloroform treatment, and purified with 100 kDA Amicon centrifugal ultrafilters and 0.22 µm PES membrane filters (Millipore). The final T3 virus stocks were stored in PBS at 4 °C. *Escherichia* virus φX174 and its bacterial host *E. coli* ATCC 13706 were kindly provided by Professor Charles Gerba's lab at the University of Arizona. φX174 virus were propagated and purified with the same method as T3, except tryptic soy agar (TSA) was used instead of regular agar.

4.2.3   Chlorine reaction

In order to investigate the impact of encapsidation on viral genome reactivity with chlorine, chlorine reactions were conducted when viral genomes were inside and outside the virus particles. For studying chlorine reaction of viral genomes within virus particles (i.e.,

encapsidated), solutions containing entire virus particles were used to react with chlorine directly. In the case of naked nucleic acids, viral genomes were extracted from the virus particles and diluted in PBS before reacting with chlorine. The PBS solution used in this study was incubated in a water bath at 90 °C for 30 minutes to inactivate nucleases. For naked nucleic acids experiment, viral genomes were extracted from the virus stock solutions immediately before the chlorine reactions using Maxwell 16 Viral Total Nucleic Acid Purification Kits according to the manufacturer's instructions. The Qubit Fluorometer 2.0 (Life Technologies) was used to measure the concentrations of the extracted genomes in ng/mL, then the readings were converted to genome copies (gc)/µL using the genome's molecular mass and Avogadro's constant. The naked nucleic acids for chlorine reactions were present at a concentration of ~10^6 gc/µL, and were prepared by diluting extracted viral genomes with nuclease free PBS. For encapsidated nucleic acids experiments, reaction solutions were prepared by directly diluting the virus stocks to a similar genome concentration ~10^6 gc/µL with PBS.

All glassware was soaked in a chlorine bath overnight before their use in the experiments. The free chlorine working solution was prepared by diluting a NaOCl stock solution with PBS in a chlorine-demand-free beaker. Chlorine reactions with viral nucleic acids were conducted in two different systems. For viral genomes that reacted with chlorine with fast kinetics (reactions less than 15 seconds), such as genomes of MS2, φ6, and φX174, a continuous quench-flow system was used. This system was built based on a reaction system reported in a previous study [197]. This allowed us to control the contact time of nucleic acids with chlorine at timescales of 4 to 15 seconds. In contrast, for viral genomes that were quite resistant to free chlorine, such as T3

dsDNA, a traditional batch reactor system was employed. In these experiments, the timescales of contact time were 1 to 8 minutes.

In the continuous quench-flow system, chlorine and virus/genome solutions were loaded into two syringes (Hamilton) that were set on a syringe pump (Kd Scientific) with a flow rate of 0.125 mL/min each. The two solutions were continuously mixed in a PEEK micro static mixing tee (IDEX Health & Science) to reach initial reaction conditions of 5 mg/L as Cl_2 for free chlorine and $\sim 1 \times 10^6$ gc/μL for viral nucleic acids. The reacting mixtures then flowed through reaction loops with various volumes and were quenched with 550 mM ultrapure Tris-HCl buffer (pH 7.5) at a flow rate of 0.025 mL min^{-1} in the end of each loop. This resulted in contact times of 4, 7, 11, and 15 seconds. Control experiments were conducted to confirm that 550 mM Tris-HCl buffer can quench free chlorine effectively, and that the reactions in nucleic acids were halted. Approximately 120 μL of quenched experimental samples were collected and stored at -80 °C before analysis. Free chlorine concentration was monitored using the DPD colorimetric method according to the standard method [198] and the chlorine losses throughout the experiment were less than 2%. Negative control experiments were conducted in the continuous quench-flow system in the same manner as the free chlorine experiments except PBS was used instead of free chlorine solutions. The experiments were repeated at least two times for each genome type. Following chlorine treatment, the encapsidated genomes were extracted from the virus samples with Maxwell 16 Viral Total Nucleic Acid Purification Kits. The chlorine-treated and negative control samples were analyzed by qPCR or RT-qPCR immediately after the completion of the chlorine experiments.

In the batch reaction setup, sacrificial reactions were conducted by adding 100 µL of free chlorine working solution into a chlorine-demand-free glass tube containing a magnetic stirrer and this was placed on a stir plate (Corning). Then, 100 µL of solutions of either viral nucleic acids or purified viruses were added into the same tube at time = 0. The initial reaction conditions in batch reactors were identical to the conditions in continuous quench-flow system. The reacting mixture was well mixed during the reaction period. 10 µL of 550 mM Tris-HCl buffer was added into the tube to quench free chlorine in order to achieve a contact time of 1, 2, 4, and 8 minutes. The consumption of free chlorine throughout the experiment was less than 9%. In negative control experiments, PBS was used to replace free chlorine solution. Similar to the continuous quench-flow system, the experimental and control samples were quantified by qPCR/RT-qPCR immediately after the chlorine reactions.

4.2.4   *qPCR assay for chlorine-treated viral genomes*

To investigate the impact of location and sequence on the reactivity of viral nucleic acids with chlorine, two sets of PCR primers were designed to target two regions (region A and B) on each viral genome type. The two regions were selected on opposite sides of the genomes for MS2, φX174, T3 and on difference genome segments for φ6 (Table B-1). The sizes of the regions were approximately 500 bases or base pairs. Detailed information regarding target regions selected for this study are provided in Table 4.1. The entire genome of ssRNA of MS2, dsRNA of φ6, and dsDNA of T3 were extracted from the purified virus stocks, and were used as qPCR standards directly; for φX174 ssDNA, gBlock gene fragments containing the two target regions (IDT) were used as standards. Both experimental and control samples were quantified in parallel in a RealPlex^2 Mastercycler system (Eppendorf). Once optimized, the standard curves of all

73

PCR/RT-qPCR assays had R^2 values greater than 0.99, and the efficiencies were consistently greater than 0.82. The free chlorine concentrations remained relatively constant throughout the reaction period and therefore the reaction rate constants of each target region were calculated based on a pseudo-first order reaction model:

$$\ln\left(\frac{C}{C_0}\right) = -k_{exp} \cdot [Cl] \cdot t$$

where C_0 is the initial concentration of the viral genome segment; C is the concentration of the chlorine-treated viral genome segment; k_{exp} is the second order rate constant; $[Cl]$ is the free chlorine concentration of 5 mg/L as Cl_2; t is the contact time (s).

Table 4.1 Location, size, and sequence compositions of the target genome regions in this study.

Virus	Region	Region location	Region size	Number of A	Number of T or U	Number of C	Number of G
MS2 (ssRNA)	A	944 to 1439	496 b	112	125	127	132
	B	2693 to 3189	497 b	115	141	121	120
φ6 (dsRNA)	A	S1141 to S1639	499 bp	221	221	278	278
	B	L1510 to L1993	484 bp	226	226	258	258
φX174 (ssDNA)	A	571 to 1074	504 b	115	144	117	128
	B	1717 to 2209	493 b	96	169	114	114
T3 (dsDNA)	A	1678 to 2186	509 bp	238	238	271	271
	B	11826 to 12324	499 bp	245	245	254	254

RT-qPCR assay for MS2 ssRNA and φ6 dsRNA

The 20 µL one-step RT-qPCR reactions for MS2 included 10 µL of 2× GoTaq qPCR Master Mix (Promega), 0.4 µL of 50× GoScript RT Mix, 0.6 µL of 10 µM forward primer, 0.6 µL of 10 µM reverse primer, 6.4 µL of nuclease-free water, and 2 µL of the MS2 RNA sample. For φ6

genome samples, dsRNA samples were first mixed with 10 μM forward and reverse primer solutions at a volume ratio of 10:1.5:1.5. This pre-mixed sample-primer combination was then incubated at 99 °C for 5 minutes, and stored at 4 °C before use. The 20 µL RT-qPCR reactions for $\varphi6$ consisted of 10 µL of 2× GoTaq qPCR Master Mix, 0.4 µL of 50× GoScript RT Mix, 4 µL of 5 M Betaine, 0.4 µL of nuclease-free water, and 5.2 µL of the pre-treated template-primer mixture. The reverse transcription process was conducted at 40 °C for 15 minutes, followed by a 10 minute holding step at 95 °C to activate the hot start DNA polymerases. The PCR amplification consists of 40 cycles of DNA denaturation at 95 °C for 15 s, primer annealing at 55 °C (59 °C for $\varphi6$) for 30 s, and extension at 72 °C for 45 s. Melting curve analysis was conducted by increasing temperature from 60 to 95 °C for 10 minutes.

qPCR assays for φX174 ssDNA and T3 dsDNA

In the case of φX174 ssDNA and T3 dsDNA, each qPCR reaction had a total volume of 10 µL, consisting of 5 µL of EvaGreen qPCR Master Mix, 0.25 µL of 25 mg/mL bovine serum albumin (BSA) solution, 0.4 µL of 10 µM forward primer, 0.4 µL of 10 µM reverse primer, 2.95 µL of nuclease-free water, and 1 µL of DNA samples. The qPCR amplification procedures for φX174 ssDNA include a holding step of 5 min at 95 °C, followed by 40 cycles of 95 °C for 20 s, 55 °C for 20 s, and 72 °C for 20 s, and a melting curve analysis from 68 to 95 °C for 5 minutes. For T3 dsDNA, the following thermocycling conditions were used: 2 min at 95 °C, 35 cycles of 95 °C for 5 s, 60 °C for 5 s, and 72 °C for 25 s, followed by a melting curve analysis from 55 to 95 °C for 5 minutes.

4.2.5   Statistical analysis

For the chlorine experiment, pseudo-first order reaction rate constants were determined by linear regression analyses of $\ln(C/C_0)$ versus time (s) on pooled data from replicate experiments of each tested region ($n \geq 2$). To test whether there were significant differences between the rate constants of two groups (i.e. naked versus encapsidated nucleic acids, ssRNA versus dsRNA), analysis of covariance (ANCOVA) tests were conducted with Prism 7 (GraphPad Software, La Jolla, CA). The null hypothesis was that the rate constants of two groups were not significantly different. The null hypothesis was rejected only when *p* value was less than 0.05.

4.3   Results and discussion

4.3.1   Chlorine reaction with naked nucleic acids

The reactions of both region A and region B of each naked viral genome with free chlorine generally followed pseudo-first order kinetics over the studied range (Figure 4.1; Figure 4.2), in which the free chlorine concentration was relatively constant. Therefore, we conducted linear regressions on duplicated experimental data to calculate pseudo-first order rate constant (s^{-1}) for each genome region. Then the second-order rate constants (L mg^{-1} s^{-1}) were obtained by dividing the pseudo-first order rate constants by chlorine concentration (5 mg L^{-1}). Replicate experiments resulted in similar kinetics. For naked ssDNA and dsDNA, there were no statistically significant differences observed between the second order rate constants of the A and B regions. In contrast, the two target regions of naked $\varphi6$ dsRNA reacted in different kinetics with free chlorine, as did the two regions of naked MS2 ssRNA. In particular, the $\varphi6$ region A (dsRNA) reacted 16× faster than $\varphi6$ region B (Figure 4.3). There are some possible explanations for this observation. First, the $\varphi6$ region A has more guanine (G) bases compared to region B (278 versus 258; Table 4.1)

76

and guanine is the most reactive base with chlorine among all bases according to previous reports[178], [179]. Second, the $\varphi6$ genome consists of three segments and region A is located in the short segment (2.9 kbp) whereas region B is located in the long segment (6.4 kbp). The short and long segments likely have different structures that can impact the reactivity of nucleic acids with chlorine. A previous study has demonstrated that the location and the spatial arrangement of the target genome region appear to have a significant impact on the degradation kinetics of the extracted viral RNA when reacting with chlorine dioxide [13]. Similarly, the MS2 regions A and B also had different reaction kinetics with free chlorine according to ANCOVA analysis ($p = 0.02$), although the difference was minor (~1.3×). In summary, we did not observe an impact of genome location on chlorine reactivity for naked DNA genomes, but we did see statistical differences in two different regions of the RNA genomes. The numbers of reactive bases in each studied viral genome region are listed in Table 4.1. This demonstrates that the region As had similar numbers of reactive bases to region Bs in most cases.
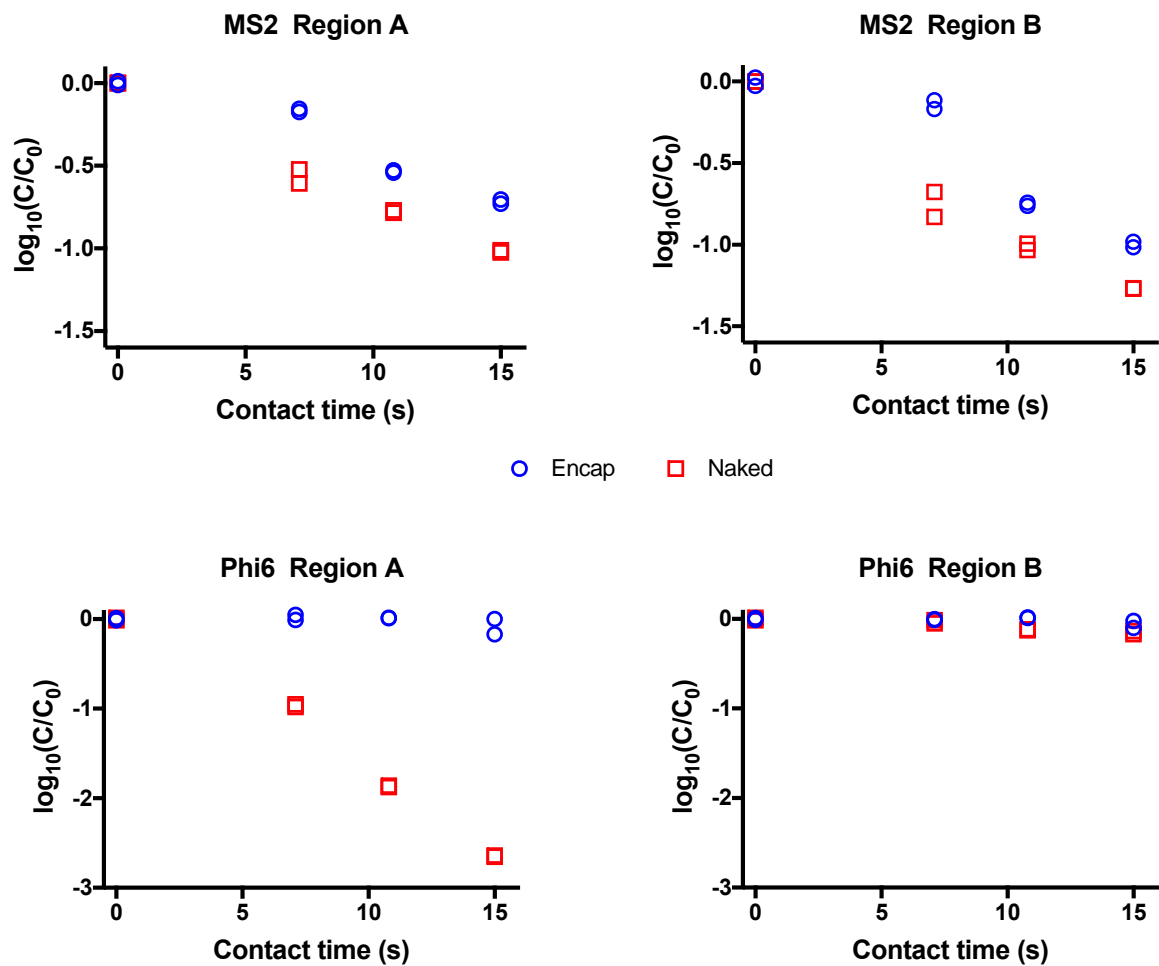
Figure 4.1 Reactions of encapsidated and naked viral genomes with free chlorine in two RNA viruses: MS2 and $\varphi6$. The concentrations of ssRNA (MS2) and dsRNA ($\varphi6$) were measured with RT-qPCR and two regions (Region A and Region B) were targeted in each genome.
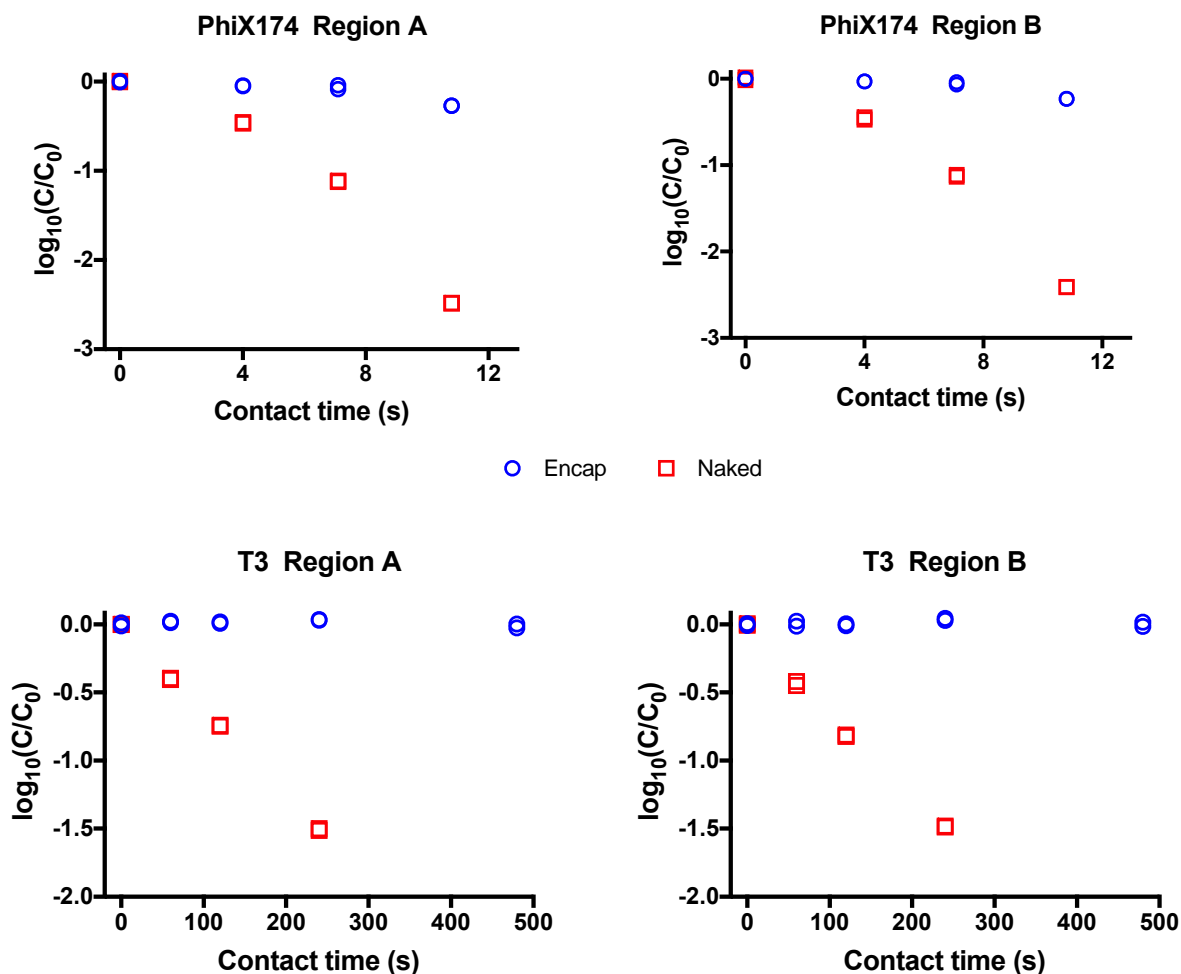
Figure 4.2 Reactions of encapsidated and naked viral genomes with free chlorine in two DNA viruses: φX174 and T3. The concentrations of ssDNA (φX174) and dsDNA (T3) were measured with qPCR and two regions (Region A and Region B) were targeted in each genome.

A comparison of the chlorine reaction constants of the naked ssRNA with the naked ssDNA demonstrates that the two ssDNA regions reacted, on average, 2.9× faster than the two ssRNA regions (Figure 4.3). In the case of naked dsRNA versus naked dsDNA, we observed the opposite trend: the two dsRNA regions were more reactive with free chlorine than the two dsDNA regions (Figure 4.3). This was unlikely due to the difference in primary sequence composition since they had similar numbers of reactive bases (Table 4.1). The exact reason that

DNA is more reactive with chlorine than RNA in single-stranded structure whereas RNA is more reactive than DNA in double-stranded structure is not clear, but may involve the circularity of the φX174 ssDNA genome and the segmentation of the φ6 dsRNA genome. Further research will be needed to verify if this trend applies to other viruses with the same genome type.
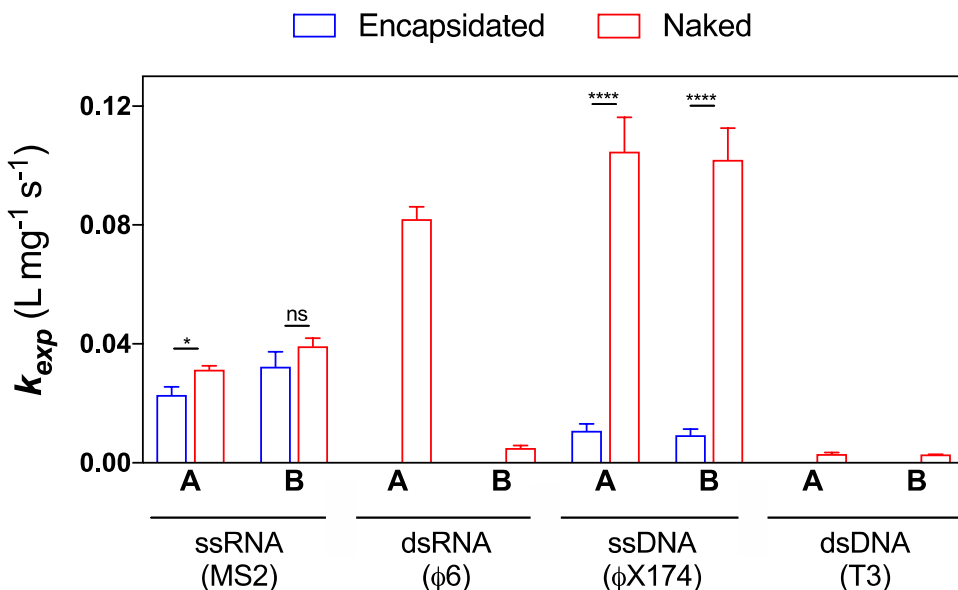
Figure 4.3 Second-order chlorine reaction rate constants of viral genome regions A and B in encapsidated form (blue bars) and in naked form (red bars). Data is not available for encapsidated genomes of φ6 (dsRNA) and T3 (dsDNA) because a decrease in genome region concentrations was not detected over the studied experimental doses. Error bars represent standard error for duplicate experiments. ANCOVA tests were conducted to calculate p values. Asterisks indicate rate constants are significantly different (one asterisk for $0.01 < p < 0.05$, four asterisks for $p < 0.0001$) and ns indicates that rate constants are not significantly different ($p > 0.05$).

4.3.2   Comparison of chlorine reactivity of nucleic acids in single stranded structure versus in double stranded structure

The genomes of $\varphi6$ and T3 virus are double-stranded, and the genomes of MS2 and φX174 virus are single-stranded. Consequently, there are twice the number of reactive bases in the target 500 bp regions of $\varphi6$ and T3 compared to the 500 b regions of MS2 and φX174. Consequently, the experimental reaction rate constants of single-stranded regions and double-stranded regions were not directly comparable. We therefore normalized the second-order rate constants by the number of bases in analyzed genome regions to get the chlorine reaction rate constants at per base level (L mg^{-1} s^{-1} base^{-1}). By comparing normalized rate constants of single-stranded regions with double-stranded regions, we were able to evaluate the impact of double-stranded structures on viral genome reactivity. We would expect the bases in single-stranded regions to react as fast as the bases in double-stranded regions if incorporation in the double helix did not impact the nucleic acid reactivity with chlorine.

Our results demonstrated that the naked RNA bases reacted, on average, 1.6× faster in the single-stranded regions than in the double-stranded regions. The naked DNA bases reacted, on average, 72× faster in the single-stranded genome than in the double-stranded genome (Table 4.2). The observed differences were not due to variances in sequence compositions because the single-stranded and double-stranded RNA regions had similar proportions of reactive bases, as did the ss and ds DNA regions (Table 4.1). Hence, we conclude that the slower reaction kinetics of double-stranded genomes compared to single-stranded genomes was primarily due to the impact of the double helix structure. This is likely the consequence of that nucleotide bases in single-stranded genomes are more readily exposed to excess chlorine molecules in solution compared to

bases in double-stranded genomes. In antiparallel double helical structure, bases from one strand are paired with corresponding bases from adjacent complementary strand through hydrogen bonding (e.g., A-T base pair and C-G base pair), which can protect primary reactive sites in bases from chlorine attack. An early study of reaction of HOCl with nucleic acids also found that heat denatured DNA and RNA (i.e., ssDNA and ssRNA) reacted 10 fold faster than native dsDNA, which agrees with our observation [179].

Table 4.2 Chlorine second order rate constants of target viral genome regions normalized by the number of bases in corresponding region, k_{exp} (L mg^{-1} s^{-1} base^{-1}). SE stands for standard error. NS indicates that decay is not significant. The concentration of free chlorine was 5 mg/L as Cl$_2$.

		ssRNA (MS2)		dsRNA (φ6)	
		Region A	**Region B**	**Region A**	**Region B**
$k_{exp} \pm$ SE	Encapsidated	4.5E-5 ± 5.3E-6	6.5E-5 ± 1.0E-5	NS	NS
	Naked	6.3E-5 ± 2.8E-6	7.9E-5 ± 5.3E-6	8.2E-5 ± 4.1E-6	5.2E-6 ± 8.6E-7
		ssDNA (φX174)		dsDNA (T3)	
		Region A	**Region B**	**Region A**	**Region B**
$k_{exp} \pm$ SE	Encapsidated	2.1E-5 ± 4.6E-6	1.9E-5 ± 4.1E-6	NS	NS
	Naked	2.1E-4 ± 2.3E-5	2.1E-4 ± 2.2E-5	2.9E-6 ± 4.8E-7	2.8E-6 ± 7.5E-8

Our results also illustrated that incorporation into the double helix structure had a much greater influence on the reactivity of DNA bases with chlorine than on the reactivity of RNA bases with chlorine. We observed that naked dsDNA of T3 was most resistant to free chlorine treatment amongst all four viral genomes. Specifically, a 1.5 log loss in the genome regions were observed after 4 minutes reaction with chlorine (Figure 4.2), whereas other naked viral genomes reacted this much within seconds (Figure 4.1; Figure 4.2). This highlight the high resistant of dsDNA to free chlorine compared to other nucleic acids. It was reported previously that high chlorine doses (~180 mg L^{-1} min) were required to cause fragmentation of a pETBlue plasmid dsDNA that

originated from *E.coli* [193], which again suggests the high resistance of dsDNA to free chlorine. This has direct environmental implications as certain antibiotic resistant genes (ARGs) located in plasmid DNA may persist for long time in the environment after nucleic acids in other forms has degraded by chlorination.

4.3.3 Chlorine reaction with encapsidated nucleic acids

To investigate the influence of encapsidation on viral nucleic acids reactivities with free chlorine, we treated the purified virus solutions with chlorine with various doses. For $\varphi6$ (dsRNA) and T3 (dsDNA), we did not detect a statistical decrease in the encapsidated genome regions after doses of 75 mg L^{-1} s and 2400 mg L^{-1} s, although we had observed statistically significant degradations following these doses when the genomes were naked (Figure 4.1; Figure 4.2). In case of φX174 ssDNA, the target regions reacted with chlorine at a significantly faster pace ($p < 0.0001$) when the genomes were naked compared to when they were incorporated in the virus particles (Figure 4.2). Specifically, the two regions in the naked form reacted, on average, 10× faster than in the encapsidated form (Figure 4.3). For ssRNA of MS2, the naked nucleic acids reacted ~1.4× faster than encapsidated nucleic acids in region A ($p = 0.016$). In region B, however, the chlorine reaction rate constants of naked and encapsidated genome were not significantly different according to ANCOVA tests. In general, we have observed a profound impact of incorporation in virus particles on viral nucleic acids reactivity except for in one of the two regions measured in the ssRNA genome of MS2. These results demonstrate that capsid proteins protect viral genomes from attack by free chlorine.

When comparing the influence of encapsidation on DNA versus RNA, we found that the discrepancy between the rate constants of naked and encapsidated regions in ssDNA was much larger than in ssRNA ($10\times$ versus $1.4\times$). This suggests that incorporation in the virus particles had greater impact on reactivity of the DNA bases than on reactivity of the RNA bases. Additional viruses will need to be studied to determine if this is true for all RNA and DNA viruses. Another interesting result is that in naked form, the two regions in ssDNA reacted, on average, $2.9\times$ faster than the regions in ssRNA (Figure 4.3), whereas in encapsidated form, the opposite is true: the regions in ssRNA reacted, on average, $2.8\times$ faster than the regions in ssDNA (Figure 4.3). This flip of reaction kinetics highlights the impact of encapsidation on viral nucleic acid reactivity. φX174 ssDNA became much less reactive once it was incorporated into virus particles. This might be due to the φX174 protein capsid shell limiting the chlorine penetration more effectively or consuming more chlorine than the MS2 protein capsid. As discussed above, the reactivity of DNA bases is also more impacted by incorporation in the double helix. Therefore, all these results together suggest that higher order structure had a larger impact on DNA base reactivity than on RNA base reactivity during chlorine disinfection.

The discrepancies between the chlorine reaction kinetics of naked and encapsidated genomes have several potential explanations. First, the viral proteins, such as capsid proteins and nucleocapsid proteins in close contact with the nucleic acids, can protect the genomes from damage by consuming part of chlorine molecules that are attacking viral genomes. It was reported previously that free chlorine reacts primarily with the outer layers of bacterial cells, such as membrane proteins [194]. We expect a similar case in chlorine reactions with viruses. A recent study from our group has demonstrated that the membrane proteins and lipids in the

envelope layer of $\varphi 6$ can also react with free chlorine, which contributes to chlorine consumption [166]. Second, the protein capsid shell may inhibit the penetration of free chlorine into the virus particles, which makes the encapsidated genomes less accessible for free chlorine molecules. Last but not least, as observed above, higher order structures such as incorporation in double helices can result in decreases in base reactivity; therefore, nucleic acids in viral particles may be more compact or have more strict higher order structure which makes some of the bases less reactive with chlorine. These protective mechanisms are absent when the nucleic acids are in naked form in the solution. Further research is needed to characterize the specific mechanisms responsible for viral genome reactivity and how it is impacted by encapsidation.

4.4   Environmental implications

Our research demonstrates that when reacting with chlorine, nucleic acids that are incorporated in virus capsids can have markedly different reaction kinetics than naked nucleic acids. The region B in MS2 ssRNA was the only region unaffected by the encapsidation. This identifies a profound impact of encapsidation on viral genome reactivity with chlorine. Therefore, we expect the nucleic acids pollutant in naked form such as extracellular antibiotic resistant genes and plant-incorporated protectants, will have different fate during chlorine disinfection compared to intact microorganisms that cause environmental concerns such as antibiotic resistant bacteria and pathogens. Future research will be needed to determine if the discrepancy between reaction kinetics in naked and encapsidated genomes applies to other viruses with the same genome types.

Another important observation of this work is the relatively high resistance of the T3 dsDNA compared to other bacteriophage genomes studied in this work. Specifically, we did not detect significant decay of encapsidated dsDNA, even after 8 minutes of reacting with free chlorine at a concentration of 5 mg/L. Even without the protection of capsid, the rate constants of naked T3 dsDNA were ~72× lower, on average, than rate constants of naked φX174 ssDNA, when the rate constants were normalized by the segment size. The naked dsDNA rate constants from this work are also relevant for the persistence of extracellular dsDNA that contain ARGs in chlorinated waters.

Chapter 5   Conclusions

The overall objective of this dissertation project was to explore the reactions that take place in viral nucleic acids during photolysis and chlorine disinfection, from the short oligomer level, to the entire naked genome, and up to the genome incorporated in a virus particle. The results from this study provide insightful knowledge on reaction kinetics of viral nucleic acids by photolysis and chlorine oxidation, and improve our understanding on the impact of higher order structure on viral genome reactivity. This information can assist scientists and engineers in designing and applying appropriate disinfection technologies to battle newly emerging virus pathogens and other nucleic acid pollutants in water and air environments.

In terms of the impact of primary sequence on nucleic acids reactivity, our work on the photochemical reactivity of purified MS2 RNA oligomers demonstrated that the nucleic acid regions with more pyrimidine bases are more susceptible to direct UV photolysis and nucleic acid sequences with more guanine bases are more susceptible to indirect photolysis. This underlines the influence of genome sequence on RNA reactivity during water disinfection processes. Our work also suggests that high proportions of neighboring pyrimidine bases in a genome can lead to earlier photostationary states in the reaction kinetics.

Beyond primary sequence structure, our work characterized how RNA reactivity compares to DNA reactivity, and how single strands compare to double strands. For UV_{254} photolysis of

entire naked genomes, the rate constants normalized by the number of bases measured exhibited the following trend: ssDNA > dsDNA ≈ ssRNA > dsRNA. In contrast, the order of reactivity from chlorine had the following trend: ssDNA > ssRNA > dsRNA > dsDNA. By comparing the measured rate constants of the single-stranded regions with double-stranded regions, our results suggest that the double helix has a greater impact on RNA photoreactivity than on DNA photoreactivity, and that the impact of the double helix was enhanced in buffer solution compared to ultrapure water. For chlorine, on the other hand, we found double helix had profound impact on both DNA and RNA reactivity. For viruses, this suggests the most resistant nucleic acids for chlorine will be dsDNA genomes and the most resistant genomes for UV_{254} will be dsRNA genomes. There are additional factors beyond nucleic acid reactivity that influence virus inactivation by disinfectants. For example, host cells can sometimes repair dsDNA photoproducts, and this makes some dsDNA viruses highly resistant to UV. The same repair mechanisms are not observed in ssDNA, ssRNA, and dsRNA. With chlorine disinfection, reactions in the protein capsids can inactivate the virus, in addition to reactions in the nucleic acids. Beyond viruses, the results also have important implications for dsRNA plant-incorporated protectants, and suggest these environmental pollutants will persist after other forms of nucleic acids have degraded from direct photolysis.

Another important conclusion from this work is that water chemistry has a significant impact on naked virus nucleic acid photochemistry. Specifically, nucleic acids in PBS were substantially less photoreactive than in ultrapure water. This is important for research going forward, because many of the quantum yields available in the literature for UV photolysis were collected with differing aqueous chemistry conditions. Future work should better characterize the quantum

yields for individual photochemical reactions that take place in both RNA and DNA, and in both single-stranded and double-stranded nucleic acids, with standardized aqueous solution conditions.

The impact of genome encapsidation on genome reactivity with UV and free chlorine was also characterized. We found that in nearly every case examined, naked nucleic acids reacted with chlorine significantly faster than encapsidated nucleic acids. This highlights the protective role of capsid proteins on viral genome reactivity with chlorine, and suggests it will be difficult to predict the inactivation of virus genomes based on their sequence alone. Future work will need to assess if the relative effects of encapsidation observed with the different genome types here are representative of all ssRNA, dsRNA, ssDNA, and dsDNA viruses. In contrast to chlorine, we observed little or no impact of encapsidation on the UV_{254} photolysis of nucleic acids.

Finally, this dissertation work identifies biases due to commonly applied methods for measuring nucleic acid reactions. The quantitative MALDI-TOF-MS technique detected significantly more RNA modifications than RT-qPCR after UV_{254} irradiation, suggesting that certain types of UV-induced RNA modifications were not detected by the reverse transcriptase enzyme. High-resolution ESI-Orbitrap MS analyses identified pyrimidine photohydrates as the major UV_{254} products, which may have contributed to the discrepancy between reaction kinetics determined by mass spectrometry and RT-qPCR. With indirect photolysis, however, RT-qPCR tracked as much $^1O_2$-induced RNA damage as MALDI-TOF-MS. This implies that MS and RT-qPCR may be equally sensitive at detecting RNA modifications caused by oxidants. Because the detection of RNA modifications that cause virus inactivation are of most interest, future research should

characterize the specific lesions measured by the reverse transcriptases used in RT-qPCR, as well as the photoproducts that impact the biological functions of viral nucleic acids. Furthermore, the same experiments conducted here for RNA should be expanded to DNA with the polymerase enzymes that are used with qPCR.

Appendices

Appendix A. Supporting information for Chapter 2

Rate Constant Analysis. For the UV experiments, first-order reaction rate constants for each oligomer with each quantification method were calculated with linear regressions of ln (C/C_0) versus UV_{254} dose. Regressions on the MALDI decay data included all of the experimental data, as did the regressions on RT-qPCR data. For the $^1O_2$ experiments, pseudo first-order reaction rate constants were determined by linear regression analyses of ln (C/C_0) versus time. Second-order reaction rate constants were then calculated by dividing the pseudo first-order rate constants by the steady-state singlet oxygen concentration (9.0×10^{-11} M).

Prediction of Oligomer Rate Constants with $^1O_2$. We compiled the limited data available from two previous publications to predict reaction rate constants of our oligomers. Wilkinson *et al.* reported that the second-order rate constant for guanosine was $\leq 1 \times 10^6$ $M^{-1}s^{-1}$ in water and 6.2×10^6 $M^{-1}s^{-1}$ in D_2O [132]. Clagett and Galen reported the relative reaction rate constants of guanine, uridine, cytidine, and adenosine were 26:13:8:1 [130]. Using a value for guanosine equal to 1×10^6 $M^{-1}s^{-1}$, we used the ratios suggested by Clagett and Galen to calculate the maximum rate constants for uridine, cytodine, and adenosine (5×10^5 $M^{-1}s^{-1}$, 3.1×10^5 $M^{-1}s^{-1}$, and 3.9×10^4 $M^{-1}s^{-1}$, respectively). There are several assumptions made here, including that the

guanosine rate constant is equal to $1 \times 10^6\,M^{-1}s^{-1}$, despite the fact that Wilkinson reported this as a maximum value, that nucleotides and nucleosides have the same reactivity with $^1O_2$, and that incorporation into an RNA oligomer does not impact the rate constants of the individual nucleotides. This prediction could be improved with more accurate rate constants for the reactions between nucleotides and $^1O_2$.
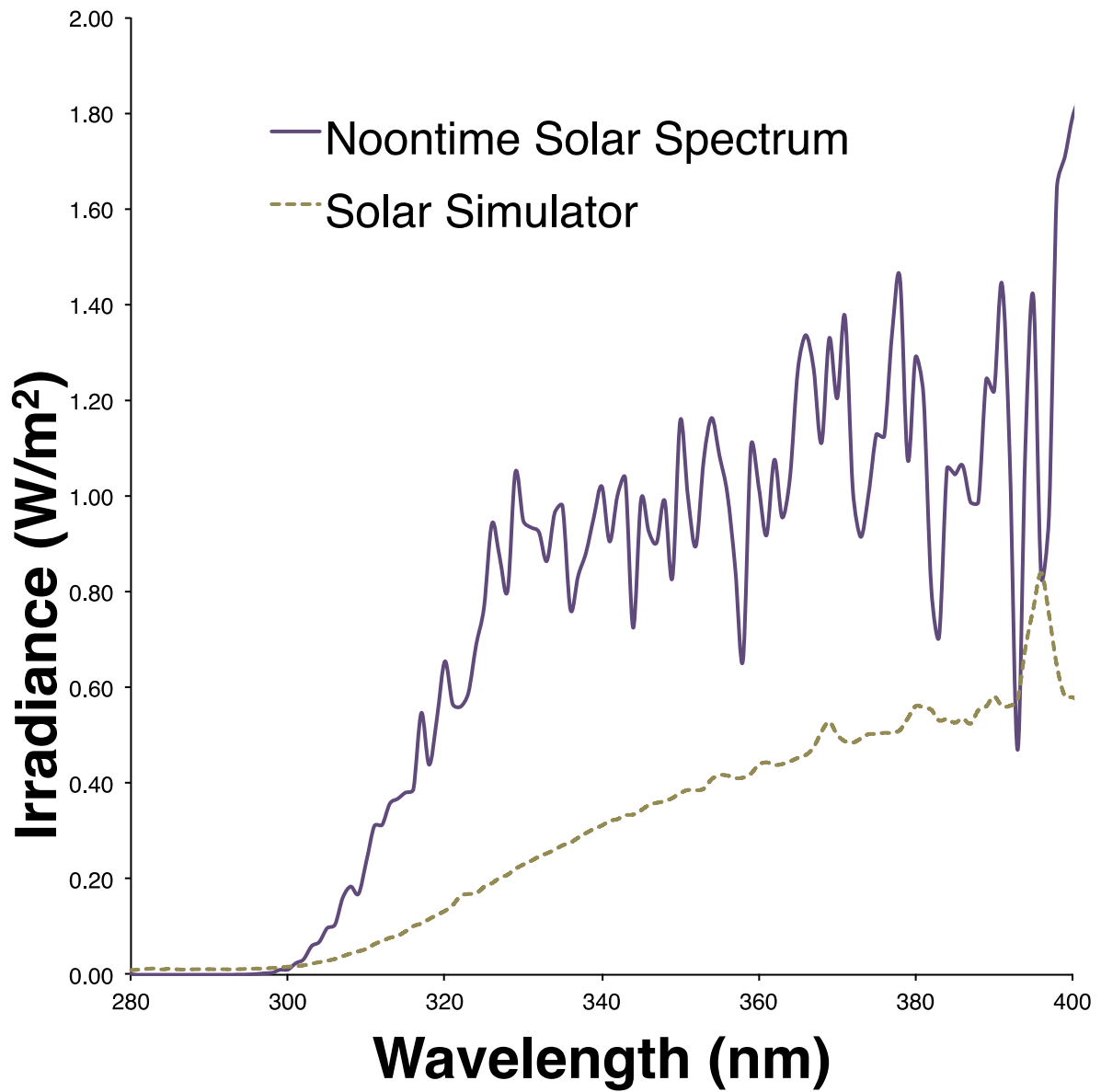
Figure A-1. Comparison of solar simulator output spectrum and solar spectrum in Ann Arbor, MI (42.3º N, 83.7º W, 7/30/16, noontime, estimated with Quick TUV Caliculator, http://cprm.acom.ucar.edu/Models/TUV/Interactive_TUV/).
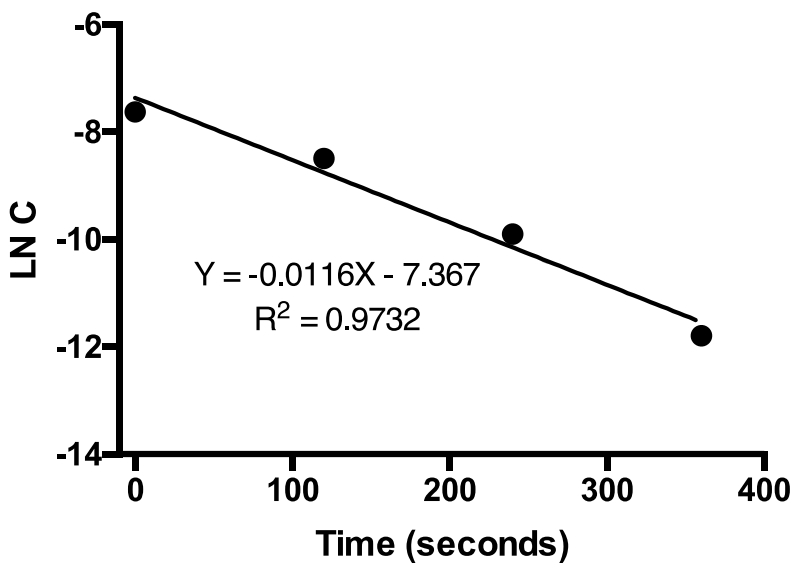
Figure A-2. Decrease of furfuryl alcohol (FFA) concentration with simulated solar treatment. FFA serves as probe compound for measuring $^1O_2$ concentration.
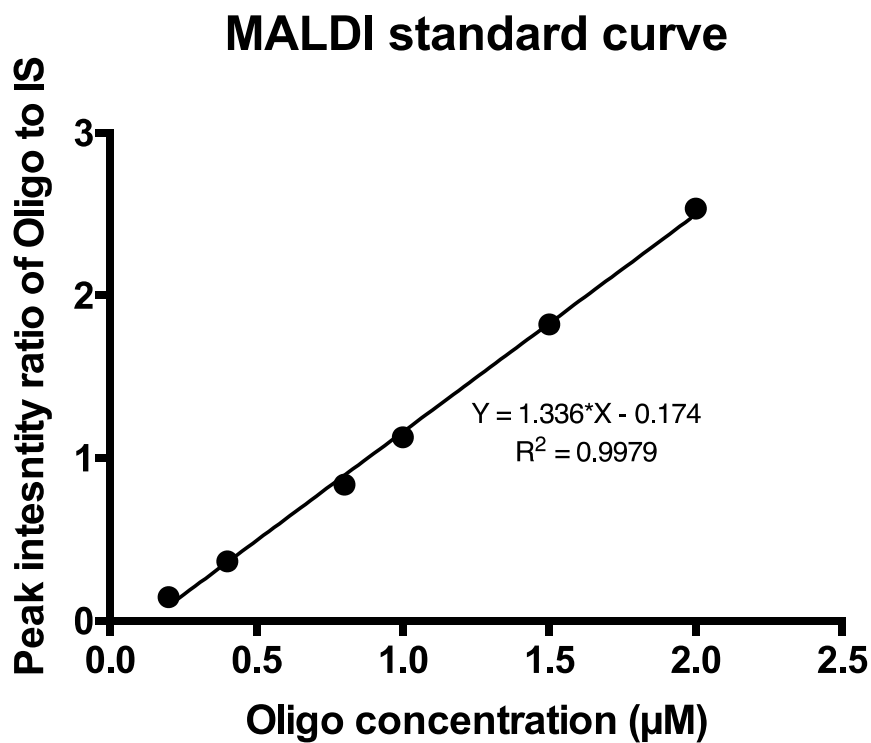
Figure A-3. Quantitative MALDI-TOF-MS standard curve of Oligomer A. The concentration of 26-mer internal standard is 1 μM.
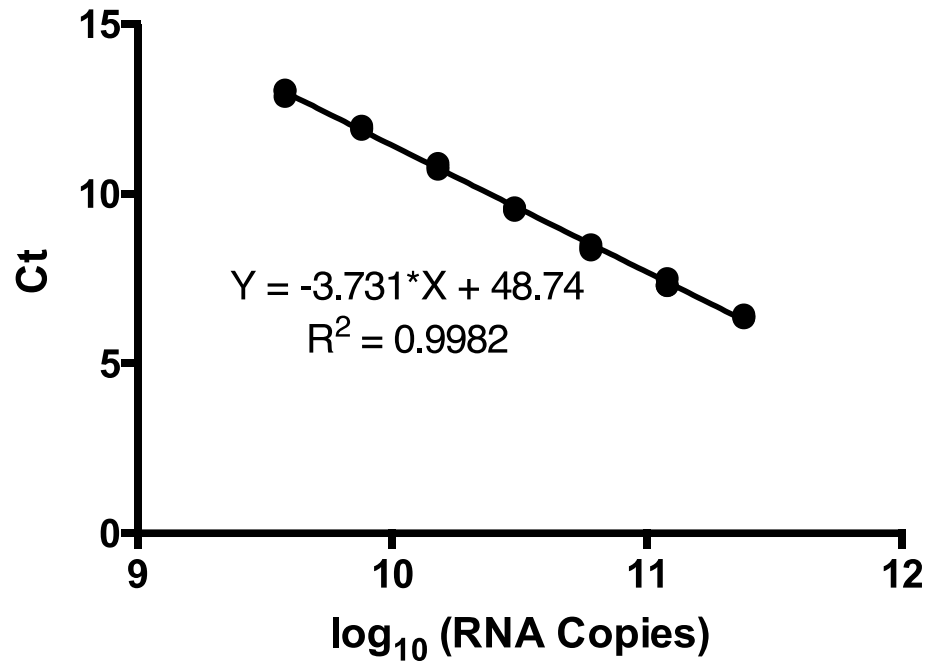
Figure A-4. Step-loop RT primer based RT-qPCR standard curve of oligomer A.
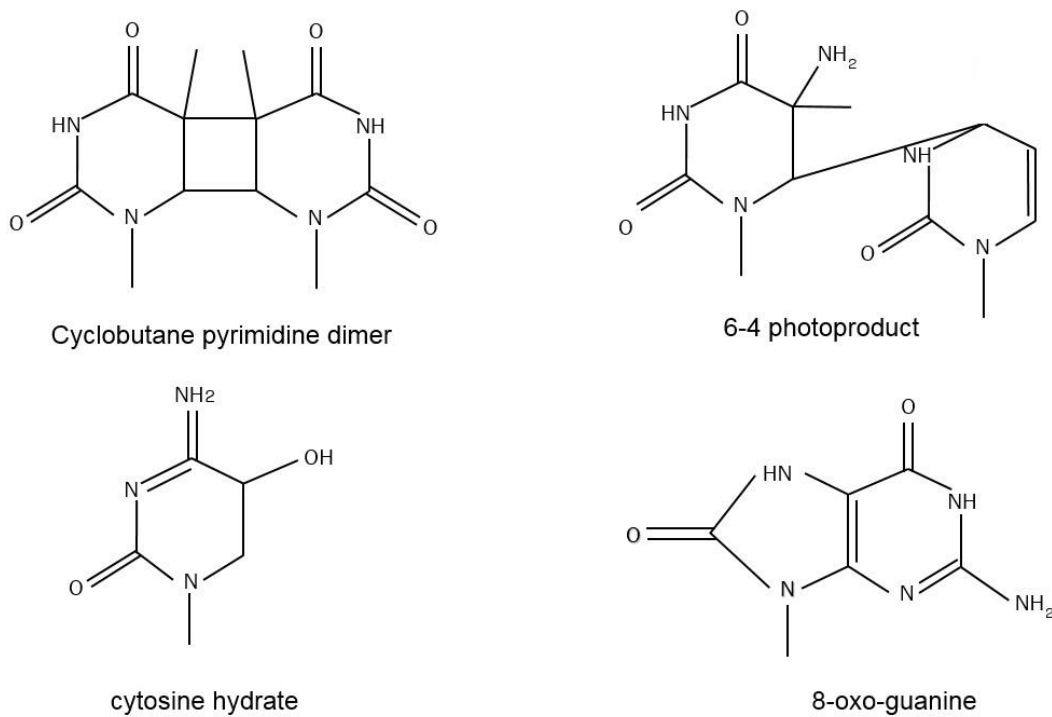
Figure A-5. Chemical structure of three major DNA photoproducts and one major oxidation product reported in the literature.
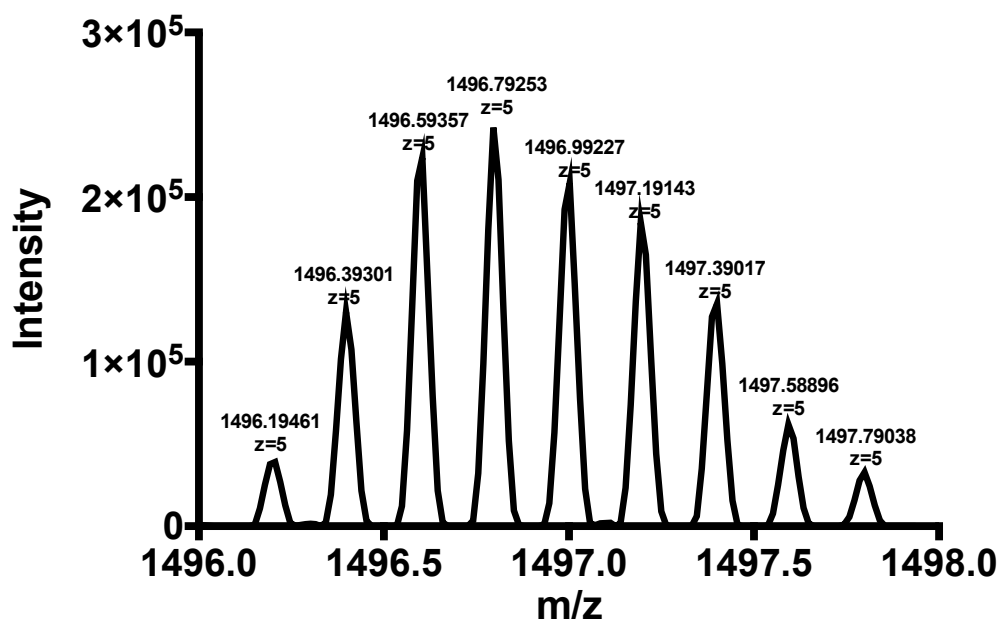
Figure A-6. High-resolution mass spectra for double pyrimidine photohydrate after 20 minutes UVC reaction obtained by ESI-Orbitrap mass spectrometer.

Table A-1. Time gradient of solvent A (2% HFIP + 0.4% TEA in Water) and solvent B (2% HFIP + 0.4% TEA in Methanol) for ESI-Orbitrap-MS analysis. The flow rate was 300 µL/min.

Time (min)	Solvent A (%)	Solvent B (%)
0.0	90	10
5.0	60	40
6.0	10	90
8.0	10	90
8.1	90	10

Table A-2. Prediction of reaction rate constants for the two oligomers with $^1O_2$. The rate constants were predicted by summing up the products of the nucleoside rate constants (described above) and the number of each nucleoside in the oligomers. The sequences of Oligomer A and Oligomer B are provided in Table 2.1.

RNA segment	# A	# C	# G	# U	Rate constant ($M^{-1}s^{-1}$)
Oligomer A	6	10	1	7	7.8×10^6
Oligomer B	7	5	10	2	1.3×10^7

Appendix B.   Supporting information for Chapter 3

Experiments probing the role of reactive oxygen species

In order to investigate the role of indirect photolysis in the nucleic acid reactions, we tested if singlet oxygen ($^1O_2$) or hydroxyl radicals ($\cdot OH$) were contributing to the observed dsDNA T3 reactions. To probe the role of $^1O_2$, experiments were conducted in deuterium oxide (D_2O). Two groups of reaction solution were prepared. The extracted T3 dsDNA was diluted with ultrapure water or D_2O to test the role of singlet oxygen. The initial DNA concentrations of both groups were the same, namely $\sim 2.0 \times 10^5$ gc/μL. Both solutions were irradiated up to 150 mJ cm^{-2} at room temperature and aliquots of experimental samples were collected periodically. Similarly, methanol was utilized to scavenge hydroxyl radicals ($\cdot OH$) that were potentially generated. Here, extracted T3 dsDNA was diluted with 20 mM methanol to reach a final concentration of 2×10^5 gc/μL, and this solution was exposed to UV$_{254}$ along with the naked T3 dsDNA in ultrapure water. For all experiments, control samples were stored in the dark for the duration of the experiments. Following UV exposure, the samples and dark controls were quantified by qPCR.
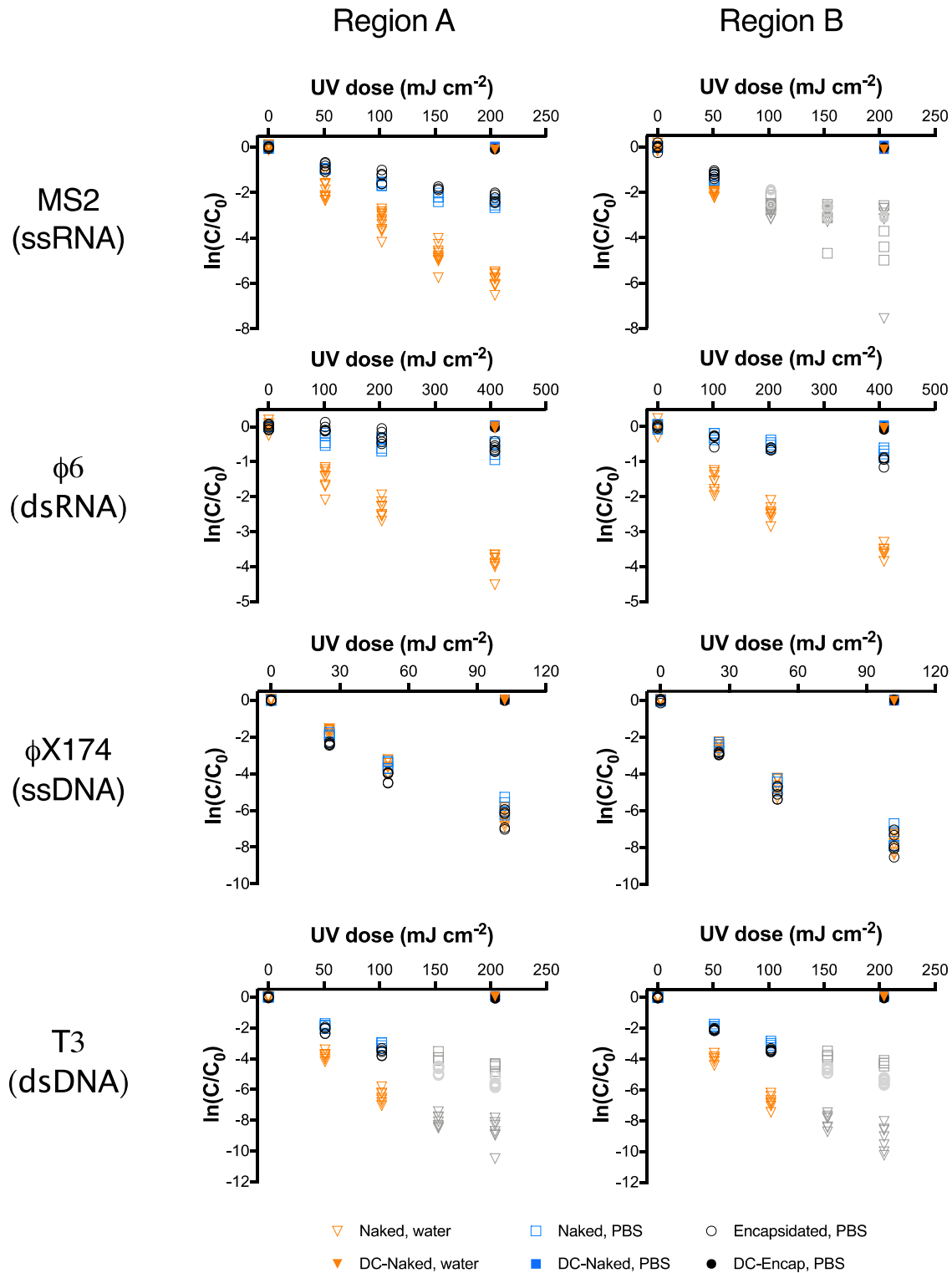
Figure B-1. Pooled data from all replicate experiments on the reactions of encapsidated and naked viral nucleic acids by UV254 irradiation. The nucleic acid concentrations were measured by qPCR (for ssDNA and dsDNA) or RT-qPCR (for ssRNA and dsRNA) and two regions

(Region A and Region B) were analyzed in each genome. We modeled regions of the reactions that followed first order kinetics; these data that were included in linear regression analyses and ANCOVA analyses are represented in color. The data points that exhibited tailing in MS2 region B, T3 region A and B are represented in grey; these were excluded from the linear regression and ANCOVA analyses.
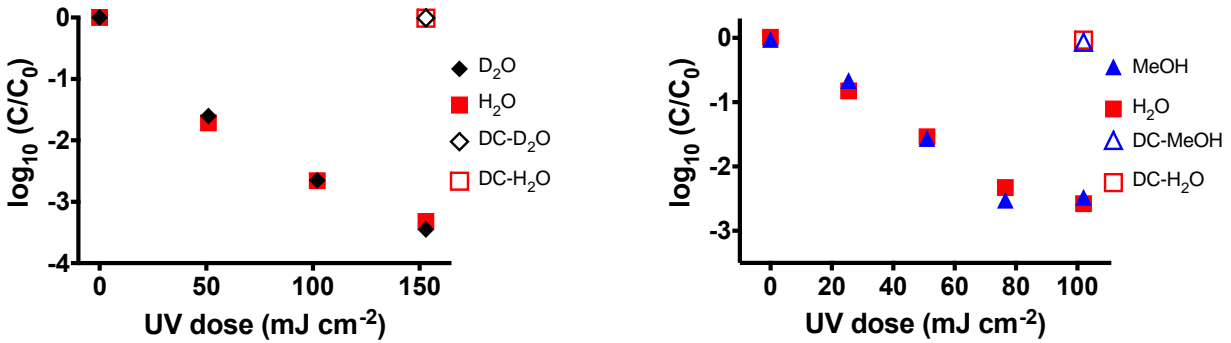
Figure B-2. Experiments to assess the potential role of reactive oxygen species when dsDNA exposed to UV_{254}. Experiments to determine role of $^1O_2$ were conducted in ultrapure water (H_2O) and D_2O (left). Experiments to determine the role of $\cdot OH$ were conducted in ultrapure water (H_2O) and methanol (MeOH; right). Control experiments were conducted in the dark (dark control; DC).

Table B-1. Viruses, primer sets, and the target genome regions utilized in this study.

Virus	Genome accession #	Regions analyzed	Direction	Primer sequence (5' to 3')	Region size (bases or base pairs)	Region location
MS2 (ssRNA)	JQ966307	Region A	F	TTTGGCCTGGTTGTCGTCTC	496 b	944 to 1439
			R	TAATCCATTCAGCGACCCCG		
		Region B	F	ACCTTTGAGCTAGAGTCCATGA	497 b	2693 to 3189
			R	TGAAAGTGAGAGAGGGTGCG		
φ6 (dsRNA)	NC_003714 (S) NC_003716 (M) NC_003715 (L)	Region A	F	GCAGACCCAGCTGACTTCTT	499 bp	S1141 to S1639
			R	AAGGCGCTATCCTTGGACAC		
		Region B	F	GCCTACCAGCTCCACCAAAT	484 bp	L1510 to L1993
			R	CGTACCCCATGTTGAGCAGT		
φX174 (ssDNA)	NC_001422	Region A	F	GTACGCTGGACTTTGTGGGA	504 b	571 to 1074
			R	ATCTGACCAGCAAGGAAGCC		
		Region B	F	GCGCTCTAATCTCTGGGCAT	493 b	1717 to 2209

			F	AACGCAAGGTCAAACGCATC		
T3 (dsDNA)	NC_003298	Region A	R	CTGCATGACGCTGAATGTCG	509 bp	1678 to 2186
		Region B	F	GAGACGACACGTTCCACCTT	499 bp	11826 to 12324
			R	TCTCCTTCTCCGCCAGTGTA		

Table B-2. Prediction of photolysis rate constants of reactive bases ($k_{pred,i}$) in different regions using published quantum yields for relevant RNA and DNA reactions. Double strand regions contained approximately twice the number of reactive bases as the single strand regions.

Reaction	Reactive base	Molar Extinction Coefficient at 254 nm (ε_{254}, M⁻¹cm⁻¹)	Quantum yield (Φ, mol eins⁻¹)	Total number in region A (b)	Total number in region B (b)	$k_{pred,i}$, region A[a] (cm² mJ⁻¹)	$k_{pred,i}$, region B[a] (cm² mJ⁻¹)	Quantum yield citations[b]
				ssRNA (MS2)				
C hydrate	C	5518 (CMP)	0.01	127	121	0.034	0.033	[199], [200]
U hydrate	U	7571 (UMP)	0.01	125	141	0.046	0.052	[199], [201]
UU dimer	UU	15140 (UMP-UMP)	0.02	19	32	0.028	0.047	[118], [199], [201]
CC dimer	CC	11040 (CMP-CMP)	Negligible	21	19			[199], [200], [202]
				dsRNA (φ6)				
C hydrate	C	4580 (CMP)	0.003[c]	278	226	0.019	0.015	[203]
U hydrate	U	6284 (UMP)	0.001	221	226	0.0068	0.0069	[106], [201]
UU dimer	UU	12570 (UMP-UMP)	0.004	44	41	0.011	0.010	[106], [201]
CC dimer	CC	9160 (CMP-CMP)	Negligible	60	48			[199], [200], [202]
				ssDNA (φX174)				
C hydrate	C	5410 (dCMP)	0.01	117	114	0.031	0.030	[199], [200]
TT dimer	TT	12210 (TMP-TM)	0.03	36	48	0.065	0.086	[199], [202], [204]
CT dimer	CT	11510 (dCMP-TMP)	0.004[d]	34	40	0.0077	0.0090	[199], [205]-[207]
TC dimer	TC	11510 (TMP-dCMP)	0.02[d]	31	35	0.035	0.039	[199], [205]-[207]
CC dimer	CC	11040 (dCMP-dCMP)	Negligible	19	24			[199], [200], [202]
				dsDNA (T3)				
C hydrate	C	4490 (dCMP)	0.002[c]	271	254	0.012	0.011	[203]
TT dimer	TT	10130 (TMP-TMP)	0.02	46	47	0.046	0.047	[199], [205]-[207]
CT dimer	CT	9556 (dCMP-TMP)	0.004[e]	67	84	0.013	0.016	[199], [205]-[207]
TC dimer	TC	9556 (TMP-dCMP)	0.02[e]	62	59	0.058	0.055	[205]-[207]
CC dimer	CC	9160 (dCMP-dCMP)	Negligible	43	45			[199], [200], [202]

a. $k_{pred,i}$ is the predicted photolysis rate constant of a reactive base, $k_{pred,i} = \frac{2.3}{U} b \cdot \varepsilon_{254} \cdot \Phi$, where $U = 4.7 \times 10^5$ J eins⁻¹.

b. Quantum yields were collected from earlier studies. When multiple quantum yields were found in the literature for the same reaction, the multiple values were averaged.

c. C hydrate quantum yields reported for dsRNA and dsDNA, but UV wavelengths not characterized.

d. These are the same CT and TC quantum yields used for dsDNA. A report suggested that denaturing DNA did not have major impact on the quantum yields of CT and TC [208].

e. Quantum yield data estimated using the relative quantum yields of dsCT and dsTC compared to dsTT, as reported in [142].

Table B-3. Photolysis rate constants based on linear regressions of experimental data presented in Figure S1 (k_{exp}) and based on the predictions presented in Table S2 (k_{pred}).

		ssRNA (MS2)		dsRNA (φ6)	
		Region A	**Region B**	**Region A**	**Region B**
$k_{exp} \pm$ SE	Encapsidated, PBS	0.011 ± 0.001	0.024 ± 0.002	0.0016 ± 0.0002	0.0023 ± 0.0002
	Naked, PBS	0.012 ± 0.001	0.027 ± 0.001	0.0015 ± 0.0003	0.0018 ± 0.0002
	Naked, water	0.029 ± 0.001	0.039 ± 0.001	0.0092 ± 0.0004	0.0083 ± 0.0005
k_{pred}		0.11	0.13	0.036	0.032
		ssDNA (φX174)		dsDNA (T3)	
		Region A	**Region B**	**Region A**	**Region B**
$k_{exp} \pm$ SE	Encapsidated, PBS	0.062 ± 0.003	0.074 ± 0.004	0.035 ± 0.002	0.034 ± 0.001
	Naked, PBS	0.056 ± 0.003	0.071 ± 0.004	0.030 ± 0.001	0.030 ± 0.002
	Naked, water	0.062 ± 0.002	0.075 ± 0.002	0.064 ± 0.002	0.067 ± 0.002
k_{pred}		0.14	0.17	0.13	0.13

Table B-4. P values obtained when comparing the UV_{254} photolysis kinetics of two different regions or two different conditions with ANCOVA analyses. We conducted ANCOVA tests to evaluate the impact of encapsidation (encapsidated nucleic acids in PBS vs. naked nucleic acids in PBS), water chemistry (naked nucleic acids in PBS vs. naked nucleic acids in water), different regions of the same genome (region A vs. region B), and different genome types (ssRNA vs. ssDNA; dsRNA vs. dsDNA). Statistical tests were not conducted on ssDNA vs. dsDNA and ssRNA vs. ds RNA because these sequences contained different numbers of bases.

		ssRNA (MS2)						dsRNA (φ6)						ssDNA (φX174)						dsDNA (T3)					
		Encap A	Water A	PBS A	Encap B	Water B	PBS B	Encap A	Water A	PBS A	Encap B	Water B	PBS B	Encap A	Water A	PBS A	Encap B	Water B	PBS B	Encap A	Water A	PBS A	Encap B	Water B	PBS B
ssRNA (MS2)	Encap A			0.084	<1E-4																				
	Water A			<1E-4		0.001																			
	PBS A	0.084	<1E-4				<1E-4																		
	Encap B	<1E-4					0.095																		
	Water B		0.001				<1E-4																		
	PBS B			<1E-4	0.095	<1E-4																			
dsRNA (φ6)	Encap A									0.883	0.005														
	Water A									<1E-4		0.153													
	PBS A							0.883	<1E-4				0.456												
	Encap B							0.005					0.050												
	Water B								0.153				<1E-4												

103

	PBS B									0.456	0.050	<1E-4													
ssDNA (φX174)	Encap A	<1E-4			<1E-4											0.171	0.016								
	Water A		<1E-4			<1E-4										0.041		<1E-4							
	PBS A			<1E-4			<1E-4							0.171	0.041				0.001						
	Encap B	<1E-4			<1E-4									0.016					0.596						
	Water B		<1E-4			<1E-4									<1E-4				0.351						
	PBS B			<1E-4			<1E-4									0.001	0.596	0.351							
dsDNA (T3)	Encap A							<1E-4			<1E-4											0.034	0.449		
	Water A								<1E-4			<1E-4											<1E-4		0.317	
	PBS A									<1E-4			<1E-4							0.034	<1E-4				0.785
	Encap B							<1E-4			<1E-4									0.449					0.047
	Water B								<1E-4			<1E-4									0.317				<1E-4
	PBS B									<1E-4			<1E-4									0.785	0.047	<1E-4	

Table B-5. Photolysis rate constants of encapsidated viral nucleic acids and naked plasmids by UV$_{254}$ reported previously in the literature. In those studies, genome reactions were measured by qPCR or RT-qPCR methods.

	Amplicon size	Base number[*]	Rate constant per base ($cm^2 mJ^{-1} base^{-1}$)	Reference
ssDNA				
φX174	108	108	1.60E-04	[161]
	250	250	1.56E-04	
	456	456	1.50E-04	
	568	568	1.52E-04	
	955	955	1.91E-04	
	1125	1,125	1.97E-04	
	1546	1,546	1.97E-04	
	1764	1,764	2.26E-04	
dsDNA				
Human adenovirus 2	1100	2200	1.14E-05	[162]
Human adenovirus 2	106	212	7.1E-06	[167]
JC polyomavirus	88	176	3.41E-05	[111]
Human adenovirus 2	68	136	1.47E-05	
ssRNA				
MS2	335	335	2.75E-05	[20]
	303	303	5.61E-05	
	289	289	3.36E-05	
	317	317	4.73E-05	
	309	309	4.53E-05	
MS2	81	81	1.73E-05	[163]
	111	111	1.80E-05	
	111	111	2.52E-05	
	692	692	9.54E-06	
	1298	1298	6.55E-06	
	1909	1909	1.00E-05	
MS2	1185	1185	3.88E-05	[119]
	2169	2169	2.67E-05	
Poliovirus 1	76	76	4.08E-05	[163]
	145	145	3.79E-05	
Noroviurs GI.1	157	157	5.80E-05	[164]
dsRNA				
φ6	499	998	2.40E-06	[166]
	472	944	1.27E-06	
	484	968	2.48E-06	
Rotavirus SA11	318	636	1.56E-05	[160]
Naked dsDNA (plasmid)				
bla_{TEM-1} (pWH1266)	209	418	1.32E-05	[151]
	861	1722	3.95E-05	
$tetA$ (pWH1266)	216	432	9.26E-06	
	1200	2400	2.42E-05	

amp^R (pUC4k)	850	1700	6.47E-05	
kan^R (pUC4k)	806	1612	9.31E-05	[165]
amp^R (pUC4k)	850	1700	5.88E-05	
kan^R (pUC4k)	806	1612	8.06E-05	

*For dsDNA and dsRNA genomes, base numbers are two times of the amplicon sizes; for ssDNA and ssRNA, base numbers are the same with the amplicon sizes.

Bibliography

[1]   R. D. Smith, "Responding to global infectious disease outbreaks: Lessons from SARS on the role of risk perception, communication and management," *Social Science & Medicine*, vol. 63, no. 12, pp. 3113–3123, Dec. 2006.

[2]   "The Global Risks Report 2016 11th Edition," World Economic Forum, Jan. 2016.

[3]   N. P. Johnson and J. Mueller, "Updating the accounts: global mortality of the 1918-1920' Spanish' influenza pandemic," *Bulletin of the History of Medicine*, pp. 105–115, 2002.

[4]   N.-A. M. Molinari, I. R. Ortega-Sanchez, M. L. Messonnier, W. W. Thompson, P. M. Wortley, E. Weintraub, and C. B. Bridges, "The annual impact of seasonal influenza in the US: Measuring disease burden and costs," *Vaccine*, vol. 25, no. 27, pp. 5086–5096, Jun. 2007.

[5]   E. Scallan, R. M. Hoekstra, F. J. Angulo, R. V. Tauxe, M.-A. Widdowson, S. L. Roy, J. L. Jones, and P. M. Griffin, "Foodborne Illness Acquired in the United States—Major Pathogens," *Emerging Infectious Diseases*, vol. 17, no. 1, pp. 7–15, Jan. 2011.

[6]   A. J. Hall, J. Vinjé, B. Lopman, G. W. Park, C. Yen, N. Gregoricus, and U. Parashar, "Updated norovirus outbreak management and disease prevention guidelines," *Morbidity and Mortality Weekly Report: Recommendations and Reports*, vol. 60, no. 3, pp. 1–15, 2011.

[7]   N. Pica and N. M. Bouvier, "Environmental factors affecting the transmission of respiratory viruses," *Current Opinion in Virology*, vol. 2, no. 1, pp. 90–95, Feb. 2012.

[8]   K. R. Wigginton, Y. Ye, and R. M. Ellenberg, "Emerging investigators series: the source and fate of pandemic viruses in the urban water cycle," *Environmental Science: Water Research & Technology*, vol. 1, no. 6, pp. 735–746, 2015.

[9]   D. Rodríguez-Lázaro, N. Cook, F. M. Ruggeri, J. Sellwood, A. Nasser, M. S. J. Nascimento, M. D'Agostino, R. Santos, J. C. Saiz, A. Rzeżutka, A. Bosch, R. Girones, A. Carducci, M. Muscillo, K. Kovač, M. Diez-Valcarce, A. Vantarakis, C.-H. von Bonsdorff, A. M. de Roda Husman, M. Hernández, and W. H. M. van der Poel, "Virus hazards from food, water and other contaminated environments," *FEMS Microbiol. Rev.*, vol. 36, no. 4, pp. 786–814, Jul. 2012.

[10]   S. A. Boone and C. P. Gerba, "Significance of Fomites in the Spread of Respiratory and Enteric Viral Disease," *Appl. Environ. Microbiol.*, vol. 73, no. 6, pp. 1687–1696, Mar. 2007.

[11]   H. R. Gelderblom, "Structure and Classification of Viruses," in *Medical Microbiology.*

4th edition, University of Texas Medical Branch at Galveston, 1996.

[12] S. J. Flint, L. W. Enquist, V. R. Racaniello, and A. M. Skalka, "Principles of Virology: Vol. 1. Molecular Biology.," 2009.

[13] J. Simonet and C. Gantzer, "Degradation of the Poliovirus 1 genome by chlorine dioxide," *J. Appl. Microbiol.*, vol. 100, no. 4, pp. 862–870, Apr. 2006.

[14] G. W. Park, K. G. Linden, and M. D. Sobsey, "Inactivation of murine norovirus, feline calicivirus and echovirus 12 as surrogates for human norovirus (NoV) and coliphage (F+) MS2 by ultraviolet light (254 nm) and the effect of cell association on UV inactivation," *Letters in Applied Microbiology*, vol. 52, no. 2, pp. 162–167, Feb. 2011.

[15] J. K. Choe, D. H. Richards, C. J. Wilson, and W. A. Mitch, "Degradation of Amino Acids and Structure in Model Proteins and Bacteriophage MS2 by Chlorine, Bromine, and Ozone," *Environ. Sci. Technol.*, vol. 49, no. 22, pp. 13331–13339, Nov. 2015.

[16] W. A. Rutala, S. L. Barbee, N. C. Aguiar, M. D. Sobsey, and D. J. Weber, "Antimicrobial Activity of Home Disinfectants and Natural Products Against Potential Human Pathogens," *Infection Control & Hospital Epidemiology*, vol. 21, no. 1, pp. 33–38, 2000.

[17] National Research Council and S. D. W. Committee, "The disinfection of drinking water," 1980.

[18] G. McDonnell and A. D. Russell, "Antiseptics and Disinfectants: Activity, Action, and Resistance," *Clin. Microbiol. Rev.*, vol. 12, no. 1, pp. 147–179, Jan. 1999.

[19] K. R. Wigginton and T. Kohn, "Virus disinfection mechanisms: the role of virus composition, structure, and function," *Current Opinion in Virology*, vol. 2, no. 1, pp. 84–89, Feb. 2012.

[20] K. R. Wigginton, B. M. Pecson, T. Sigstam, F. Bosshard, and T. Kohn, "Virus inactivation mechanisms: impact of disinfectants on virus function and structural integrity," *Environ. Sci. Technol.*, vol. 46, no. 21, pp. 12069–12078, Nov. 2012.

[21] A. M. Gall, J. L. Shisler, and B. J. Mariñas, "Analysis of the Viral Replication Cycle of Adenovirus Serotype 2 after Inactivation by Free Chlorine," *Environ. Sci. Technol.*, vol. 49, no. 7, pp. 4584–4590, Mar. 2015.

[22] M. A. Page, J. L. Shisler, and B. J. Mariñas, "Mechanistic Aspects of Adenovirus Serotype 2 Inactivation with Free Chlorine," *Appl. Environ. Microbiol.*, vol. 76, no. 9, pp. 2946–2954, May 2010.

[23] J. W. Li, Z. T. Xin, X. W. Wang, J. L. Zheng, and F. H. Chao, "Mechanisms of inactivation of hepatitis a virus by chlorine.," *Appl. Environ. Microbiol.*, vol. 68, no. 10, pp. 4951–4955, Oct. 2002.

[24] C. L. H. and and M. J. Davies, "Hypochlorite-Induced Damage to Nucleosides: Formation of Chloramines and Nitrogen-Centered Radicals," *Chem. Res. Toxicol.*, vol. 14, no. 8, pp. 1071–1081, Jul. 2001.

[25] C. Badouard, M. Masuda, H. Nishino, J. Cadet, A. Favier, and J.-L. Ravanat, "Detection of chlorinated DNA and RNA nucleosides by HPLC coupled to tandem

mass spectrometry as potential biomarkers of inflammation," *Journal of Chromatography B*, vol. 827, no. 1, pp. 26–31, Nov. 2005.

[26]   T. P. A. Devasagayam, S. Steenken, M. S. W. Obendorf, W. A. Schulz, and H. Sies, "Formation of 8-hydroxy(deoxy)guanosine and generation of strand breaks at guanine residues in DNA by singlet oxygen," *Biochemistry*, vol. 30, no. 25, pp. 6283–6289, May 2002.

[27]   E. Kvam, K. Berg, and H. B. Steen, "Characterization of singlet oxygen-induced guanine residue damage after photochemical treatment of free nucleosides and DNA," *BBA-Gene Struct. Expr.*, vol. 1217, no. 1, pp. 1–8, Jan. 1994.

[28]   J. Cadet, M. Berger, T. Douki, B. Morin, and S. Raoul, "Effects of UV and visible radiation on DNA-final base damage.," *Biol. Chem.*, vol. 378, no. 11, pp. 1275–1286, 1997.

[29]   J.-L. Ravanat, G. R. Martinez, M. H. G. Medeiros, P. Di Mascio, and J. Cadet, "Mechanistic aspects of the oxidation of DNA constituents mediated by singlet molecular oxygen," *Arch. Biochem. Biophys.*, vol. 423, no. 1, pp. 23–30, Mar. 2004.

[30]   E. J. Wurtmann and S. L. Wolin, "RNA under attack: Cellular handling of RNA damage," *Critical Reviews in Biochemistry and Molecular Biology*, vol. 44, no. 1, pp. 34–49, Feb. 2009.

[31]   S. Nuanualsuwan and D. O. Cliver, "Capsid Functions of Inactivated Human Picornaviruses and Feline Calicivirus," *Appl. Environ. Microbiol.*, vol. 69, no. 1, pp. 350–357, Jan. 2003.

[32]   W. A. Rutala and D. J. Weber, "Uses of inorganic hypochlorite (bleach) in health-care facilities.," *Clin. Microbiol. Rev.*, vol. 10, no. 4, pp. 597–610, Oct. 1997.

[33]   K. P. Cantor, "Water chlorination, mutagenicity, and cancer epidemiology.," *American Journal of Public Health*, vol. 84, no. 8, pp. 1211–1213, 1994.

[34]   R. D. Morris, A. M. Audet, I. F. Angelillo, T. C. Chalmers, and F. Mosteller, "Chlorination, chlorination by-products, and cancer: a meta-analysis.," *American Journal of Public Health*, vol. 82, no. 7, pp. 955–963, Oct. 2011.

[35]   C. M. Villanueva, K. P. Cantor, S. Cordier, J. J. K. Jaakkola, W. D. King, C. F. Lynch, S. Porru, and M. Kogevinas, "Disinfection Byproducts and Bladder Cancer," *Epidemiology*, vol. 15, no. 3, pp. 357–367, 2004.

[36]   USEPA (US Environmental Protection Agency), "National Primary Drinking Water Regulations: Stage 2 Disinfectants and Disinfection Byproducts Rule: Final Rule," *Fed. Reg.*, vol. 71, no. 2, p. 388, 2006.

[37]   C. J. Seidel, M. J. McGuire, R. S. Summers, and S. Via, "Have utilities switched to chloramines?," *Journal - American Water Works Association*, vol. 97, no. 10, pp. 87–97, Oct. 2005.

[38]   G. Hua and D. A. Reckhow, "Comparison of disinfection byproduct formation from chlorine and alternative disinfectants," *Water Res.*, vol. 41, no. 8, pp. 1667–1678, Apr. 2007.

[39]   B. R. Kim, J. E. Anderson, S. A. Mueller, W. A. Gaines, and A. M. Kendall, "Literature review—efficacy of various disinfectants against Legionella in water systems," *Water Res.*, vol. 36, no. 18, pp. 4433–4444, Nov. 2002.

[40]   Y. E. Lin, J. E. Stout, and V. L. Yu, "Controlling Legionella in Hospital Drinking Water: An Evidence-Based Review of Disinfection Methods," *Infection Control & Hospital Epidemiology*, vol. 32, no. 2, pp. 166–173, Feb. 2011.

[41]   G. Bitton, *Microbiology of Drinking Water Production and Distribution*. John Wiley & Sons, 2014.

[42]   V. W. Riesser, J. R. Perrich, B. B. Silver, and J. R. McCammon, "Possible mechanisms of poliovirus inactivation by ozone," pp. 186–192, 1977.

[43]   G.-A. Shin and M. D. Sobsey, "Reduction of Norwalk Virus, Poliovirus 1, and Bacteriophage MS2 by Ozone Disinfection of Water," *Appl. Environ. Microbiol.*, vol. 69, no. 7, pp. 3975–3978, Jul. 2003.

[44]   S. Chowdhury, M. J. Rodriguez, and R. Sadiq, "Disinfection byproducts in Canadian provinces: Associated cancer risks and medical expenses," *Journal of Hazardous Materials*, vol. 187, no. 1, pp. 574–584, Mar. 2011.

[45]   P. C. Singer, "Control of disinfection by-products in drinking water," *Journal of environmental engineering*, vol. 120, no. 4, pp. 727–744, 1994.

[46]   D. S. Blanc, P. Carrara, G. Zanetti, and P. Francioli, "Water disinfection with ozone, copper and silver ions, and temperature increase to control Legionella: seven years of experience in a university teaching hospital," *Journal of Hospital Infection*, vol. 60, no. 1, pp. 69–72, May 2005.

[47]   L. C. Simões and M. Simões, "Biofilms in drinking water : problems and solutions," *RSC Advances*, vol. 3, no. 8, pp. 2520–2533, 2013.

[48]   R. J. Davis-Colley, A. M. Donnison, and D. J. Speed, "Towards a mechanistic understanding of pond disinfection," *Water Sci. Technol.*, vol. 42, no. 10, pp. 149–158, Nov. 2000.

[49]   J. Jagger, "Solar-UV actions on living cells," Jan. 1985.

[50]   T. Kohn and K. L. Nelson, "Sunlight-mediated inactivation of MS2 coliphage via exogenous singlet oxygen produced by sensitizers in natural waters," *Environ. Sci. Technol.*, vol. 41, no. 1, pp. 192–197, Dec. 2006.

[51]   L. W. Sinton, C. H. Hall, P. A. Lynch, and R. J. Davies-Colley, "Sunlight inactivation of fecal indicator bacteria and bacteriophages from waste stabilization pond effluent in fresh and saline waters.," *Appl. Environ. Microbiol.*, vol. 68, no. 3, pp. 1122–1131, Mar. 2002.

[52]   K. R. Wigginton, L. Menin, T. Sigstam, G. Gannon, M. Cascella, H. B. Hamidane, Y. O. Tsybin, P. Waridel, and T. Kohn, "UV radiation induces genome-mediated, site-specific cleavage in viral proteins," *ChemBioChem*, vol. 13, no. 6, pp. 837–845, Apr. 2012.

[53]   W. J. Cooper, R. G. Zika, R. G. Petasne, and A. M. Fischer, "Sunlight-induced photochemistry of humic substances in natural waters: major reactive species," *Aquatic Humic Substances: Influence on Fate and Treatment of Pollutants. American Chemical Society, Washington DC. 1989. p 333-362, 6 fig, 5 tab, 136 ref.*, 1989.

[54]   T. P. Curtis, D. D. Mara, and S. A. Silva, "Influence of pH, Oxygen, and Humic Substances on Ability of Sunlight To Damage Fecal Coliforms in Waste Stabilization Pond Water.," *Appl. Environ. Microbiol.*, vol. 58, no. 4, pp. 1335–1343, Apr. 1992.

[55]   R. B. Thurman and C. P. Gerba, "Molecular mechanisms of viral inactivation by water disinfectants ," *Adv. Appl. Microbiol.*, vol. 33, pp. 75–105, 1988.

[56]   B. M. Pecson, M. Ackermann, and T. Kohn, "Framework for using quantitative PCR as a nonculture based method to estimate virus infectivity," *Environ. Sci. Technol.*, vol. 45, no. 6, pp. 2257–2263, Mar. 2011.

[57]   A. C. Eischeid and K. G. Linden, "Molecular indications of protein damage in adenoviruses after UV disinfection.," *Appl. Environ. Microbiol.*, vol. 77, no. 3, pp. 1145–1147, Feb. 2011.

[58]   M. Barbatti, A. Aquino, and J. J. Szymczak, "Relaxation mechanisms of UV-photoexcited DNA and RNA nucleobases," *Proc. Natl. Acad. Sci. U.S.A.*, vol. 107, no. 50, pp. 21453–21458, 2010.

[59]   J. Cadet, E. Sage, and T. Douki, "Ultraviolet radiation-mediated damage to cellular DNA," *Mutat. Res.-Fund. Mol. M.*, vol. 571, no. 1, pp. 3–17, Apr. 2005.

[60]   J. Cadet, C. Anselmino, T. Douki, and L. Voituriez, "New trends in photobiology: Photochemistry of nucleic acids in cells," vol. 15, no. 4, pp. 277–298, Sep. 1992.

[61]   M. H. Patrick and J. M. Snow, "Studies on thymine-derived UV photo-products in DNA—ii. a comparative analysis of damage caused by 254 nm irradiation and triplet-state photosensitization," *Photochem. Photobiol.*, vol. 25, no. 4, pp. 373–384, 1977.

[62]   R. B. Setlow and J. K. Setlow, "EVIDENCE THAT ULTRAVIOLET-INDUCED THYMINE DIMERS IN DNA CAUSE BIOLOGICAL DAMAGE," *Proc. Natl. Acad. Sci. U.S.A.*, vol. 48, no. 7, pp. 1250–1257, Jul. 1962.

[63]   L. S. Kan, L. Voituriez, and J. Cadet, "The Dewar valence isomer of the (6-4) photoadduct of thymidylyl-(3′–5′)-thymidine monophosphate: Formation, alkaline lability and conformations properties," *J. Photoch. Photobio. B*, vol. 12, no. 4, pp. 339–357, 1992.

[64]   D. L. Mitchell, L. A. Applegate, and R. S. Nairn, "Photoreactivation of cyclobutane dimers and (6-4) photoproducts in the epidermis of the marsupial, Monodelphis domestica.," *Photochem. Photobiol.*, vol. 51, no. 6, pp. 653–658, 1990.

[65]   J. L. Ravanat, T. Douki, and J. Cadet, "UV damage to nucleic acid components," *Compr. Seri. Photosci.*, vol. 3, pp. 207–230, 2001.

[66]   E. C. Friedberg and G. C. Walker, *DNA repair and mutagenesis*. Trends in …, 1995.

[67]   M. D. Weitzman, C. T. Carson, R. A. Schwartz, and C. E. Lilley, "Interactions of

viruses with the cellular DNA repair machinery," *DNA Repair*, vol. 3, no. 8, pp. 1165–1173, Aug. 2004.

[68]   C. D. Lytle, S. A. Aaronson, and E. Harvey, "Host-cell Reactivation in Mammalian Cells," *International Journal of Radiation Biology and Related Studies in Physics, Chemistry and Medicine*, vol. 22, no. 2, pp. 159–165, Aug. 2009.

[69]   R. E. Raudales, J. L. Parke, C. L. Guy, and P. R. Fisher, "Control of waterborne microbes in irrigation: A review," *Agricultural Water Management*, vol. 143, pp. 9–28, Sep. 2014.

[70]   N. Okafor, "Environmental microbiology of Aquatic and waste systems," Department of Biological Sciences, Clemson University, Clemson, 29634, South Carolina, USA. Publisher," 2011.

[71]   D. Pūle, "Conventional and Alternative Disinfection Methods of Legionella in Water Distribution Systems – Review," *Construction Science*, vol. 19, no. 1, pp. 21–26, Dec. 2016.

[72]   A. Fraisse, S. Temmam, N. Deboosere, L. Guillier, A. Delobel, P. Maris, M. Vialette, T. Morin, and S. Perelle, "Comparison of chlorine and peroxyacetic-based disinfectant to inactivate Feline calicivirus, Murine norovirus and Hepatitis A virus on lettuce," *Int. J. Food Microbiol.*, vol. 151, no. 1, pp. 98–104, Nov. 2011.

[73]   R. S. Fujioka and B. S. Yoneyama, "Sunlight inactivation of human enteric viruses and fecal bacteria," *Water Sci. Technol.*, vol. 46, no. 11, pp. 291–295, Dec. 2002.

[74]   A. I. Silverman, B. M. Peterson, A. B. Boehm, K. McNeill, and K. L. Nelson, "Sunlight inactivation of human viruses and bacteriophages in coastal waters containing natural photosensitizers," *Environ. Sci. Technol.*, vol. 47, no. 4, pp. 1870–1878, Feb. 2013.

[75]   W. P. Rowe, W. E. Pugh, and J. W. Hartley, "Plaque assay techniques for murine leukemia viruses," *Virology*, vol. 42, no. 4, pp. 1136–1139, 1970.

[76]   S. J. Martin, *The Biochemistry of Viruses*. CUP Archive, 1978.

[77]   A. Yakimovich, V. Andriasyan, R. Witte, I.-H. Wang, V. Prasad, M. Suomalainen, and U. F. Greber, "Plaque2.0—A High-Throughput Analysis Framework to Score Virus-Cell Transmission and Clonal Cell Expansion," *PLOS ONE*, vol. 10, no. 9, p. e0138760, Sep. 2015.

[78]   E. S. Koo, C.-H. Yoo, Y. Na, S. Y. Park, H. R. Lyoo, and Y. S. Jeong, "Reliability of non-culturable virus monitoring by PCR-based detection methods in environmental waters containing various concentrations of target RNA," *J Microbiol.*, vol. 50, no. 5, pp. 726–734, Nov. 2012.

[79]   N. Albinana-Gimenez, M. P. Miagostovich, B. Calgua, J. M. Huguet, L. Matia, and R. Girones, "Analysis of adenoviruses and polyomaviruses quantified by qPCR as indicators of water quality in source and drinking-water treatment plants," *Water Res.*, vol. 43, no. 7, pp. 2011–2019, Apr. 2009.

[80]   M. Kitajima, B. C. Iker, I. L. Pepper, and C. P. Gerba, "Relative abundance and

treatment reduction of viruses during wastewater treatment processes — Identification of potential viral indicators," *Sci. Total Environ.*, vol. 488, pp. 290–296, Aug. 2014.

[81]   J. M. S. Bartlett and D. Stirling, *A Short History of the Polymerase Chain Reaction*. 2003, pp. 3–6.

[82]   J. Logan, J. M. Logan, K. J. Edwards, and N. A. Saunders, "Real-time PCR: current technology and applications," 2009.

[83]   B. M. Pecson, L. V. Martin, and T. Kohn, "Quantitative PCR for determining the infectivity of bacteriophage MS2 upon inactivation by heat, UV-B radiation, and singlet oxygen: advantages and limitations of an enzymatic treatment to reduce false-positive results," *Appl. Environ. Microbiol.*, vol. 75, no. 17, pp. 5544–5554, Aug. 2009.

[84]   Y. M. D. Lo, S.-F. Leung, L. Y. S. Chan, A. T. C. Chan, K.-W. Lo, P. J. Johnson, and D. P. Huang, "Kinetics of Plasma Epstein-Barr Virus DNA during radiation therapy for nasopharyngeal carcinoma," *Cancer Res.*, vol. 60, no. 9, pp. 2351–2355, May 2000.

[85]   Y. S. Ahi and S. K. Mittal, "Components of Adenovirus Genome Packaging," *Front. Microbiol.*, vol. 7, no. 318, p. 1325, Sep. 2016.

[86]   J. T. Watson and O. D. Sparkman, *Introduction to Mass Spectrometry*. John Wiley & Sons, 2013.

[87]   B. Thomas and A. V. Akoulitchev, "Mass spectrometry of RNA," *Trends in Biochemical Sciences*, vol. 31, no. 3, pp. 173–181, Mar. 2006.

[88]   M. Kullolli, E. Knouf, M. Arampatzidou, M. Tewari, and S. J. Pitteri, "Intact MicroRNA Analysis Using High Resolution Mass Spectrometry," *J. Am. Soc. Mass Spectrom.*, vol. 25, no. 1, pp. 80–87, Oct. 2013.

[89]   D. Su, C. T. Y. Chan, C. Gu, K. S. Lim, Y. H. Chionh, M. E. McBee, B. S. Russell, I. R. Babu, T. J. Begley, and P. C. Dedon, "Quantitative analysis of ribonucleoside modifications in tRNA by HPLC-coupled mass spectrometry," *Nat Protoc*, vol. 9, no. 4, pp. 828–841, Mar. 2014.

[90]   E. Nordhoff, F. Kirpekar, and P. Roepstorff, "Mass spectrometry of nucleic acids," *Mass Spectrometry Reviews*, vol. 15, no. 2, pp. 67–138, Jan. 1996.

[91]   Z. Qiao and K. R. Wigginton, "Direct and indirect photochemical reactions in viral RNA measured with RT-qPCR and mass spectrometry," *Environ. Sci. Technol.*, vol. 50, no. 24, pp. 13371–13379, Nov. 2016.

[92]   Z. M. and and P. A. Limbach, "Quantitation of Ribonucleic Acids Using 18O Labeling and Mass Spectrometry," *Anal. Chem.*, vol. 77, no. 6, pp. 1891–1895, Feb. 2005.

[93]   S. Sun, "Analysis and quantification of oligonucleotides," *AB SCIEX Technical Note*, pp. 1–2, 2010.

[94]   R. T. O'Brien and J. Newman, "Structural and compositional changes associated with chlorine inactivation of polioviruses.," *Appl. Environ. Microbiol.*, vol. 38, no. 6, pp. 1034–1039, Dec. 1979.

[95]   D. Roy, P. K. Wong, R. S. Engelbrecht, and E. S. Chian, "Mechanism of enteroviral inactivation by ozone.," *Appl. Environ. Microbiol.*, vol. 41, no. 3, pp. 718–723, Mar. 1981.

[96]   C. K. Kim, D. M. Gentile, and O. J. Sproul, "Mechanism of Ozone Inactivation of Bacteriophage f2," *Appl. Environ. Microbiol.*, vol. 39, no. 1, pp. 210–218, Jan. 1980.

[97]   T. Sigstam, A. Rohatschek, Q. Zhong, M. Brennecke, and T. Kohn, "On the cause of the tailing phenomenon during virus disinfection by chlorine dioxide," *Water Res.*, vol. 48, no. C, pp. 82–89, Jan. 2014.

[98]   E. A. Permyakov, S. E. Permyakov, G. Y. Deikus, L. A. Morozova Roche, V. M. Grishchenko, L. P. Kalinichenko, and V. N. Uversky, "Ultraviolet illumination-induced reduction of α-lactalbumin disulfide bridges," *Proteins: Structure, Function, and Bioinformatics*, vol. 51, no. 4, pp. 498–503, Jun. 2003.

[99]   V. G. Artiukhov, V. V. Gusinskaia, and E. A. Dvurekova, "UV-Light induced structural and functional changes of protein C4 of the complement system," *Biofizika*, 2006.

[100]   C. Prinsze, T. M. A. R. Dubbelman, and J. Van Steveninck, "Protein damage, induced by small amounts of photodynamically generated singlet oxygen or hydroxyl radicals," *Biochimica et Biophysica Acta (BBA) - Protein Structure and Molecular Enzymology*, vol. 1038, no. 2, pp. 152–157, Apr. 1990.

[101]   W. H. Dennis, V. P. Olivieri, and C. W. Krusé, "Mechanism of disinfection: Incorporation of Cl-36 into f2 virus," *Water Res.*, vol. 13, no. 4, pp. 363–369, 1979.

[102]   A. K. da Silva, J. C. Le Saux, and S. Parnaudeau, "Evaluation of removal of noroviruses during wastewater treatment, using real-time reverse transcription-PCR: different behaviors of genogroups I and II," *Applied and ...*, 2007.

[103]   M. Kertesz, Y. Wan, E. Mazor, J. L. Rinn, R. C. Nutter, H. Y. Chang, and E. Segal, "Genome-wide measurement of RNA secondary structure in yeast," *Nature*, vol. 467, no. 7311, pp. 103–107, Sep. 2010.

[104]   M. McCullagh, M. Hariharan, F. D. Lewis, D. Markovitsi, T. Douki, and G. C. Schatz, "Conformational control of TT dimerization in DNA conjugates. A molecular dynamics study," *J. Phys. Chem. B.*, vol. 114, no. 15, pp. 5215–5221, Mar. 2010.

[105]   Z. Pan, M. Hariharan, J. D. Arkin, A. S. Jalilov, M. McCullagh, G. C. Schatz, and F. D. Lewis, "Electron donor–acceptor interactions with flanking purines influence the efficiency of thymine photodimerization," *J. Am. Chem. Soc.*, vol. 133, no. 51, pp. 20793–20798, Dec. 2011.

[106]   M. Pearson and H. E. Johns, "Suppression of hydrate and dimer formation in ultraviolet-irradiated poly (A + U) relative to poly U," *J. Mol. Biol.*, vol. 20, no. 2, pp. 215–229, Sep. 1966.

[107]   A. D. McLaren and W. N. Takahashi, "Inactivation of infectious nucleic acid from tobacco mosaic virus by ultraviolet light (2537 A)," *Radiat. Res.*, vol. 6, no. 5, p. 532, 1957.

[108] W. Harm, "Biological effects of ultraviolet radiation," *Int. Union Pure Appl. Bio*, vol. 1, 1980.

[109] J. Cadet and R. Teoule, "Comparative study of oxidation of nucleic acid components by hydroxyl radicals, singlet oxygen and superoxide anion radicals," *Photochem. Photobiol.*, vol. 28, no. 4, pp. 661–665, Oct. 1978.

[110] A. Steen Steenken and S. V. Jovanovic, "How easily oxidizable is DNA? One-electron reduction potentials of adenosine and guanosine radicals in aqueous solution," *J. Am. Chem. Soc.*, vol. 119, no. 3, pp. 617–618, Jan. 1997.

[111] B. Calgua, A. Carratalà, L. Guerrero-Latorre, A. de Abreu Corrêa, T. Kohn, R. Sommer, and R. Girones, "UVC inactivation of dsDNA and ssRNA viruses in water: UV fluences and a qPCR-based approach to evaluate decay on viral infectivity," *Food Environ. Virol.*, vol. 6, no. 4, pp. 260–268, 2014.

[112] D. J. Lane, B. Pace, G. J. Olsen, D. A. Stahl, M. L. Sogin, and N. R. Pace, "Rapid determination of 16S ribosomal RNA sequences for phylogenetic analyses.," *Proc. Natl. Acad. Sci. U.S.A.*, vol. 82, no. 20, pp. 6955–6959, Oct. 1985.

[113] R. O. Rahn, "Potassium iodide as a chemical actinometer for 254 nm radiation: use of iodate as an electron scavenger," *Photochem. Photobiol.*, vol. 66, no. 6, pp. 885–885, Dec. 1997.

[114] C. Chen, D. A. Ridzon, A. J. Broomer, Z. Zhou, D. H. Lee, J. T. Nguyen, M. Barbisin, N. L. Xu, V. R. Mahuvakar, M. R. Andersen, K. Q. Lao, K. J. Livak, and K. J. Guegler, "Real-time quantification of microRNAs by stem-loop RT-PCR.," *Nucleic Acids Res.*, vol. 33, no. 20, pp. e179–e179, 2005.

[115] J.-L. Ravanat, T. Douki, and J. Cadet, "Direct and indirect effects of UV radiation on DNA and its components," vol. 63, no. 1, pp. 88–102, Oct. 2001.

[116] "FRAMEWORKS FOR ASSESSING RELIABILITY OF MULTIPLE, WATER REUSE," pp. 1–8, Feb. 2015.

[117] R. L. Miller and P. Plagemann, "Effect of ultraviolet light on mengovirus: formation of uracil dimers, instability and degradation of capsid, and covalent linkage of protein to viral RNA," *J. Virol.*, vol. 13, no. 3, pp. 729–739, 1974.

[118] P. A. Swenson and R. B. Setlow, "Kinetics of dimer formation and photohydration in ultraviolet-irradiated polyuridylic acid," *Photochem. Photobiol.*, vol. 2, no. 4, pp. 419–434, Oct. 1963.

[119] S. E. Beck, R. A. Rodríguez, M. A. Hawkins, T. M. Hargy, T. C. Larason, and K. G. Linden, "Comparison of UV-induced inactivation and RNA damage in MS2 phage across the germicidal UV spectrum," *Appl. Environ. Microbiol.*, vol. 82, no. 5, pp. 1468–1474, Mar. 2016.

[120] T. Climent, I. González-Ramírez, R. González-Luque, M. Merchán, and L. Serrano-Andrés, "Cyclobutane Pyrimidine Photodimerization of DNA/RNA Nucleobases in the Triplet State," *J. Phys. Chem. Lett.*, vol. 1, no. 14, pp. 2072–2076, Jun. 2010.

[121] H. Görner, "New trends in photobiology: Photochemistry of DNA and related

biomolecules: Quantum yields and consequences of photoionization," vol. 26, no. 2, pp. 117–139, Nov. 1994.

[122] W. J. Schreier, T. E. Schrader, F. O. Koller, P. Gilch, C. E. Crespo-Hernández, V. N. Swaminathan, T. Carell, W. Zinth, and B. Kohler, "Thymine dimerization in DNA is an ultrafast photoreaction," *Science*, vol. 315, no. 5812, pp. 625–629, Feb. 2007.

[123] J. A. Sikorsky, D. A. Primerano, T. W. Fenger, and J. Denvir, "Effect of DNA damage on PCR amplification efficiency with the relative threshold cycle method," *Biochem. Bioph. Res. Co.*, vol. 323, no. 3, pp. 823–830, Oct. 2004.

[124] J. P. McDonald, A. Hall, D. Gasparutto, J. Cadet, J. Ballantyne, and R. Woodgate, "Novel thermostable Y-family polymerases: applications for the PCR amplification of damaged or ancient DNAs." *Nucleic Acids Res.*, vol. 34, no. 4, pp. 1102–1111, 2006.

[125] D. Polo and I. García-Fernández, "Solar water disinfection (SODIS): Impact on hepatitis A virus and on a human Norovirus surrogate under natural solar conditions," *Int. Microbiol.*, vol. 18, no. 1, pp. 41–49, 2015.

[126] F. Bosshard, F. Armand, R. Hamelin, and T. Kohn, "Mechanisms of human adenovirus inactivation by sunlight and UVC light as examined by quantitative PCR and quantitative proteomics." *Appl. Environ. Microbiol.*, vol. 79, no. 4, pp. 1325–1332, Feb. 2013.

[127] A. I. Silverman, M. T. Nguyen, I. E. Schilling, J. Wenk, and K. L. Nelson, "Sunlight inactivation of viruses in open-water unit process treatment wetlands: modeling endogenous and exogenous inactivation rates," *Environ. Sci. Technol.*, vol. 49, no. 5, pp. 2757–2766, Mar. 2015.

[128] T. Kohn, M. J. Mattle, M. Minella, and D. Vione, "A modeling approach to estimate the solar disinfection of viral indicator organisms in waste stabilization ponds and surface waters," *Water Res.*, vol. 88, pp. 912–922, Jan. 2016.

[129] Z. Kuluncsics, D. Perdiz, E. Brulay, B. Muel, and E. Sage, "Wavelength dependence of ultraviolet-induced DNA damage distribution: Involvement of direct or indirect mechanisms and possible artefacts," vol. 49, no. 1, pp. 71–80, Mar. 1999.

[130] D. C. Clagett and T. J. Galen, "Ribonucleoside reactivities with singlet (1Δg) molecular oxygen," *Arch. Biochem. Biophys.*, vol. 146, no. 1, pp. 196–201, Sep. 1971.

[131] X. Gong, R. Tao, and Z. Li, "Quantification of RNA damage by reverse transcription polymerase chain reactions," *Anal. Biochem.*, vol. 357, no. 1, pp. 58–67, Oct. 2006.

[132] F. Wilkinson, W. P. Helman, and A. B. Ross, "Rate constants for the decay and reactions of the lowest electronically excited singlet state of molecular oxygen in solution. An expanded and revised compilation," *J. Phys. Chem. Ref. Data*, vol. 24, no. 2, pp. 663–677, Mar. 1995.

[133] S. Shibutani, M. Takeshita, and A. P. Grollman, "Insertion of specific bases during DNA synthesis past the oxidation-damaged base 8-oxodG," *Nature*, vol. 349, no. 6308, pp. 431–434, Jan. 1991.

[134] C. L. Simms, B. H. Hudson, J. W. Mosior, A. S. Rangwala, and H. S. Zaher, "An

active role for the ribosome in determining the fate of oxidized mRNA," *Cell Reports*, vol. 9, no. 4, pp. 1256–1264, Nov. 2014.

[135]   X. Shan, Y. Chang, and C.-L. G. Lin, "Messenger RNA oxidation is an early event preceding cell death and causes reduced protein expression.," *FASEB J.*, vol. 21, no. 11, pp. 2753–2764, Sep. 2007.

[136]   X. Shan, H. Tashiro, and C. G. Lin, "The identification and characterization of oxidized RNAs in Alzheimer's disease," *J. Neurosci.*, vol. 23, no. 12, pp. 4913–4921, 2003.

[137]   M. Tanaka, P. B. Chock, and E. R. Stadtman, "Oxidized messenger RNA induces translation errors.," *Proc. Natl. Acad. Sci. U.S.A.*, vol. 104, no. 1, pp. 66–71, Jan. 2007.

[138]   P. J. Vikesland, A. Pruden, P. J. J. Alvarez, D. Aga, H. Bürgmann, X.-D. Li, C. M. Manaia, I. Nambi, K. Wigginton, T. Zhang, and Y.-G. Zhu, "Toward a comprehensive strategy to mitigate dissemination of environmental sources of antibiotic resistance," *Environ. Sci. Technol.*, vol. 51, no. 22, pp. 13061–13069, 2017.

[139]   K. M. Parker and M. Sander, "Environmental fate of insecticidal plant-incorporated protectants from genetically modified crops: knowledge gaps and research opportunities," *Environ. Sci. Technol.*, vol. 51, no. 21, pp. 12049–12057, Oct. 2017.

[140]   "Disinfection market set for billion dollar growth up to 2019," *waterworld.com*, 2018. [Online]. Available: http://www.waterworld.com/articles/wwi/print/volume-28/issue-4/regulars/news/analysis/disinfection-market-set-for-billion-dollar.html. [Accessed: 28-Apr-2018].

[141]   T. Douki, "The variety of UV-induced pyrimidine dimeric photoproducts in DNA as shown by chromatographic quantification methods," *Photochem. Photobiol. Sci.*, vol. 12, no. 8, pp. 1286–1302, 2013.

[142]   T. Douki and J. Cadet, "Individual determination of the yield of the main UV-induced dimeric pyrimidine photoproducts in DNA suggests a high mutagenicity of CC photolesions," *Biochemistry*, vol. 40, no. 8, pp. 2495–2501, 2001.

[143]   T. Douki, "Low ionic strength reduces cytosine photoreactivity in UVC-irradiated isolated DNA," *Photochem. Photobiol. Sci.*, vol. 5, no. 11, pp. 1045–1051, Nov. 2006.

[144]   D. E. Lemaire and B. P. Ruzsicska, "Quantum yields and secondary photoreactions of the photoproducts of dTpdT, dTpdC and dTpdU," *Photochem. Photobiol.*, vol. 57, no. 5, pp. 755–757, May 1993.

[145]   Z. Pan, M. McCullagh, G. C. Schatz, and F. D. Lewis, "Conformational control of thymine photodimerization in purine-containing trinucleotides," *J. Phys. Chem. Lett.*, vol. 2, no. 12, pp. 1432–1438, May 2011.

[146]   Y. K. Law, R. A. Forties, X. Liu, M. G. Poirier, and B. Kohler, "Sequence-dependent thymine dimer formation and photoreversal rates in double-stranded DNA," *Photochem. Photobiol. Sci.*, vol. 12, no. 8, pp. 1431–1439, 2013.

[147]   G. J. Fisher and H. E. Johns, *Pyrimidine photodimers*. 1976, pp. 225–294.

[148]   C. P. Gerba, D. M. Gramos, and N. Nwachuku, "Comparative inactivation of

enteroviruses and adenovirus 2 by UV light," *Appl. Environ. Microbiol.*, vol. 68, no. 10, pp. 5167–5169, Oct. 2002.

[149] M. J. Mattle and T. Kohn, "Inactivation and tailing during UV254 disinfection of viruses: contributions of viral aggregation, light shielding within viral aggregates, and recombination," *Environ. Sci. Technol.*, p. 120830135926005, Aug. 2012.

[150] C. W. McKinney and A. Pruden, "Ultraviolet disinfection of antibiotic resistant bacteria and their antibiotic resistance genes in water and wastewater," *J. Am. Chem. Soc.*, vol. 46, no. 24, pp. 13393–13400, Nov. 2012.

[151] P. H. Chang, B. Juhrend, T. M. Olson, C. F. Marrs, and K. R. Wigginton, "Degradation of extracellular antibiotic resistance genes with UV254 treatment," *Environ. Sci. Technol.*, vol. 51, no. 11, pp. 6185–6192, May 2017.

[152] C. W. Helleiner, M. L. Pearson, and H. E. Johns, "The ultraviolet photochemistry of deoxyuridylyl (3′→5′) deoxyuridine," *Proc. Natl. Acad. Sci. U.S.A.*, vol. 50, no. 4, pp. 761–767, Oct. 1963.

[153] H. E. Johns, M. L. Pearson, J. C. LeBlanc, and C. W. Helleiner, "The ultraviolet photochemistry of thymidylyl-(3′→5′)-thymidine," *J. Mol. Biol.*, vol. 9, no. 2, pp. 503–IN1, Aug. 1964.

[154] L. M. Kundu, U. Linne, M. Marahiel, and T. Carell, "RNA is more UV resistant than DNA: The formation of UV-induced DNA lesions is strongly sequence and conformation dependent," *Chem. Eur. J.*, vol. 10, no. 22, pp. 5697–5705, Nov. 2004.

[155] G. J. Fisher and H. E. Johns, "Pyrimidine Photohydrates," in *Photochemistry and Photobiology of Nucleic Acids*, Elsevier, 1976, pp. 169–224.

[156] R. P. Schwarzenbach, P. M. Gschwend, and D. M. Imboden, *Environmental organic Chemistry 2 nd Edition*.

[157] I. H. Brown and H. E. Johns, "Photochemistry of uracil. Intersystem crossing and dimerization in aqueous solution," *Photochem. Photobiol.*, vol. 8, no. 4, pp. 273–286, Oct. 1968.

[158] N. A. Evans and A. D. McLaren, "Quantum yields for inactivation of tobacco mosaic virus nucleic acid by ultraviolet radiation (254 nm.)," *J. Gen. Virol.*, vol. 4, no. 1, pp. 55–63, Jan. 1969.

[159] Z. Tarmer, K. L. Wierzchowski, and D. Shugar, "Influence of polynucleotide secondary structure on thymine photodimerization," *Acta Biochim Pol*, vol. 16, no. 1, pp. 83–107, 1696.

[160] D. Li, A. Z. Gu, M. He, H.-C. Shi, and W. Yang, "UV inactivation and resistance of rotavirus evaluated by integrated cell culture and real-time RT-PCR assay," *Water Res.*, vol. 43, no. 13, pp. 3261–3269, Jul. 2009.

[161] J. Ho, M. Seidel, R. Niessner, J. Eggers, and A. Tiehm, "Long amplicon (LA)-qPCR for the discrimination of infectious and noninfectious phix174 bacteriophages after UV inactivation," *Water Res.*, vol. 103, pp. 141–148, Oct. 2016.

[162] S. E. Beck, R. A. Rodríguez, K. G. Linden, T. M. Hargy, T. C. Larason, and H. B.

Wright, "Wavelength dependent UV inactivation and DNA damage of adenovirus as measured by cell culture infectivity and long range quantitative PCR," *Environ. Sci. Technol.*, vol. 48, no. 1, pp. 591–598, 2013.

[163] J. Simonet and C. Gantzer, "Inactivation of poliovirus 1 and F-specific RNA phages and degradation of their genomes by UV irradiation at 254 nanometers.," *Appl. Environ. Microbiol.*, vol. 72, no. 12, pp. 7671–7677, Dec. 2006.

[164] B. A. Dancho, H. Chen, and D. H. Kingsley, "Discrimination between infectious and non-infectious human norovirus using porcine gastric mucin," *Int. J. Food Microbiol.*, vol. 155, no. 3, pp. 222–226, Apr. 2012.

[165] Y. Yoon, H. J. Chung, D. Y. Wen Di, M. C. Dodd, H.-G. Hur, and Y. Lee, "Inactivation efficiency of plasmid-encoded antibiotic resistance genes during water treatment with chlorine, UV, and UV/H2O2," *Water Res.*, vol. 123, pp. 783–793, Oct. 2017.

[166] Y. Ye, P. H. Chang, J. Hartert, and K. R. Wigginton, "Reactivity of enveloped virus genome, proteins, and lipids with free chlorine and UV254," *Environ. Sci. Technol.*, vol. 52, no. 14, pp. 7698–7708, 2018.

[167] B. Vazquez-Bravo, K. Gonçalves, J. L. Shisler, and B. J. Mariñas, "Adenovirus replication cycle disruption from exposure to polychromatic ultraviolet irradiation," *Environ. Sci. Technol.*, vol. 52, no. 6, pp. 3652–3659, 2018.

[168] S. P. Jackson and J. Bartek, "The DNA-damage response in human biology and disease," *Nature*, vol. 461, no. 7267, pp. 1071–1078, Oct. 2009.

[169] K. K. Khanna and S. P. Jackson, "DNA double-strand breaks: signaling, repair and the cancer connection," *Nature Genetics 2001 27:3*, vol. 27, no. 3, pp. 247–254, Mar. 2001.

[170] G. N. Wogan, S. S. Hecht, J. S. Felton, A. H. Conney, and L. A. Loeb, "Environmental and chemical carcinogenesis," *Seminars in Cancer Biology*, vol. 14, no. 6, pp. 473–486, Dec. 2004.

[171] K. Scarlett, D. Collins, L. Tesoriero, L. Jewell, F. van Ogtrop, and R. Daniel, "Efficacy of chlorine, chlorine dioxide and ultraviolet radiation as disinfectants against plant pathogens in irrigation water," *European Journal of Plant Pathology*, vol. 145, no. 1, pp. 27–38, 2015.

[172] G.-A. Shin and M. D. Sobsey, "Inactivation of norovirus by chlorine disinfection of water," *Water Res.*, vol. 42, no. 17, pp. 4562–4568, Nov. 2008.

[173] C. Le Dantec, J.-P. Duguet, A. Montiel, N. Dumoutier, S. Dubrou, and V. Vincent, "Chlorine Disinfection of Atypical Mycobacteria Isolated from a Water Distribution System," *Appl. Environ. Microbiol.*, vol. 68, no. 3, pp. 1025–1032, Mar. 2002.

[174] J. C. Morris, "The Acid Ionization Constant of HOCl from 5 to 35°," *The Journal of Physical Chemistry*, vol. 70, no. 12, pp. 3798–3805, 1966.

[175] M. Deborde and U. von Gunten, "Reactions of chlorine with inorganic and organic compounds during water treatment—Kinetics and mechanisms: A critical review,"

Water Res., vol. 42, no. 1, pp. 13–51, Jan. 2008.

[176]   H. HAYATSU, S. PAN, and T. UKITA, "Reaction of Sodium Hypochlorite with Nucleic Acids and Their Constituents," *Chem. Pharm. Bull.*, vol. 19, no. 10, pp. 2189–2192, Oct. 1971.

[177]   C. L. H. and and M. J. Davies, "Hypochlorite-Induced Damage to DNA, RNA, and Polynucleotides: Formation of Chloramines and Nitrogen-Centered Radicals," *Chem. Res. Toxicol.*, vol. 15, no. 1, pp. 83–92, Jan. 2002.

[178]   W. A. Prütz, "Hypochlorous Acid Interactions with Thiols, Nucleotides, DNA, and Other Biological Substrates," *Arch. Biochem. Biophys.*, vol. 332, no. 1, pp. 110–120, Aug. 1996.

[179]   W. A. Prütz, "Interactions of Hypochlorous Acid with Pyrimidine Nucleotides, and Secondary Reactions of Chlorinated Pyrimidines with GSH, NADH, and Other Substrates," *Arch. Biochem. Biophys.*, vol. 349, no. 1, pp. 183–191, 1998.

[180]   J. P. Gould, J. T. Richards, and M. G. Miles, "The kinetics and primary products of uracil chlorination," *Water Res.*, vol. 18, no. 2, pp. 205–212, Jan. 1984.

[181]   Y. Hoyano, V. Bacon, R. E. Summons, W. E. Pereira, B. Halpern, and A. M. Duffield, "Chlorination studies. IV1. The reaction of aqueous hypochlorous acid with pyrimidine and purine bases," *Biochem. Bioph. Res. Co.*, vol. 53, no. 4, pp. 1195–1199, Aug. 1973.

[182]   M. Whiteman, A. Jenner, and B. Halliwell, "8-Chloroadenine: a novel product formed from hypochlorous acid-induced damage to calf thymus DNA," *Biomarkers*, vol. 4, no. 4, pp. 303–310, 1999.

[183]   W. Patton, V. Bacon, A. M. Duffield, B. Halpern, Y. Hoyano, W. Pereira, and J. Lederberg, "CHLORINATION STUDIES. I. THE REACTION OF AQUEOUS HYPOCHLOROUS ACID," *Biochem. Bioph. Res. Co.*, vol. 48, no. 4, 1972.

[184]   J. P. Gould, J. T. Richards, and M. G. Miles, "The formation of stable organic chloramines during the aqueous chlorination of cytosine and 5-methylcytosine," *Water Res.*, vol. 18, no. 8, pp. 991–999, 1984.

[185]   J. P. Henderson, J. Byun, and J. W. Heinecke, "Chlorination of nucleobases, RNA and DNA by myeloperoxidase: a pathway for cytotoxicity and mutagenesis by activated phagocytes," *Redox Report*, vol. 4, no. 6, pp. 319–320, Jul. 2013.

[186]   X. Liang, H. Kuhn, and M. D. Frank-Kamenetskii, "Monitoring Single-Stranded DNA Secondary Structure Formation by Determining the Topological State of DNA Catenanes," *Biophysical Journal*, vol. 90, no. 8, pp. 2877–2889, Apr. 2006.

[187]   A. Buhot and A. Halperin, "Effects of stacking on the configurations and elasticity of single-stranded nucleic acids," *Phys. Rev. E*, vol. 70, no. 2, p. 020902, Aug. 2004.

[188]   Y. Zhang, H. Zhou, and Z.-C. Ou-Yang, "Stretching Single-Stranded DNA: Interplay of Electrostatic, Base-Pairing, and Base-Pair Stacking Interactions," *Biophysical Journal*, vol. 81, no. 2, pp. 1133–1143, Aug. 2001.

[189]   W. D. Wilson, M.-H. Dotrong, E. T. Zuo, and G. Zon, "Unusual duplex formation in

purine rich oligodeoxyribonucleotides," *Nucleic Acids Res.*, vol. 16, no. 11, pp. 5137–5151, Jun. 1988.

[190] T. Suda, Y. Mishima, H. Asakura, and R. Kominami, "Formation of a parallel-stranded DNA homoduplex by d(GGA) repeat oligonucleotides," *Nucleic Acids Res.*, vol. 23, no. 18, pp. 3771–3777, Sep. 1995.

[191] P. R. Cook and I. A. Brazell, "Supercoils in human DNA," *Journal of Cell Science*, vol. 19, no. 2, pp. 261–279, Nov. 1975.

[192] S. Kadauke and G. A. Blobel, "Chromatin loops in gene regulation," *Biochimica et Biophysica Acta (BBA) - Gene Regulatory Mechanisms*, vol. 1789, no. 1, pp. 17–25, Jan. 2009.

[193] C. Suquet, J. J. Warren, N. Seth, and J. K. Hurst, "Comparative study of HOCl-inflicted damage to bacterial DNA ex vivo and within cells," *Arch. Biochem. Biophys.*, vol. 493, no. 2, pp. 135–142, Jan. 2010.

[194] M. C. Dodd, "Potential impacts of disinfection processes on elimination and deactivation of antibiotic resistance genes during water and wastewater treatment," *Journal of Environmental Monitoring*, vol. 14, no. 7, pp. 1754–1771, 2012.

[195] Y.-C. Hsu, "Resistance of Infectious RNA and Transforming DNA to Iodine which Inactivates ƒ2 Phage and Cells," *Nature*, vol. 203, no. 4941, p. 152, 1964.

[196] R. W. Pero, Y. Sheng, A. Olsson, C. Bryngelsson, and M. Lund-Pero, "Hypochlorous acid/N-chloramines are naturally produced DNA repair inhibitors," *Carcinogenesis*, vol. 17, no. 1, pp. 13–18, Jan. 1996.

[197] M. C. Dodd, N. D. Vu, A. Ammann, Van Chieu Le, R. Kissner, H. V. Pham, T. H. Cao, M. Berg, and U. von Gunten, "Kinetics and mechanistic aspects of As(iii) oxidation by aqueous chlorine, chloramines, and ozone: relevance to drinking water treatment," *Environ. Sci. Technol.*, vol. 40, no. 10, pp. 3285–3292, 2006.

[198] W. E. Federation and A. P. H. Association, "Standard methods for the examination of water and wastewater," *American Public Health Association (APHA): Washington, DC, USA*, 2005.

[199] D. N. Nikogosyan, "Two-quantum UV photochemistry of nucleic acids: comparison with conventional low-intensity UV photochemistry and radiation chemistry," *International Journal of Radiation Biology*, vol. 57, no. 2, pp. 233–299, 1990.

[200] D. F. Rhoades and S. Y. Wang, "Photochemistry of polycytidylic acid, deoxycytidine, and cytidine," *Biochemistry*, vol. 10, no. 25, pp. 4603–4611, 1971.

[201] M. Pearson, D. W. Whillans, J. C. LeBlanc, and H. E. Johns, "Dependence on wavelength of photoproduct yields in ultraviolet-irradiated poly U," *J. Mol. Biol.*, vol. 20, no. 2, pp. 245–261, Sep. 1966.

[202] D. L. Mitchell and J. M. Clarkson, "Use of synthetic polynucleotides to characterise an antiserum made against UV-irradiated DNA," *Photochem. Photobiol.*, vol. 40, no. 6, pp. 743–748, 1984.

[203] L. Grossman and E. Rodgers, "Evidence for the presence of cytosine photohydrates in

UV irradiated nucleic acids," *Biochem. Bioph. Res. Co.*, vol. 33, no. 6, pp. 975–983, 1968.

[204]   R. A. Deering and R. B. Setlow, "Effects of ultraviolet light on thymidine dinucleotide and polynucleotide," *Biochimica et Biophysica Acta*, vol. 68, pp. 526–534, 1963.

[205]   D. L. Wulff, "Kinetics of thymine photodimerization in DNA," *Biophysical Journal*, vol. 3, no. 5, pp. 355–362, Sep. 1963.

[206]   M. H. Patrick, "Studies on thymine-derived UV photoproducts in DNA—i. formation and biological role of pyrimidine adducts in DNA," *Photochem. Photobiol.*, vol. 25, no. 4, pp. 357–372, 1977.

[207]   F. Garcés and C. A. Dávila, "Alterations in DNA irradiated with ultraviolet radiation— i. the formation process of cyclobutylpyrimidine dimers: cross sections, action spectra and quantum yields," *Photochem. Photobiol.*, vol. 35, no. 1, pp. 9–16, 1982.

[208]   T. Douki, "Effect of denaturation on the photochemistry of pyrimidine bases in isolated DNA," vol. 82, no. 1, pp. 45–52, 2006.